NATURE AND EVOLUTION OF MANTLE SECTION IN THE NIDAR OPHIOLITE SUITE, LADAKH, INDIA

By

SOUVIK DAS

Under the Guidance of

DR. BARUN K MUKHERJEE, SCEINTIST – C

WADIA INSTITUTE OF HIMALAYAN GEOLOGY
DEHRADUN

Submitted

IN PARTIAL FULFILLMENT OF THE REQUIREMENT OF THE DEGREE OF DOCTOR OF PHILOSOPHY

IN

GEOSCIENCE

TO

UNIVERSITY OF PETROLEUM AND ENERGY STUDIES
DEHRADUN

July, 2014

Wadia Institute of Himalayan Geology
(an autonomous institution of Dept. of Science & Technology)
33 GMS Road,Dehra Dun-248 001 (Uttarakhand)

Dr. Barun Kumar Mukherjee, PhD,
JSPS, (Japan)
Scientist-C

Certificate

This is to certify that the thesis entitled "Nature and Evolution of Mantle Section in the Nidar Ophiolite Suite, Ladakh, India" is a bonafied work of Mr Souvik Das, which has been completed under my supervision. Further it is certified that he has fulfilled all the terms and conditions pertaining to PhD ordinances of the University of Petroleum & Energy Studies, Dehra Dun and Wadia Institute of Himalayan Geology, Dehra Dun and that he is entitled to submit this original thesis work for the Ph.D. Degree in University of Petroleum & Energy Studies.

The content of the thesis, in full or parts have not been submitted to any other Institute or University for the award of any other degree or diploma.

Date: July, 2014

Place: Dehra Dun

FAX: 0135-2625212 Tel (off): 01352525189
E-Mail:baun@wihg.res.in : mukherjeebarun@yahoo.co.in
Web:www.wihg.res.in

Declaration

"I hereby declare that this submission is my own work and that, to the best of my knowledge and belief, it contains no material previously published or written by another person nor material which has been accepted for the award of any other degree or diploma of the university or other institute of higher learning, except where due acknowledgment has been made in the text".

(Souvik Das, July, 2014)

TO MY
PARENTS

CONTENTS

PREFACE

The origin of ophiolite have long been a conundrum in the history of Earth science as it is linked with mantle circulation processes. Through this thesis work an attempt has been made through detail in situ mineralogical studies of primary rock bodies of ultramafic part of a classical ophiolite sequence along Indus Suture Zone, Ladakh Himalaya, India to understand the primitive phases and composition of spreading centre upwelling. Though it is a daunting task to decode the Earth's deep interior from natural rocks still the study was carried out on the relatively primary features as recovered from the field. Starting from field work to microscopic studies relatively primary portions are considered to find the initial material of ophiolite. For further characterization in situ Laser Raman Spectroscope and Electron Micro Probe Analyser were employed. In this thesis some exciting results from ophiolite ultramafic rocks have been summarised which will put us one step ahead to understand the mantle petrology.

Additionally I tried to explain the presence of mantle rocks in the core of the orogeny. Their presence indicate intimate connection between tectonics of the lithosphere and the deep Earth processes which may demand more attention in near future to consider them key players behind the orogenic processes.

Souvik Das

ACKNOWLEDGEMENTS

I would like to express my sincere gratitude to my supervisor Dr Barun Kumar Mukherjee, Scientist 'C', Wadia Institute of Himalayan Geology (WIHG), Dehradun. As a mentor he not only directed me to the solution but always inspired me. His critics also helped me a lot to improve my work.

Present Director WIHG – Prof Anil K Gupta is acknowledged for providing me "Wadia National Fellowship in Himalayan Geology" and extending the necessary facilities and the required infrastructure for the research work in Wadia Institute of Himalayan Geology. The former directors Prof B R Arora & Dr A K Dubey are thanked for the same.

I extend my sincere thanks to University of Petroleum and Energy Studies for their supports. The priceless inputs from the FRC (UPES) during synopsis and abstract presentation helped me a lot to improve my thesis. I would like to express my sincere gratitude to CCE, UPES for their timely cooperation and encouragement.

I am also thankful to Prof Asish R Basu (Chair, Dept. of Earth & Environmental Sciences, University of Texas at Arlington) for his priceless suggestions during my PhD. Besides, he also provided me the laboratory facilities (EPMA and Raman spectroscopy in Cornell University, XRD in University of Rochester) for the analyses of my samples and arranged my 1 week stay in Rochester for the above mentioned analyses.

I am thankful to the American Geophysical Union (AGU) for Berkner Travel Fellowship which gave me a great opportunity to present my research at AGU Fall meeting in December, 2011 held at San Francisco, California (USA).

I would like to thank Dr. P P Khanna, Dr. D. R. Rao, Dr. Rajesh Sharma and Dr. S. S. Thakur for their immense help while operating the EPMA, Raman spectroscope & other instruments in Goechemistry group, WIHG. I also sincerely acknowledge Kit Umbach (Cornell University, USA) and John Hunt (Cornell University, USA) for basic training in Raman spectroscopy and EPMA respectively.

Mr. Koushick Sen and Dr. Koushik Sen are thanked for several discussion session and helping in field work. I thank Dr. Yogesh Ray (NCAOR), Dr Sumit K Ghosh and Dr. Vimal Singh (Delhi University) for encouraging me. Dr. V. C. Thakur is thanked for discussing regional geology in Ladakh. Dr. Pradeep Srivastava, Dr. V. C. Tewari and Dr. R Islam are thanked for both scientific and official helps. Mr Mainak Palit (University of Calcutta) is thanked for discussions regarding instrument handling. I extend this thanks giving for Registrar and Finance and accounting officer (WIHG) for numerous official helps.

I would also like to express heartiest gratitude to Dr. Santanu Bose (Assist. Prof, University of Calcutta) for inspiring and motivating me in research from my M. Sc. Days. At the time of first field work (July – August, 2010) our field team was trapped into flash flood took place in Ladakh. I sincerely thank Indian army for rescuing us to the Leh. Dr. C. P. Dorjey and our drivers and porters are also thanked for helping us that time to reach Delhi and sending the collected samples after the road blockages get cleared.

I am grateful to Mr. Shekhar Nandan for his careful hands at time of thin section preparation. I would also like to acknowledge Mr. N K Juyal and Mr. Samay Singh for analyses of SEM and XRD respectively. I would like to acknowledge Rakhi Rawat for helping me at the time of Raman spectroscopic analyses. I would like to acknowledge Library (S Ahmed and S S Bhandari) and Publication section of WIHG for their immense helps.

Last but not the least I am grateful to all of my well-wishers. Particularly among them, I sincerely thank Mrs Tamanna Mukherjee, Mr S P Bose & Dr Neeti Sethi Bose for motivating and inspiring me. Mrs Nabanita Sen, Mr Reetam Choudhury, Subhra Sharma & Nandini Prakash are thanked for moral support and many co operations. Finally, I take this opportunity to thank all those unnamed individuals participated in various ways to complete this task successfully.

Date: July, 2014

(Souvik Das)

LIST OF FIGURES

Chapter 3

	initiated by a deep oceanic subduction followed by dehydration of serpentines released a huge amount of free water. The water was responsible for melting in mantle wedge. This process created a vacuum in mantle which attracted the regular mantle flow towards the open "window" in the pre Himalayan intra oceanic arc where the deep Earth phases are emplaced on to the surface. The flow began its journey from the transition zone upwards by solid – state flow, arrived below the ophiolite's volcanic crust at spreading center in an intra-oceanic arc.	

LIST OF TABLES

Chapter 5

EXECUTIVE SUMMARY

The ophiolites preserve signatures of variety of geologic processes which provide researchers important insights into the development of our planet. But the main problem with these ophiolites are that, their origin is still a matter of debate over a hundred years because of their mysterious occurrences along tectonic suture zones. The Nidar valley in Indus Suture Zone (ISZ, NW Himalaya, India) displays classical exposures of ophiolite which represents a palaeo spreading center. In the basal section, crosscutting discordant dunite channels carry lherzolite xenoliths which include very high pressure minerals – *C2/c* clinoenstatite, disordered coesite, α - Fe_2O_3 glass and probably β - Mg_2SiO_4. These phase discoveries are confirmed by combining petrography, electron probe micro analyses and Raman spectroscopy. Phase stabilities of the minerals require derivation from at least mantle transition zone (410 - 660 km depth). Unlike previous studies that reported minerals of high - pressure origin in similar rocks, here a set of minerals and supportive micro textures are reported. The systematic phase transitions along with micro textural evidences infer continuous pathway from the mantle transition zone to the uppermost mantle region. The phase transitions show systematic evolution of MgO – FeO - SiO_2 terminating beneath the mid-ocean-ridge basalt eruption temperatures of ~1300^0 C.

Several micro structures and exsolution micro textures supports the deep mantle origin of at least some part of Nidar ophiolite ultramafics. Exsolution needles

of Cr - spinel in olivine, lamellar inclusions of *C2/c* clinoenstatite in orthoenstatite and many other micro textures infer systematic fall of P – T condition from deep mantle to the ocean ridges.

The thesis also reports rare natural evidences of highly reducing environment in and around mantle transition zone. The very high pressure lherzolites bear dense primary hydrocarbon fluid inclusions along with unusual inclusions of carbons and $\alpha - Fe_2O_3$ in olivine.

The signatures of serpentine dehydration and formation of garnet bearing serpentinite infer deep and steep subduction of primary oceanic lithosphere which releases free high volume of water in sub arc depth. This phenomena facilitate melting at the overlying mantle wedge and potential of volcanism in intra oceanic arc. Additionally due to dehydration and ascent of magma a sudden vacuum can be formed in mantle wedge which may trigger upwelling from mantle transition depth (410 – 660 km). Thus subduction induced mantle flow may create the ‘geodynamo’ which initiated the Himalaya building process.

Besides all, present work documents first site of natural CO_2 sequestration in Himalaya. The dunites and serpentinites in Nidar valley react with CO_2 at low temperature to produces magnesite as patches on skin and as veins. Understanding the carbonation process is important in terms of global carbon cycle, weathering and fluid rock interaction during serpentinization.

CHAPTER 1

INTRODUCTION

CHAPTER 1

INTRODUCTION

1.1 STATEMENT OF THE THESIS

This thesis is an attempt to study the behaviour of deep Earth mineralogy and mineral phases of Mantle Transition Zone (MTZ). These deep Earth mineral phases have been collected on the Earth surface at basal ultramafic part of Nidar Ophiolite, Ladakh Himalaya. This thesis draws a perspective of possible evolution path of mineral phase transition from mantle transition zone (410 – 660 Km). To substantiate the evolution path, field geology, petrology, mineralogy, mineral chemistry, mineral phase characterization and role of volatiles are examined.

1.2 MOTIVATION FOR THE STUDY

Issue concerning the origin and evolution of our planet Earth, have inevitably been of special importance to scientists. The Earth is a dynamic and active planet changes its size and shape with time and this dynamism of the earth can be explained by plate tectonic concept. The outer rigid layer of the Earth is called lithosphere which diverges at mid-ocean ridges and converges at the other plate margin to create the orogenic belts. Although theory of plate tectonics is widely accepted, the dynamo that drives the motion of the lithospheric plates is overlooked. Yet in order to really understand the geodynamo, we must look below the plates themselves – into the Earth's deep interior. The large scale convection is believed to drive the plate tectonic processes. But the problem with the upper mantle (extends from 40 km below our feet to a depth of 660 km) is that we cannot go there and we cannot drill this deep till date. Therefore we rely on indirect observations, such as from seismic signals, or from parts of the mantle that have been lifted to the Earth's surface (such as small mantle fragments in volcanoes – "xenoliths", or larger segments of ocean floor that have been emplaced to the surface – "ophiolites"). Detail studies of these mantle rocks allow us to determine the nature of the mantle. The present research is focused on the mantle rocks present in the core of the orogeny to crack the mystery of "geodynamo" which links the relationship between tectonics of the lithosphere and the deep mantle.

1.3 DEFINITION OF THE PROBLEM

Mantle convection flow is thought as the most plausible causative factor for plate movement. It is more or less accepted by geoscientists that mantle convection controls the lithosphere movement - to diverge at mid ocean ridge and collides at subduction zone. But the nature of mantle upwelling beneath a mid ocean ridge or spreading center is poorly known. The main problem is to sample the mantle rocks from spreading center. For this we are dependent on the ophiolites present along suture zones. The ophiolites are generally considered as fossil mid-oceanic ridges (Moores and Vine, 1971; Malpas, 1978), island arcs (Menzies, 1973; Miyashiro, 1973) or back-arc basins (Upadhyay and Neale, 1979; Ewart, 1982) and supposed to retain the primitive signatures of mantle upwelling. Geophysical studies show that the root of the mantle upwelling beneath a spreading center is at around 400 km (Su et al., 1992; Zhao et al., 1997). But ophiolite peridotites, which are generally spinel peridotites, do not cross the stability field across 2 GPa (~ 60 km depth). Petrological knowledge of mid oceanic basalt generation also suggests that the melting in an upwelling mantle is restricted in 70 – 90 km depth (O'Leary et al., 2010). Though recent experimental studies suggested huge volume of melt can be present at ~ 200 km depth (Dasgupta et al., 2013).

The present work has been carried out to examine connection between ophiolite evolution and deep Earth. The study was done on ultramafic part of Nidar ophiolite, Indus Suture Zone (ISZ), Ladakh Himalaya as the ophiolite suite has a thick basal section (~7 km). One hand, these mantle rocks provide insights into the upper mantle processes and on the other hand they bear important information regarding geodynamic setting because of their presence along suture zones.

The greatest disadvantage with the ophiolite is that their original setting is not exactly known and their significance is sometimes a subject of speculation. Since appearance of plate tectonic concept the birth environment of ophiolites (mid oceanic ridges versus suprasubduction settings – e.g., Nicolas, 1989) have long been a stubborn mystery which lead Earth scientists to the famous ‘ophiolite conundrum’. Similarity between ophiolite internal structure and modern oceanic environment forced the earlier Geo scientists to consider ophiolites as representative of ancient oceanic crust. A preferred hypothesis was that the ophiolites originate in a mid-oceanic ridge and then rammed into continent in a subduction set up and ultimately emplaced over the continental crust. Meanwhile a revolutionary thought started in 1980’s and 1990’s. Geochemical data started to advocate for derivation from depleted upper and the condition is similar to the subduction zone environment. Since then geologists started to believe that ophiolites originate in fore arc of subduction zone. But the mantle structures and mineralogical compositions of tectonically emplaced mantle rocks are generally re equilibrated by deformation and metamorphic recrystallization during emplacement. These metamorphic processes involve high temperature recrystallization in the stability field of plagioclase peridotites (Rampone et al 1993) to complete serpentinization (Burkhard and O’Neill, 1988). Most often, the chemical signatures of ultramafic rocks are strongly modified and cannot be used directly to assess actual mantle compositions (e.g. Baker and Beckett, 1999). So it is far from primary signature of ophiolites from whole rock geochemical data.

To solve the debate regarding the primitive signature of ophiolite composition, a direct attempt has been employed on ultramafic rocks of Nidar ophiolite by studying in situ mineralogical and textural evidences.

1.4 WHAT IS OPHIOLITE?

The geologists of early days were puzzled by looking a peculiar set of rock types in the European Alps that never been observed before on land: bodies of dark and heavy peridotite associated with deep-seated gabbro, volcanic rocks and bodies of serpentinite, with a thin cap of deep-sea sedimentary rocks. In 1813 Alexandre Brongniart first used the term “ophiolite” (in Greek language *ophio* – means snake, *lite* – means stone) because of shiny surfaces with a snake skin like texture of serpentinite. Steinmann (1905, 1927) later used the ophiolite for a broader association of serpentinite, pillow lava and radiolarian chert occur in the Alps which was often referred as “Steinmann’s Trinity”. But he did not consider any relationship between them with respect to their origin. Later Dewey and Bird (1971) have argued that the term ophiolite should be restricted to a full sequence of (i) ultramafic rocks, (ii) gabbro, (iii) sheeted dyke complex, and (iv) pillow lava with chert from bottom to top. That time people started to consider this assemblage as analogue of oceanic crust and mantle as the general structure of the oceanic lithosphere resembles with the ophiolite. The observation of sheeted dyke complex within the Troodos Ophiolite (Cyprus) (Gass 1968) indicates formation through repetitive extension of ocean crust and intrusion of magma. Moores and Vine (1971) concluded that the sheeted dyke complex at Troodos could only form by a process similar to the seafloor spreading proposed by Vine and Matthews (1963). From then it became widely accepted that ophiolites represent oceanic crust that had been emplaced on land. Fractured, altered and faulted, with almost no fossil evidence to date them, ophiolites were stubborn mysteries until plate tectonics revealed their important role? A hundred and fifty years after Brongniart, the advent of plate tectonics gave ophiolites a place in the big cycle: they appear to be small pieces of oceanic crust that have been attached to the continents.

Most researchers presume an idealized picture of pseudostratigraphic section of ophiolite. Miyashiro (1973, 1975) emphasized, however "most of the mafic and ultramafic masses now exposed in ancient subduction zones (or high-pressure metamorphic belts) do not show such a sequence". There is strong evidence indicating that many of them had no regular sequence from the beginning. Mafic volcanic rocks usually form beds conformable with the underlying and overlying sedimentary beds, and thus do not represent fragments of any ophiolite sequences". Coleman (1977) argued that these basalts are chemically similar to oceanic basalts but are not sequentially associated with sheeted dykes, layered gabbro, and peridotites, so they cannot be referred to as ophiolites.

The term "ophiolite" is regarded as generally descriptive, and its usage should be independent of its supposed origin (Anonymous, 1972, Gass et al., 1975). Personally I believe in Steinmann's original concept about ophiolite is more logical – "ophiolite is an association of serpentinite, pillow lava and radiolarian chert disregarding any interpretation of its origin".

1.5 IMPORTANCE OF THE OPHIOLITE STUDY

Ophiolites are widely accepted as remnants of oceanic lithosphere. They show significant variations in their internal structures, geochemical fingerprints and emplacement mechanisms. Ophiolites retain signatures of many significant processes some of which are discussed below.

In ocean floors mantle rocks are generally not exposed. Even if they are somewhere exposed it is hard to sample them. Classical ophiolite suites are widely considered as remnants of ancient oceanic crust and upper mantle rocks. Ophiolites provide a great opportunity to study the architecture of oceanic lithosphere. Importantly ophiolitic mantle rocks bear signatures of Upper mantle process which show systematic litho units evolved from a pristine magma chamber. Detailed studies of ophiolitic and orogenic peridotites provide valuable insights into melt extraction mechanisms, such as melt flow in lithospheric vein conduits and wall rock interactions (Bodinier et al., 1990), melt extraction from mantle sources via channelled porous flow (Kelemen et al 1995) or propagation of kilometre scale melting fronts associated with thermal erosion of lithospheric mantle (Lenoir et al., 2001). In contrast, mantle fragments may be used to infer either much smaller or much larger scale mantle heterogeneities, such as micro-inclusions in minerals (Schiano and Clocchiatti, 1994) or lateral variations between lithospheric provinces (O'Reilly et al., 2001).

Ophiolites also provide many indispensable materials for human cultures and civilizations because they are enriched in mineral and ore deposits. The precious metals gold, silver, and platinum-group elements (PGEs), iron, chromium, manganese, titanium, and the base metals cobalt, copper, nickel are obtained in ophiolites. For example - the discovery of copper in the Troodos ophiolite contributed to the development of the Bronze Age (~2400 BC) and triggered a critical era in human history during which the use of bronze brought about drastic changes in farming, hunting and warfare. Non-metallic chrysotiles, asbestos and jade are mainly found in serpentinized peridotites.

1.6 BASIC CONCEPTS REGARDING OPHIOLITE

Initially ophiolites were defined as fragments of oceanic lithosphere because of their structural similarity (Dewey and Bird 1971; Coleman 1977) which were emplaced on to the continents through a process called obduction (Coleman 1971). It was considered that ophiolites originate in mid oceanic ridges. But geochemical studies however not supported this view as it was found that crustal part of the “Troodos ophiolite” follows calc – alkaline trend suggesting characteristic of subduction zone origin (Miyashiro 1973). Subsequently Pearce (1975) proposed marginal basin origin for the Troodos massif. Since then due to advancement of knowledge of the ocean floor it became evident that sea-floor spreading could take place in a number of settings, not just at ridges in the centres of large ocean basins. The problem then switched from answering the question of whether or not ophiolites formed at ocean ridges to determining the precise nature and setting of the ridges at which they formed.

The various types of ophiolites have recently been defined and described in detail by Dilek and Furnes (2011, 2014). Broadly they are classified as subduction related and subduction unrelated types. Subduction unrelated ophiolites are of those, whose magmatic constructions are not affected by subduction. They are generally of three types –

a) **Normal mid ocean ridges**

   This geodynamic set up forms when an ocean opened sufficiently for steady state spreading and they have no influences of either subduction zones or plumes. Most of the melting takes place as a result of decompression at shallow depths (<60 km) as the mantle rises beneath the ridge (e.g. Langmuir et al. 1992). The dominant magma type is known as normal mid-ocean ridge basalt (N – MORB) whose source is depleted with respect to the average mantle.

   Example – Masirah ophiolite, Oman

b) **Plume related mid ocean ridges**

   Plume mantle is hotter than mantle beneath normal ridges. This leads to melting columns in which melting begins at greater depth than at plume distal ridges. As a result, more melting takes place within the deeper garnet facies compared to the shallower spinel facies, and the overall degree of melting is higher. The magma types in this setting are termed as P (plume)-MORB (Dilek and Furnes 2014).

Example – Nicoya ophiolite, Costa Rica

c) **Continental margin ophiolites**

These ridges form when continents break up and a steady-state spreading center has formed. The volcanic-rifted margins are generally driven by plume-associated extension and the lavas may be of P - MORB character. At the non-volcanic rifted margins (e.g. Whitmarsh et al. 2001) lavas are more typically E (enriched)-MORB. The involvement of continental lithosphere in this process can lead to C (contaminated) – MORB compositions.

Example – Jormua ophiolite, Finland

Subduction related ophiolites are formed in a subduction zone magmatism environment. These ophiolites are called as suprasubduction zone ophiolites. They are also broadly classified in three types –

d) **Subduction initiation ophiolite**

According to the Stern-Bloomer (1992) the ophiolites form immediately after the start of convergence during an extensional event that accompanies the roll-back and sinking of the newly subducting plate. In this setting, mantle flows into the nascent mantle wedge and interacts with a small and variable contribution of fluids from the sinking plate. Melting induced by the fluid augments that resulting from decompression, leading to a higher degree of melting than at mid-ocean ridges (e.g. Langmuir et al. 2006). Subduction-influenced lavas originating in this setting have been termed fore arc basalts (FAB) by Reagan et al. (2010). The ophiolite-forming spreading event is typically followed by the first products of arc volcanism. These are commonly boninites, a distinctive Mg – Si rich lava formed by the melting of depleted mantle under shallow, hydrous conditions (Ishizuka et al. 2006).

Example – Semail ophiolite, Oman; Troodos ophiolite, Cyprus

e) Back arc basin ophiolite

These ophiolites are form behind island arcs and / or volcanic arcs, at back arc basins. If the axis is sufficiently far behind the arc, the lavas resemble those from mid-ocean ridges. If it is closer to the arc, its underlying mantle incorporates fluid-rich component from the subducting plate below, as in ridges in subduction- initiation settings. Subduction-influenced lavas from this setting are termed back-arc basin basalts (BABB). Example - Rocas Verdes ophiolite, Chile

f) Ridge – subduction ophiolite

These type of ophiolites form where ridges subduct. Mantle continues to upwell as it did before subduction, but now the melting column is shortened because of the overlying lithosphere of the forearc in the overriding plate. Guivel et al. (1999) carried out a detailed geochemical study of the best example (the Taitao ophiolite in southern Chile) and revealed the co-existence of a number of magma types and a complicated petrogenetic scenario. The melting column produces both N-MORB and E-MORB compositions, commonly with a subduction component. That magma may then interact with fore arc continental lithosphere giving a C (contaminated)-MORB composition. Example – Smartville ophiolite, California

Besides all these, the mystery of ophiolite origin is not ended. Recently from podiform chromitite of a Tibetan ophiolite ultra high pressure mineral inclusions and textures are reported (Robinson et al., 2001; Yang et al., 2007; Yamamoto et al., 2009; Dobrzhinetskaya et al., 2009). It has also been inferred by many workers that the deep mantle minerals was transported by mantle upwelling. These results clearly indicate that, only podiform chromitite travelled from the depth > 300 Km whereas the major part of the ophiolite ultramafics are formed in a shallow depth < 60 Km. But the debate didn’t stopped. Recently it is claimed that the podiform chromitites actually originate in low pressure condition; the UHP minerals are produced by deep recycling of podiform chromitites via mantle convection (Arai 2013). So it is required to substantiate the formation depth of ophiolitic ultramafic rocks, especially the peridotites which constitute the majority of the ophiolite mantle part.

1.7 BROAD OBJECTIVES

The ophiolite peridotites are generally spinel peridotites and thought to have originated from < 60 km (< 2 GPa pressure) depth (Coleman 1977). But geophysical evidences suggest that root of the spreading center upwelling is > 100 km and may extend up to 400 km (Su et al., 1992; Zhao et al., 1997). Ophiolite peridotites and spreading center rocks do not bear any evidence of such deep mantle upwelling until high pressure minerals are discovered from podiform chromitites of Luobusa ophiolite (Tibet) through mineral separation technique (Robinson et al., 2001). Again this can be explained in an alternative way that, the UHP minerals have possibly xenocrystal origin and they are accidentally trapped as xenocrysts within chromitites during formation of podiform chromitites in shallow upper mantle. According to this it is not required to assume that ophiolites are connected deep rooted mantle upwelling. Recently in situ high pressure mineralogical and exsolution micro textures are reported from the same podiform chromitite (Yang et al., 2007; Yamamoto et al., 2009; Dobrzhinetskaya et al., 2009) strongly suggesting evolution of chromitites from deep mantle (> 10 GPa; may be up to mantle transition zone). This precludes the possibility of xenocrystal origin. Very soon the deep mantle mineralogical evidences are also found from other ophiolites like – Dongqiao ophiolite, Semail ophiolite and Ray Iz ophiolite (Trumbull et al., 2009) (Fig. 1.1 A).

But recently Shoji Arai (2013) rejected the deep mantle origin theory for podiform chromitites and suggested alternative view by deep recycling of low pressure chromitites via mantle convection. Podiform chromitites are not essential part of MORB derived ultramafics as they are not consistently observed in all ophiolite sections throughout the globe. So it is really necessary to fix the formation depth of the primitive material of the ophiolite ultramafics. The primary goal of the present research is to substantiate the depth of origin of MORB derived ophiolite in spreading center.

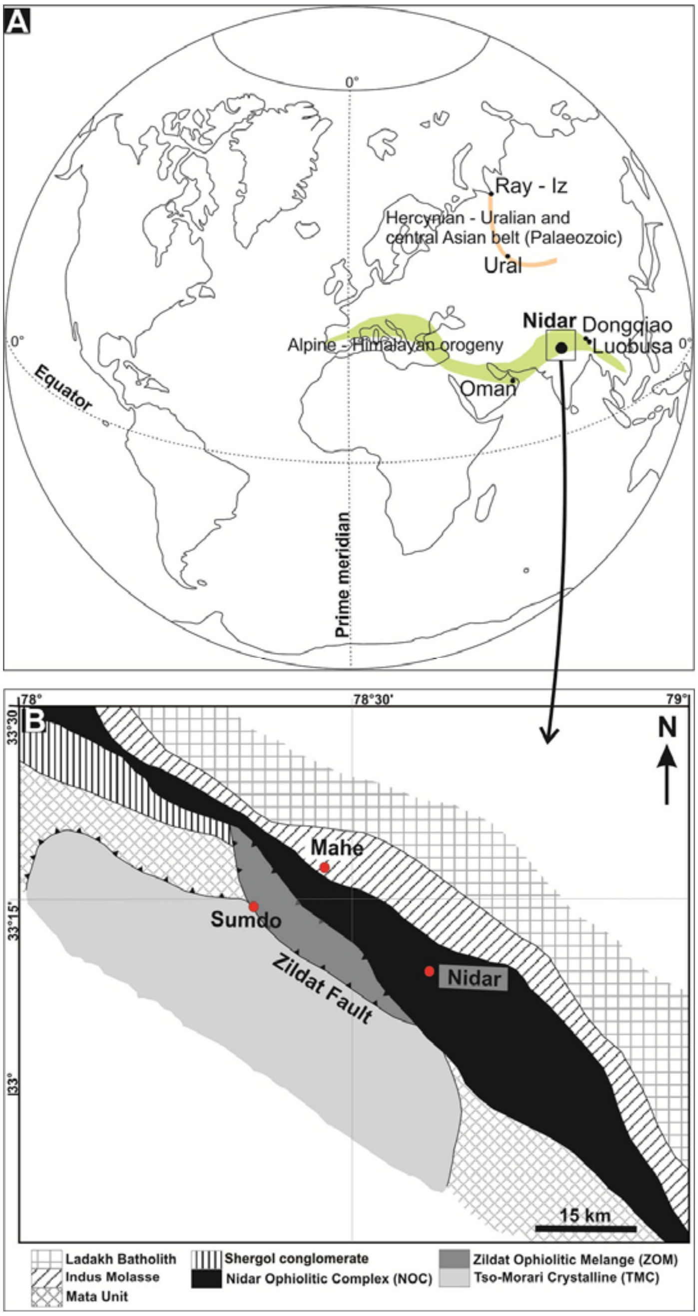

Fig.1.1.A. Ophiolites with high pressure mineral phase bearing podiform chromitites are marked with simple bullet. The locations of the ophiolites along the respective orogenic belts are shown. The study area (Nidar ophiolite) has been marked. B. Simplified geological map of the study area showing part of Indus Suture Zone, NW Himalaya (modified after Thakur and Misra 1984).

It is also strongly believed that nature of different discontinuities depend on intrinsic properties of the minerals. But those mineral phases are rare in the nature. If the primary goal of the study is achieved this area may emerged as potential sites to study the seismic discontinuities in deep Earth.

Apart from the main aim of the study the role of mantle dynamics to build an orogeny is also examined. It is believed that orogenic processes are essentially restricted within the crustal scale. But in any orogenic belt in the planet Earth mantle rocks or ophiolites are observed in suture zones or zone of convergence of two lithospheric plates. In this study an attempt has been made to examine the role of mantle processes in an orogeny.

Volatiles play important roles in mantle processes. From fluid inclusion study and sometimes hydrated minerals in mantle rocks bear important information about the interior of the deep Earth. It is also an aim of the present study is to constrain the role of volatiles in mantle processes.

The broad objectives are summarised below:

- The main objective of the present research is to investigate the root of ophiolite origin.

- Examine the role of mantle processes in mountain building process.

- To sample the volatile phases which bear valuable information about the environment of Earth interior.

- Sample the mineral phase transitions indicating different discontinuities in the deep Earth.

1.8 SELECTION OF THE STUDY AREA: NIDAR OPHIOLITE (ISZ, HIMALAYA)

Himalaya is considered as classic analogue of orogenic process in planet Earth. Keeping that in mind, the Himalayan ophiolites are chosen for the present study. It is a unique opportunity to study the relations between orogeny and ophiolite. Besides, the mantle section of the ophiolites can be targeted for the present research problem.

Among the Himalayan ophiolites in India Nidar ophiolite is the best exposed ophiolite section. Localized along the Indus suture zone (ISZ), Nidar ophiolite and associated Zildat mélange witness the closure of an ocean domain (Tethys) during India-Asia convergence. Earlier workers have mentioned that the Nidar area preserve thickest ophiolite section (Fig. 1.1 B) in Himalaya (Thakur and Bhat 1983). For this the present study was designed on Nidar ophiolite.

1.9 OVERVIEW OF THE RESEARCH APPROACH

Ophiolites retain huge variations in mineralogy. It was a daunting task to find out their depth of origin. For that in situ petrological approach was taken. Generally serpentinization, deformation and metamorphic recrystallization modify whole rock compositions of ultramafic rocks. Hence they cannot be used straight forwardly to assess actual mantle compositions. For this, to search primary signature of ophiolites in situ textural and mineralogical studies are carried out. Firstly from field occurrence the primary rocks are sorted for detail study. Then on the basis of hand specimen, petrography and mineral chemistry the primary signatures are identified. For petrography optical microscopes and secondary electron microscopes were used. For mineral chemistry electron probe micro analyser and energy dispersive X ray are used. Laser Raman spectroscope and X ray diffraction techniques are used to characterize incipient to major mineral phase identification.

1.10 THESIS OUTLINE

The thesis has been outlined as written below:

Chapter 1. Introduction

Statement of the thesis, Definition of the problem, What is Ophiolite, Importance of the Ophiolite Study, Basic concepts regarding ophiolite, Broad objectives, Selection of the study area: Nidar ophiolite (ISZ, Himalaya), Overview of the research approach, Thesis outline.

Chapter 2. Regional setting and geology of the study area

Chapter overview, The Himalaya, Indus Suture Zone and ophiolites, Geology of the Nidar Ophiolite, Crustal part with Moho transition zone, Basal part.

Chapter 3. Methods and analytical techniques

Introduction: overview of research approach, Field geology and sample strategy, Petrography, Sample preparation, Optical Microscope, Scanning electron Microscope, Mineral Chemistry, Energy Dispersive X Ray attached with SEM, Electron Probe Micro Analysis, Solid and fluid phase characterization, X Ray Diffractometer, Laser Raman Spectroscope.

Chapter 4. Mineralogical characterization of Ophiolite ultramafics

Chapter overview, Lithological description, Petrography, Mineral chemistry, Mineral phase characterization, Mineralogical evolution of ultramafic part, Significance of the findings.

Chapter 5. Micro textures and Volatile phases

Chapter overview, Lithological description of the studied rocks, Characterization of exsolution micro textures, Characterization of micro inclusions, Volatile phases, Evolution of micro textures and volatile phases.

Chapter 6. Discussion and model reconstruction

Chapter overview, Research summary, Major contributions from the present study, Scope of the future work.

Bibliography

Appendix

CHAPTER 2

REGIONAL SETTING AND GEOLOGY OF THE STUDY AREA

CHAPTER 2

REGIONAL SETTING AND GEOLOGY OF THE STUDY AREA

2.1 CHAPTER OVERVIEW

The chapter “2” describes the geological setting of the north western part of the Indian Himalaya. A major part of this research involve construction of stratigraphy and distribution of rocks types. The Himalaya is considered as classical site of an orogenic belt and it is store house of all types of rock unit. To sample mantle rocks Himalayan ophiolites are chosen as the study case. The principal research focus was to assess the root of mantle upwelling in a spreading center and find the role of mantle in an orogenic process. In view of this the ophiolites along the Himalayan suture zone are chosen as best suitable study area. It is well known that among Himalayan ophiolites Nidar area display the best exposed ophiolite suite (Thahur and Mishra 1984). So focus has been made on basal part of the Nidar ophiolite suite. In this chapter the geological details of the Himalaya and ISZ are discussed. It also include the details of Nidar ophiolite suite and Pseudostratigraphic reconstruction.

2.2 THE HIMALAYA

The Himalaya – (Him + alaya) means “abodes of snow” is the highest, longest mountain chain on the continent of the planet Earth. It bear most number of peaks of 8000 meters and above among all mountain belts in globe. Long Himalayan mountain chain spread over 2400 km bounded between eastern and western syntaxis which are Namche Barwa and Nanga Parbat respectively. It varies in width around 200 - 300 km along its length. The mountain range is arc-shaped, convex southwards with two syntaxial bends at the western and eastern ends (Valdiya 1980). The whole mountain belt is divided into more or less parallel five major domains from south to north: Sub - Himalaya (Lower Tertiary and Siwalik), Lower Himalaya (Lesser Himalaya), Higher Himalaya (Central Crystalline), Tethyan Himalaya and Trans Himalaya (Fig 2.1 B) (Gansser, 1964; Le fort, 1975). The north dipping Main Himalayan Thrust (MHT) is considered to be the main basal detachment fault (Zhao et al., 1993; Sharma, 1998). It is proposed that entire sequences from N-S are marked by fault planes that are progressively young towards south. The south Tibetan Detachment System (STDS), a syn orogenic extensional shear zone separates Tethyan Himalaya from Trans Himalaya. The Main Central Thrust (MCT, northernmost) separating the medium grade crystalline rocks of Higher Himalaya from the meta-sedimentary packages of the Lesser Himalaya; the Main Boundary Thrust (MBT) separates the Lesser Himalayan domain from the Sub Himalayan Lower Tertiary and Siwalik, the Siwalik thrusts over Ganga alluvium along Himalayan Frontal Thrust (HFT).

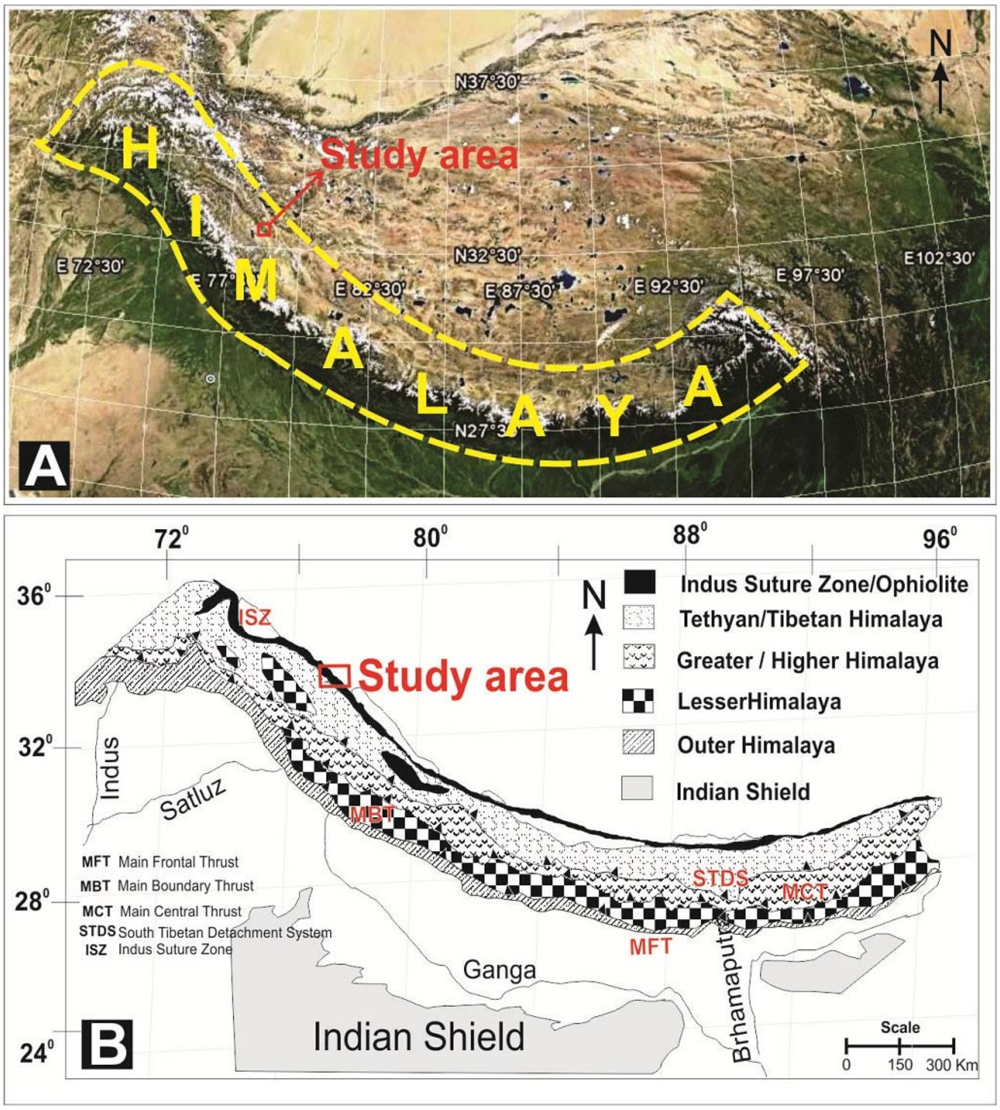

Fig. 2.1. (A) The entire Himalayan range is marked in a google Earth image. (B) Generalized geological map of Himalaya with its major subdivisions. In both the figure study area has been marked (Gansser 1964).

The rising of the Himalaya has led to flexural down warping of the under-thrusting Indian plate that lodged the sediments derived from the Himalayas, forming the world’s largest terrestrial foreland basin named as Himalayan Foreland Basin (HFB). The MCT, MBT and HFT are considered to be the imbrications of MHT. The evolution of Himalayan fold and thrust belt was mainly explained through crustal shortening (DeMets et al., 1994; Bilham et al., 1997; Larson et al., 1999; Lave and Avouac, 2000; Mugnier et al., 2003). This contraction in the northern Indian margin is accommodated by the early mentioned south - verging thrust faults, which separate the Proterozoic to Paleocene sedimentary cover (Gansser, 1964; Powell and Conaghan, 1973; LeFort, 1975; Mattauer, 1986; Hauck et al., 1998; Hodges, 2000; DeCelles et al., 2002; Murphy and Yin, 2003; Yin, 2006). To construct this geometry a critical taper model for the evolution of Himalaya was suggested (Henry et al., 1997). But it was unable to explain the presence of deep crustal rocks and inverted metamorphism from base to the top in Higher Himalayan Crystalline or MCT zone. The upward increase in metamorphic grade from lower level to upper level is noticed in different regions of Himalaya (Mallet, 1875; Heim and Gansser, 1939; Lefort, 1975; Arita, 1983; Pecher, 1989; Hubbard, 1989; Mohan et al., 1989; Jain and Manickavasagam, 1993; MacFarlane, 1995; Vannay and Grasemann, 2001; Harrison et al., 1997; Sakai et al., 1999; Stephenson et al., 2000; Searle et al., 2003). To explain the inversion of metamorphic isograds and exhumation of Higher Himalayan Crystalline an alternative channel flow model has been proposed (referring couette flow of fluids creating parabolic profile of particle movement) and implied in various sections of Himalaya (Nelson et al., 1996; Wu et al., 1998; Hodges et al., 1996; Grujic et al., 1996; Beaumont et al., 2001; Vannay and Grasemann, 2001; White et al., 2002; Grujic et al., 2002, 2006; Searle, et al., 2003; Harrison, 2006; Hodges, 2006; Yin, 2006; Robinson et al., 2006). Tectonic evolution of Himalayan fold thrust belt is believed to be formed by cenozoic India – Asia collision which largely control the Himlayan metamorphism and deformation (Dewey and Bird, 1970; Patriat and Achache, 1984; Searle et al., 1987; Molnar, 1988; Dewey et al., 1989; Le Pichon et al., 1992; Hallet and Molnar, 2001; Clark et al., 2004). Dynamic evolution of Himalayan orogen can be best studied at northern margin of Himalayan collision zone called Indus Suture Zone. The geology of the Indus Suture Zone (ISZ) will be discussed in detail in following part.

2.3 INDUS SUTURE ZONE AND OPHIOLITES

The Himalaya is the most classical analogue of a linear mountain belt formed as a consequence of continent-continent collision between India and Eurasia. The collision is witnessed by Indus Suture Zone (ISZ), the principle unit of Trans Himalaya. ISZ is discontinuously extended for nearly 2500 Km from Pakistan in the west to Lhasa block, S Tibet in the east. The Indus Suture Zone (ISZ) is a tectonic boundary represents suturing between India and Asia. It exists across the northern margin of Himalaya. The Indus Suture Zone is delineated mainly on the basis of presence of ophiolites and ophiolitic melanges in a linear and discontinuous manner. In Ladakh, (NW Himalaya, India) which is our study area, the ISZ lies between Tethys Himalaya to the south and Karakoram zone to the north (Fig. 2.1). The northern most part of the Ladakh Himalaya area is occupied by calc alkaline Ladakh batholith. The batholith has been developed between 110 – 50 Ma on the Asian continental margin during northward subduction of Neo Tethys and the Indian continent (Honegger et al., 1982; Weinberg et al., 2000). The batholith formation ceased as a consequence of end of collisional process between India and Eurasia. To the south of the Ladakh batholith Indus Molasse unit is present which is composed of clastic sediments. To the south of the Indus Molasse ophiolite suites are intermittently traceable along the whole stretch of Indus Suture Zone (ISZ). Some places patchy exposures of ophiolite melanges are present just to the south of the ophiolite suite. In places the ophiolites and some places melanges terminate at the gneissic core complex. The biggest core complex along Indus suture zone is Tso Morari Complex which bears meta basic boudins enveloped by gneisses. This unit bears relicts of eclogite facies metamorphism within those meta basics which represent subducted Indian continental margin around 55 Ma (Guillot et al., 1997; de Sigoyer et al., 2000). The eclogites experienced ultra high pressure metamorphism (Mukherjee and Sachan 2001; Mukherjee et al., 2003) around 53 Ma (Leech et al., 2005).

The Ladakh – Zanskar area exhibits two groups of ophiolitic units and associated ophiolitic mélanges: the ophiolite directly north of the ISZ and the South Ladakh ophiolites. The first group is represented by the Dras ophiolite, localized southwest of the Ladakh batholith. This ophiolite is formed during the subduction of the Indian plate beneath the oceanic margin of the Asian plate. It is developed as an arc characterized by three calc-alkaline volcanic suites set on oceanic crust (Dietrich et al., 1983; Reuber, 1989) and crosscut by granodioritic plutons between 103 and 70 Ma (Honegger et al., 1982). South of the Dras arc, the Nindam flysch corresponds to a fore-arc area filled with thick volcano sedimentary deposits (Clift et al., 2000). The Nindam flysch locally overthrusts the Sapi–Shergol ophiolitic me´lange, classically interpreted as an Accretionary prism related to the Dras arc (Cannat and Mascle, 1990).

The second group is constituted by three ophiolites and associated ophiolitic me´lange, the Spontang, Nidar and Karzog ophiolites (Mahe´o et al., 2000). The crustal part of these ophiolites has MORB affinities and originated at a mid ocean ridge (Corfield et al., 2001; Pedersen et al., 2001). The Spongtang ophiolitic melange was formed in an intra-oceanic supra subduction zone (Corfield et al., 2001; Pedersen et al., 2001). The origin of mantle units is still poorly known.

Few data have been published concerning the age of the Spontang ophiolite. Reuber et al. (1989) obtained K–Ar ages of 170 and 125–140 Ma on hydrothermal hornblendes, inferred to correspond to oceanic accretion and intra-oceanic thrusting, respectively. More recently, Pedersen et al. (2001) proposed an age of 177 Ma for oceanic accretion, based on U–Pb dating on zircon from plagiogranites sampled in the crust unit. They also proposed a minimum age of 88 Ma for the formation of the volcano-sedimentary unit, within a supra-subduction zone setting (U–Pb on zircon from dacite of the Spong arc). The Spontang ophiolite is thrust over the Spontang me´lange, which consists in two alkaline magmatic units, of Permo-Triassic and Albian ages (Reuber et al.,1987; Corfield et al., 1999). The Karzog ophiolite is located south of the Tso Morari dome within the core of a synform of Permian sediments. The Karzog ophiolite mainly consists of chromitites, serpentinites and minor gabbros which are highly deformed and altered. Because of the abundant chromitites, the Karzog ophiolite is considered as a part of transition zone between the crust and the mantle.

Among these ophiolite suites along ISZ Nidar area displays most complete ophiolite section having complete package of crustal and mantle part. The Nidar ophiolite extends along the ISZ and exhibits a complete cross section from the upper mantle to supra-ophiolitic sediments. Initially Nidar Ophiolite was considered as a typical section of oceanic crust comprised of ultramafics, gabbros, volcanic rocks and associated sediments from bottom to top of the section (Thakur and Virdi, 1979; Thakur, 1990). However, recent studies of the ultramafic rocks based on mineral chemistry data indicate that the Nidar ophiolitic rocks represent a remnant intra-oceanic island arc sequence rather than an oceanic floor sequence (Mahéo et al., 2000; Sachan, 2001). A boninitic parentage and hence suprasubduction setting origin was given by Ravikant (2004). Further Maheo (2004) proposed intra-oceanic tholeiitic arc origin for Nidar ophiolites. And the timing of intra oceanic subduction in the Neo - Tethyan Ocean is 140±32 Ma (Ahmed et al., 2008). Another available age for the formation of Nidar ophiolite is Cretaceous to Eocene based on radiolarians (Thakur and Virdi, 1979).

2.4 GEOLOGY OF THE NIDAR OPHIOLITE

The Nidar ophiolite is a well exposed ophiolite section, perhaps the best exposed ophiolite section in Indian subcontinent. The ophiolite section is named after the Nidar village (33^0 09′ 17″ N, 78^0 36′ 26.3″ E; 4232 m height). It represents the Indus Suture Zone (ISZ) in South-East Ladakh and lies exactly at the boundary between Indian plate and Asian plate (Fig. 2.3 A).

Nidar ophiolite is bounded by calc alkaline batholith and Indus molasse to the north. To south part of Indian plate consists of Tso Morari crystalline (gneissic rocks with metabasic enclaves) bounded by Mata unit (containing continent margin sedimentary rocks). Between the Nidar ophiolite and Tso Morari crystalline rocks discontinuous patch of Zildat melange is present (Sen et al 2013). The Nidar ophiolite appears as regional scale "eye" shaped in plan view (Fig.2.3.A). For this it has variation in thickness (Mahe – Sumdo section 3 Km; Nidar valley 10 Km) across its trend (NW – SE). The exposures of the Nidar ophiolite can be approached through two valleys (Fig 2.2 A) – (1) Mahe – Sumdo Valley & (2) Nidar Valley. Combining these two area a complete pseudostratigraphic section and geological map have first ever been prepared (Fig 2.3) for Nidar ophiolite. From these two sections total 134 samples are collected from 23 different rock bodies of the ophiolite suite. The Mahe – Sumdo valley and Nidar village can be approached by crossing Indus through bridge near Mahe and Nyoma respectively. The Mahe – Sumdo section is along a nala; the Nidar valley section is a glacier valley. The mineralogical details of the collected samples are given in Table 2.1.

2.4.1 CRUSTAL PART WITH MOHO TRANSITION ZONE

The crustal part of the Nidar ophiolite outcrops both in the Mahe - Sumdo Section and the Nidar ophiolite. The mapping was done in both the section to prepare a composite cross section.

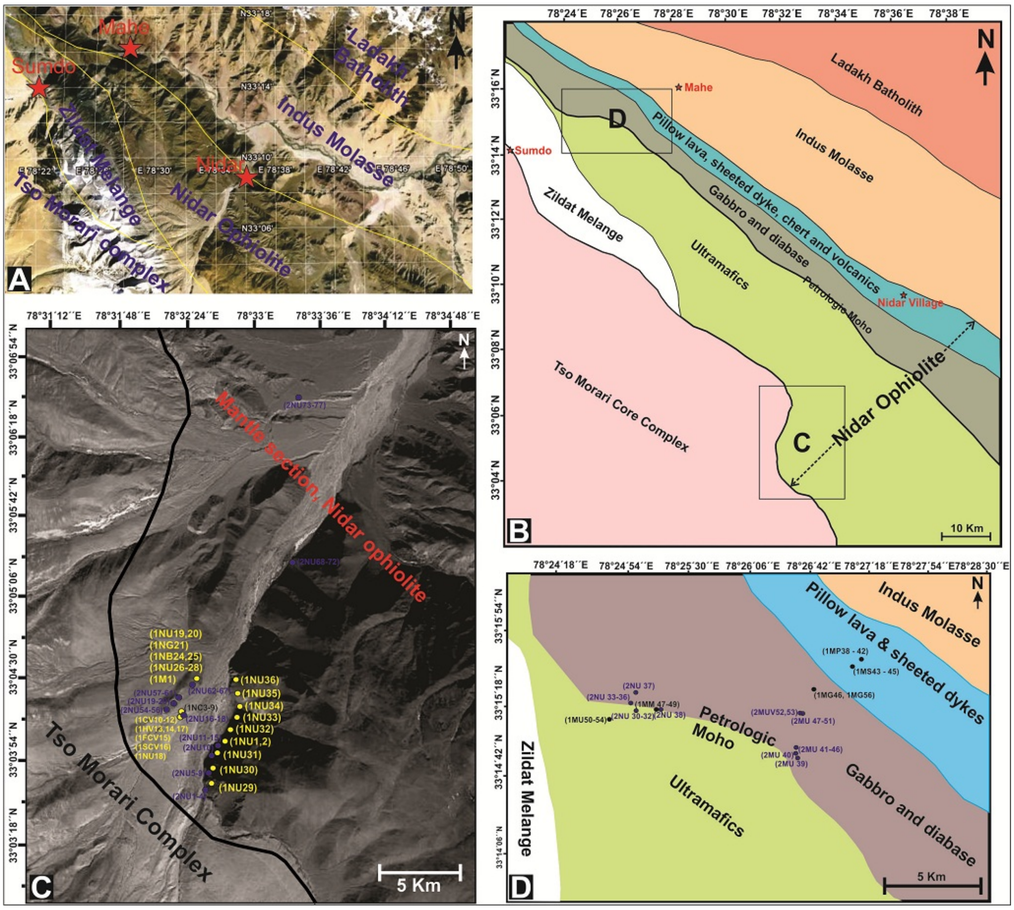

Fig. 2.2 (A) The Google Earth image of the enlarged study area shows Nidar ophiolite and the associated units. (B) Geological map of the study area. The boxes C and D indicate Mahe – Sumdo and Nidar Valley section respectively. In the next two photos the enlarged view of C and D are shown. (C) Sample distribution in mantle section of Nidar Valley. (D) Sample distribution in Mahe – Sumdo section.

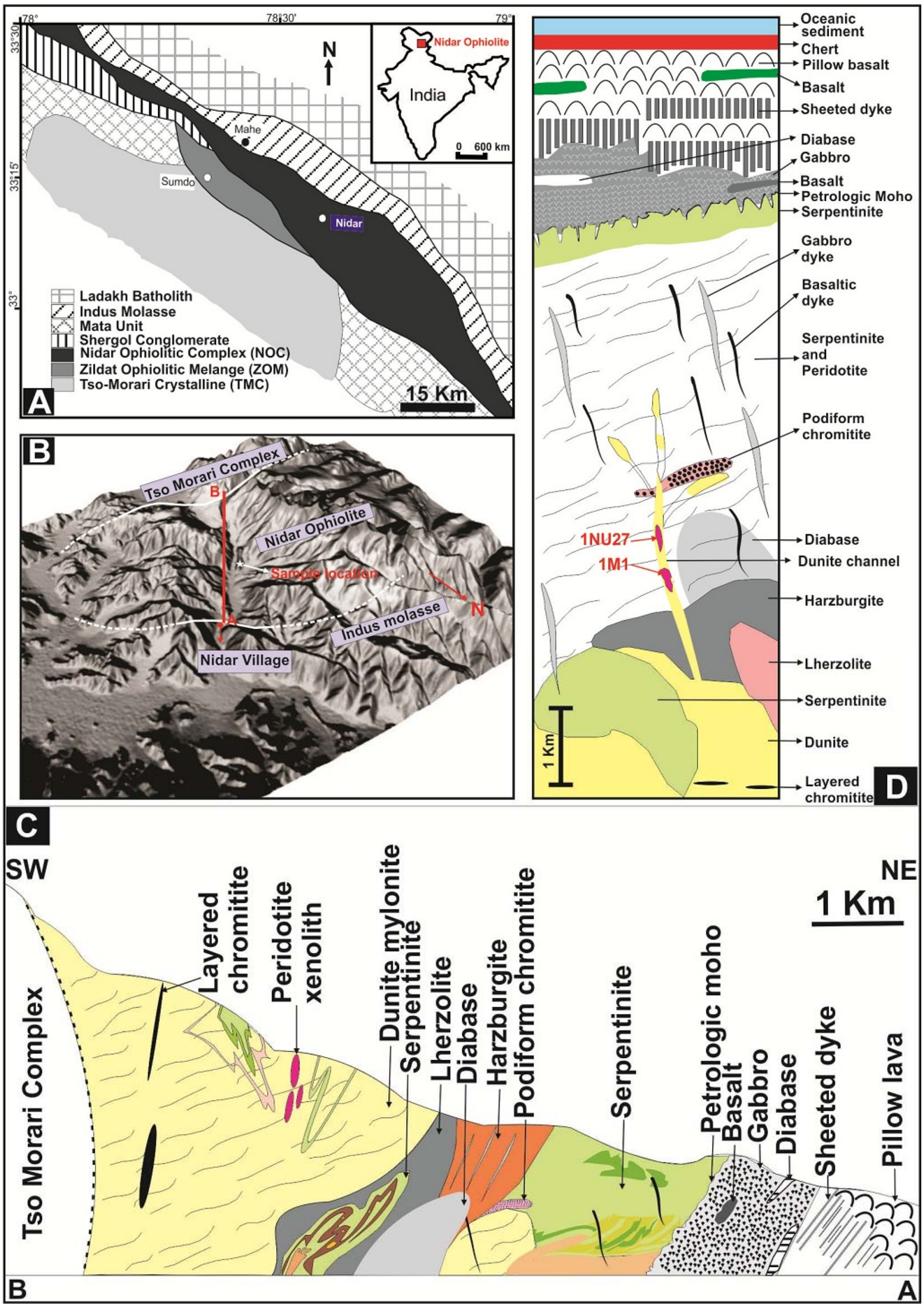

Fig. 2.3 (A) Geological map of the Nidar Ophiolite Complex (NOC) and associated units of the Indus Suture Zone (ISZ); inset shows outline of India with the location of NOC (after Thakur and Mishra 1984). (B) Digital elevation model of the NOC bounded by the surrounding geological units. A-B represents the traverse along Nidar valley for geological mapping of the ophiolite complex. (C) Cross-section of NOC along A – B showing the detailed litho - units of the ophiolite suite. (D) Pseudostratigraphic reconstruction of NOC based on our geological traverse.

But the detail sampling was possible mainly in the Mahe – Sumdo section because the crustal section is better preserved there and outcrops of the Mahe – Sumdo sections are easily approachable. The volcanics part of the crustal part of the Nidar ophiolite is composed of oceanic sediments, chert, basalt, pillow lava and sheeted dyke. To the south of Indus formation oceanic sediments and chert are first noticed as top part of ophiolite.

In Nidar valley section the thickness of chert and oceanic sediments (~ 150 m) are greater than in Mahe – Sumdo section (~ 20 m). Beneath the chert and sediments, pillow lava (thickness ~ 1 Km) a principal unit of ophiolite is present (Fig 2.3 D). The pillow lavas show characteristic interconnected lobate shaped structure. Pillow lavas are fine grained and bear vesicles of 1 – 4 mm diameter (Fig 2.4 E, F). The shape is attributed to extrusion in underwater condition preferably in sea floor. Next part is sheeted dyke complex which is connected to the pillow lava suite. The basic dykes are intruded into earlier dykes and create a sheeted dyke complex (thickness 300 – 500 m; Fig 2.4 C).

Within the sheeted dykes small scale normal faults are noticed which clearly indicate extensional feature (Fig 2.4 D). The formation of sheeted dyke complex through each injection of dykes, indicate repetitive extension. The process was proposed as analogous to the sea floor spreading (Gass 1968; Vine and Matthews 1963; Moores and Vine 1971). Beneath the sheeted dyke part 1 – 1.5 Km thick mafic cumulates are present. The mafic cumulate part is composed of layered gabbro, dolerite and basalt. In gabbro large crystals of plagioclases are observed.

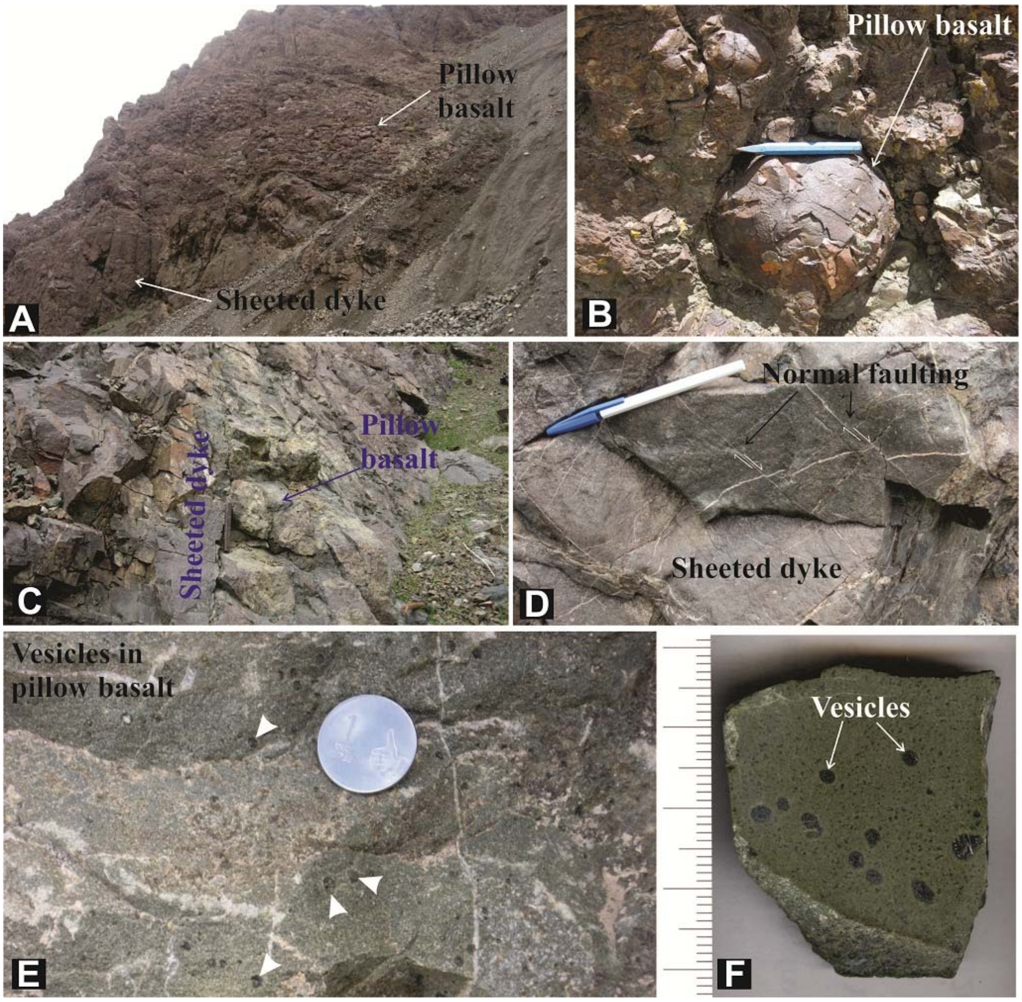

Fig.2.4 (A) A hillock of pillow lava and feeder sheeted dykes beneath it in Mahe - Sumdo section. (B) A single unit of pillow lava showing classical pillow structure. (C) Sheeted dyke intersects pillow lava. (D) Splays of normal faults are seen in sheeted dykes. (E), (F) Vesicles in pillow lava is shown in different magnifications.

Sometimes the sizes of plagioclase crystals are up to ~ 3 cm (Fig 2.5 B, D). At the bottom of the cumulate gabbro about ~ 300 m thick zigzag contact between gabbro and serpentinite is observed. The contact is characterized as Moho transition zone.

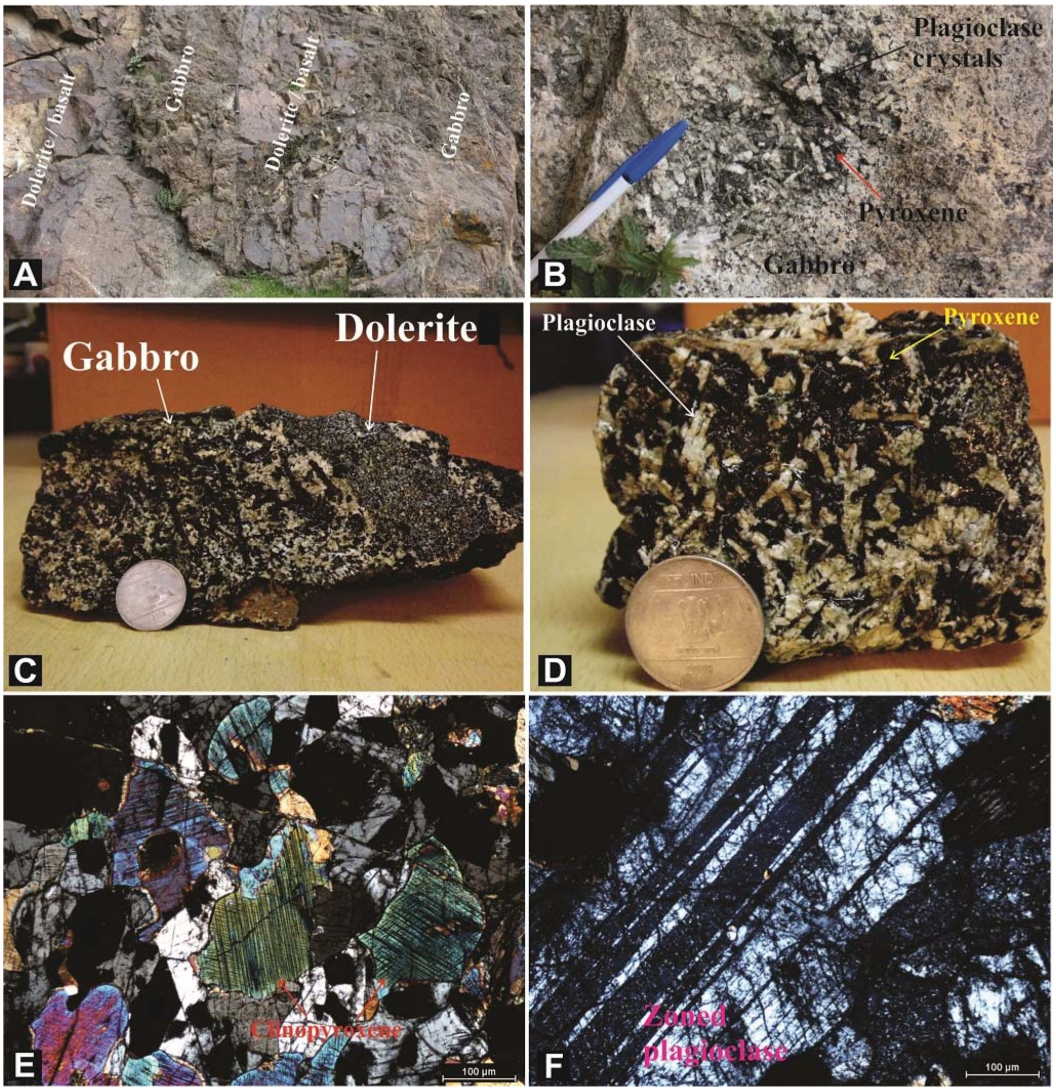

Fig. 2.5 (A) Mafic cumulate part shows layered gabbro and dolerite in Mahe – Sumdo section. (B) Large crystals of plagioclase in the gabbro of the mafic cumulate part. (C), (D) Hand specimen photos of the gabbros from crustal part of Nidar ophiolite. (E) Photomicrograph of diabasic rocks from Mahe – Sumdo section. (F) Zoning in plagioclase from crustal part of ophiolite.

Fig.2.6 (A) The zigzag gabbro – serpentinites contact represents petrologic Moho section in Mahe – Sumdo valley. (B) The sharp contact between gabbro and serpentinites. (C) A photomicrograph of serpentinites shows a relict pyroxene within it.

The mantle section of the Nidar ophiolite lies beneath the Moho transition zone. The mantle section is poorly preserved in Mahe Sumdo valley. The mapping and sample collection of crustal part of the ophiolite has been done in Mahe – Sumdo section. Total 42 rock samples are collected from Mahe – Sumdo valley.

In the Mahe – Sumdo section between Nidar Ophiolite and Tso Morari complex (TMC) a ~ 3 Km thick Zildat ophiolitic melange is present. The melange has oppositely dipping faulted contact with the TMC and NOC. The melange rocks display typical conglomeratic texture. Melange contains dismembered blocks of volcanics, chert, metasediments, large carbonate blocks (100 m size) and clasts of ophiolites. Structurally the blocks in melange are arranged in block in matrix fashion. The Zildat ophiolitic melange terminates at the Tso Morari crystalline and their boundary is marked by a fault which is named as Zildat fault.

2.4.2 BASAL PART

The mantle section of Nidar ophiolite is well preserved in Nidar valley. Detail mapping in Nidar valley suggest that Nidar ophiolite suite have the largest ultramafic section (~7 Km thick; spread over spread over ~ 7 x 3 Km^2 in Nidar valley section; Fig 2.3 D). In Nidar valley the ultramafic part of ophiolite suite has a direct contact with the Tso Morari core complex in the south. The bottom of the mantle section is occupied by a dunite body (~ 3 Km thick; Fig 2.3 D), concordant with the trend (NW – SE) of the ISZ (Fig 2.7). This dunite body is essentially composed of olivine along with sporadic spinel and serpentine mesh. A meter thick chromitite layer is seen concordant to the dunite body whereas parallel thin layers of chromitite are also noticed. Chromites are also present as disseminated crystals (~ 6 %) within the dunites. Many small randomly oriented pyroxenite layers (4 – 6 cm wide) within the dunite are noticed (Fig 2.8 B). Some channelized discordant network (~ 5 Km long, 100 – 200 m wide; trending NE – SW) with same lithology (olivine +

disseminated chromitite) emerged from the basal dunite which crosscut the entire ultramafic body which consists of lherzolite and harzburgites (Fig 2.7A, D). The upper part of basal dunite and the channelized dunite exhibit mylonite structures (Fig 2.7 B), this illustrates strain localization on multiple scales associated with the channelized melt flow.

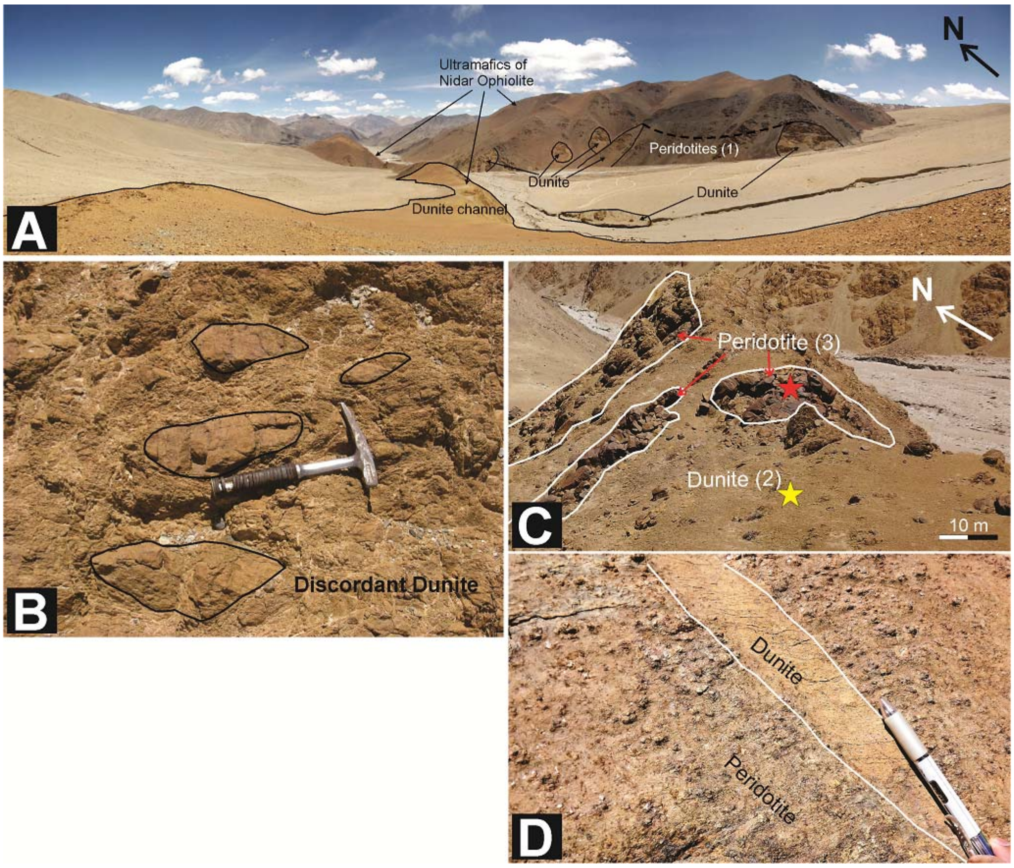

Fig.2.7 (A) Field photographs of lowermost ultramafic rocks of Nidar Ophiolite. Some channelized discordant dunites originate from the base. (B) In places the discordant dunites show mylonite structure trending NE - SW. Coarse elliptical portions of the dunite mylonite are noticed along the channel. (C) The peridotite xenoliths are trapped in dunite flow. (D) The photograph shows that dunite intruded as secondary injection in an early formed peridotite body.

There are some 10 – 30 m wide peridotite bodies which are enveloped by dunite and occur as xenolith within channel (Fig 2.7 C). Broadly the ultramafic rocks of Nidar ophiolite can be classified in three groups (Fig 2.7 A, C) – (1) The peridotites which are cut by the discordant dunite (2) The discordant dunite and its basal part with layered chromitite (3) The peridotite bodies which occur as xenoliths in dunite channel. With the group (1) peridotites some medium grained diabasic channels are also encountered which cross cut the ophiolite ultramafics. The diabasic rocks are also noticed as broad rock bodies within the ultramafic part of the Nidar ophiolite. But grain sizes of these rocks are finer with respect to the diabasic rocks of the mafic cumulate part in the crustal part of ophiolite.

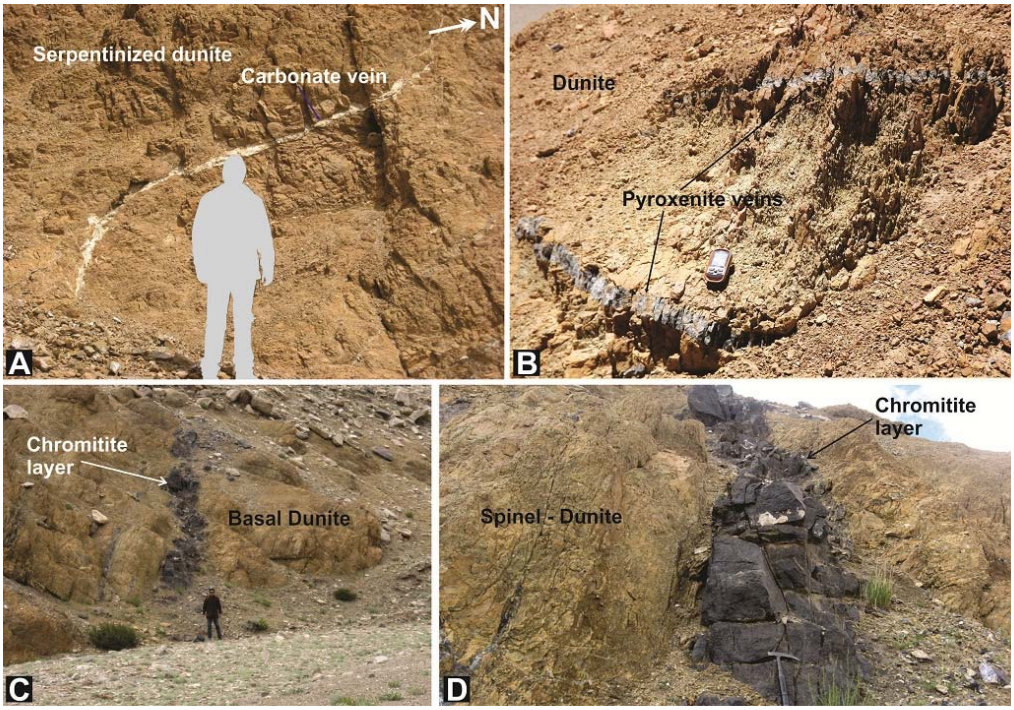

Fig. 2.8 (A) A white colour carbonate vein crosscut the serpentinized dunite in Nidar valley section. (B) Pyroxenite veins intruded within the basal dunite, Nidar valley. (C) & (D). A chromitite layer shown in different magnifications within basal dunite part, Nidar valley.

The serpentinization phenomena are prominent in all the ultramafics especially the dunites having typical mesh texture. Numerous randomly oriented massive dull network of carbonate veins (<1 cm – 10 cm wide) are seen in dunite bodies (Fig 2.8 A). The carbonates are also occurring in patches on dunite, apart from their occurrence along veins. The associated peridotites and harzburgite are much less affected by this carbonation. But in serpentinites, the complex networks of carbonate veins are present. Total 88 rock samples are collected from the Nidar valley for present study (Table 2.1). According to our research focus we study in detail the primitive part of the ophiolite.

Table 2.1. Mineralogical details of the collected rocks samples from Nidar Ophiolite suite is given below:

Rock	**Sample**	**Mineralogy**
Diabase	**1NU1 - 2**	$\mathbf{Cpx_{25}Pl_{45}Srp_{8}Amp_{20}Cb_{2}}$
Chromitite	**1NC3 - 9**	$\mathbf{Chr_{98}Srp_{2}}$
Carbonate	**1CV10 - 12**	$\mathbf{Cb_{90}Srp_{10}}$
Dunite	**1HV13 - 14**	$\mathbf{Ol_{70}Chr_{5}Srp_{20}Cb_{5}}$
Carbonate	**1FCV15**	$\mathbf{Cb_{90}Srp_{10}}$
Carbonate	**1SCV16**	$\mathbf{Cb_{90}Srp_{10}}$
Dunite	**1HV17**	$\mathbf{Ol_{65\text{-}70}Chr_{5}Srp_{20\text{-}25}Cb_{5}}$
Dunite	**1NU18**	$\mathbf{Ol_{80\text{-}85}Chr_{5}Srp_{10\text{-}15}}$
Harzburgite	**1NU19**	$\mathbf{Ol_{60}Opx_{18}Chr_{2}Srp_{20}}$
Lherzolite	**1M1**	$\mathbf{Ol_{40}Opx_{25}Cpx_{15}Chr_{2}Srp_{18}}$
Harzburgite	**1NU20**	$\mathbf{Ol_{60}Opx_{15}Chr_{5}Srp_{20}}$
Serpentinized peridotite	**1NU21**	$\mathbf{Ol_{30}Opx_{8}Cpx_{5}Chr_{2}Srp_{55}}$
Serpentinite	**1NU22**	$\mathbf{Srp_{90}Opq_{10}}$
Serpentinite	**1NU26**	$\mathbf{Ol_{5}Srp_{95}}$
Lherzolite	**1NU27**	$\mathbf{Ol_{50}Opx_{25}Cpx_{15}Chr_{5}Srp_{5}}$
Serpentinized Peridotite	**1NU28**	$\mathbf{Ol_{40}Opx_{20}Cpx_{5}Chr_{5}Srp_{30}}$
Harzburgite	**1NU29**	$\mathbf{Ol_{55}Opx_{35}Chr_{5}Srp_{5}}$

Diabase	1NU30 - 32	$Cpx_{20}Pl_{40}Srp_{5}Amp_{20}Opq_{15}$
Serpentinite	1NU33	$Ol_{20}Srp_{60}Opq_{20}$
Lherzolite	3	$Ol_{40}Opx_{20}Cpx_{17}Chr_{3}Srp_{20}$
Lherzolite	4	$Ol_{40}Opx_{20}Cpx_{17}Chr_{3}Srp_{20}$
Dunite	1NU33	$Ol_{75}Chr_{5}Srp_{20}$
Podiform Chromitite	1NU34	$Ol_{20\text{-}25}Chr_{70\text{-}75}Srp_{5}$
Serpentinite	1NB35	$Ol_{10}Srp_{80}Opq_{10}$
Dunite	1NU36	$Ol_{85}Chr_{5}Srp_{10}$
Anorthite bearing Diabase	SNU1	$Cpx_{30}Pl_{50}Srp_{10}Amp_{10}$
Serpentinized Diabase	1MM47 - 49	$Opx_{5}Cpx_{15}Pl_{25}Srp_{50}Cb_{5}$
Serpentinite	1, 2	Srp_{100}
Diabase	1MU50 - 53	$Cpx_{25}Pl_{45}Srp_{30}$
Pyroxenite	SNU31 - 36	$Opx_{50}Cpx_{45}Srp_{5}$
Lherzolite	N 018	$Ol_{40}Opx_{10}Cpx_{15}Pl_{20}Chr_{5}Srp_{10}$
Gabbro	N P 10	$Cpx_{40}Pl_{50}Srp_{10}$
Harzburgite	2NU8	$Ol_{45}Opx_{15}Cpx_{5}Chr_{5}Srp_{30}$
Harzburgite	2NU10	$Ol_{45}Opx_{15}Cpx_{5}Chr_{5}Srp_{30}$
Serpentinite	2MU40	Srp_{100}
Harzburgite	2NU61	$Ol_{45}Opx_{20}Cpx_{5}Chr_{2}Srp_{28}$
Serpentinite	2NU63	$Srp_{90}Px_{10}$
Lherzolite	2NU65	$Ol_{50}Opx_{25}Cpx_{15}Chr_{5}Srp_{5}$
Garnet Serpentinite	2NU66	$Opx_{5}Cpx_{15}Pl_{10}Srp_{40}Amp_{10}Grt_{20}$
Serpentinized peridotite	2NU72	$Ol_{30}Opx_{15}Cpx_{5}Srp_{50}$
Listwanite	2NU76	$Srp_{30}Cb_{70}$
Serpentinized peridotite (Mahe)	MUN4	$Ol_{30}Opx_{20}Cpx_{10}Srp_{40}$

CHAPTER 3

METHODS AND ANALYTICAL TECHNOQUES

CHAPTER 3

METHODS AND ANALYTICAL TECHNIQUES

3.1 INTRODUCTION: OVEVIEW OF RESERACH APPROACH

The main objective of this chapter is to elaborate the various research strategy and analytical methods to construct complete research framework. The ophiolitic mantle rocks are generally strongly affected by hydrothermal alteration and cannot be used straight forwardly to determine the primitive signature. For that the whole rock geochemical approaches are avoided and the study is focused on in situ mineralogical approaches. Rock samples from ultramafic unit of Nidar Ophiolite are used for the present study. From the rock samples thin sections are prepared for optical investigation in transmitted and reflected light under Petrographic microscope. Detailed microscopy was done with the aid of Secondary Electron Microscope (SEM). Mineral chemistry was analyzed with Electron Probe Micro Analyser and EDX (attached with SEM). For identifications of solid and fluid phases Laser Raman spectroscopy was performed on thin rock wafers. For some cases XRD (X Ray Diffraction) was used on rock powders to identify different mineral phases. Present chapter contains details of the individual methods used in the thesis.

3.2 FIELD GEOLOGY AND SAMPLE STRATEGY

The studied ophiolite in Nidar and Mahe – Sumdo area spread over ~300 km^2 area in SE Ladakh. Perhaps this is the best exposed ophiolite suite in Indian subcontinent (~ 10 km thick). The ophiolite suite displays about ~ 7 Km thick mantle section in Nidar valley (SE Ladakh, Indian Himalaya). For this the ultramafic rocks of basal part of Nidar ophiolite has been used for the present study. Field work was carried out in whole ophiolite suite to understand the internal structure of ophiolite. Two traverses across the ophiolite suite were taken (Mahe – Sumdo and Nidar valley) to prepare the map and cross section of the ophiolite. Field work as carried completed in two phases - The first phase was for 20 days (July 22 – August 10 2010); the second phase of work was for 17 days (May 07 – May 23, 2012). Total 134 rock samples were collected from the 23 different rock bodies of the whole ophiolite suite, starting from the upper most pillow lava to the lower most dunite. In field, to determine the location “GARMIN 12XL” GPS system was used. The aid of 1: 50,000 scale toposheet map (no. 52 K/7) was taken at the time of mapping. Camera was used to take photographs. For structural relationship clinometer and brunton compasses are used. Detail hand specimen study was carried out with the aid of lens (magnifier). Fresh ultramafic rocks are hard to break with geological hammer. For that 5 pound hammer was used in sample collection. The collected samples are preserved with maximum care.

According to thesis objective only ultramafic rocks of mantle section are studied in detail. Among the ultramafic rocks the fresh (unaltered) primary rocks are targeted as the aim is to find out the primitive material of ophiolite. In the present research work 15 samples collected from 8 different ultramafic rock bodies are studied in detail. The primary rock bodies are selected based on their field occurrences, crosscutting relationships. To compare the mineralogy and mineral chemistry some crosscutting ultramafic rocks are also studied in detail along with the primary ultramafic rocks. To have an idea about the conditions of hydrothermal alteration serpentines are collected.

3.3 PETROGRAPHY

Petrography is an important part of in situ mineralogical and petrological studies. For mineralogical and textural details petrography is done on rocks. The petrographic studies were done on thin wafers. To have a general idea about the ophiolite suite at least 2 – 3 thin sections are prepared from each of the 23 rock types of Nidar ophiolite. For detail study more numbers of thin sections are prepared from ultramafic rocks. Details of sample preparations are given.

3.3.1 SAMPLE PREPARATION

The collected rocks have been cut to small pieces for the preparation of thin sections. All the thin sections are prepared in “High Precision Laboratory” of Wadia Institute of Himalayan Geology, Dehradun, India. For the cutting of the rocks to small pieces “BUEHLER Delta Petrocut GEOLOGICAL CUTTER” is used. After cutting them into small pieces the one side of the rock chips are grinded to make it smooth. Then the smooth side of the rock chips are mounted on glass slide. At the time of mounting the care is taken so that there any air bubble do not exists. For that the sections are kept in Petro Bond to keep the sample under pressure for at least 24 hours. This process makes more possibilities that there will not be any bubble. Keeping in mind that the thin section may be used for Electron Probe Micro Analyses (EPMA) most of the slides are mounted in EPMA sized slides and araldite is used as adhesive. Some thin sections are also prepared with the Canada balsam adhesive. The melting temperature of the araldite is higher than Canada balsam and at the time of EPM analyses greater than the melting temperature of Canada balsam is attained. For this at the time of EPMA analyses araldite mounted thin section is used. This care is taken for the safety of the instrument and acquires good quality data.

After 24 hours the sample is taken out of Petro Bond and further cut to lower its thickness using “BUEHLER PetroThin”. After cutting in the same instrument the grinder is used to minimize its thin section up to ~ 100 µm. Rest of the grinding is done with the aid of “BUEHLER GRINDER –

POLISHER & POWER HEAD” to make the thickness further to 40 – 80 μm. Lastly the thin sections are polished with Buehler Metadi fluid along with diamond suspensions of sizes ranges from 1 – 15 μm. Ultimate care was taken so that diamond cannot enter into the sample to influence the interpretation. Diamond is highly prone to be artefact. It may be plucked or introduced into a sample during processing (sawing, grinding). For that utmost care is taken. At the time of final polishing with 3 μm and 1 μm plates, diamond suspensions are not used and only Buehler Metadi fluid is used.

For EPMA and EDS chemical analyses on thin sections of rocks it is require to make the sample conductive so that efficient interaction between electron and sample is possible. To make the slides conductive they are carbon coated. The thin section must be flat, smooth and clean before coating. The coating was done using a carbon fibre in a Polaron CC7650 carbon coater in EPMA Laboratory, Wadia Institute of Himalayan Geology, Dehradun, India (Fig 3.1). The approximate thickness of the coating was ~ 10 nm. The pressure of vacuum was kept 2×10^{-2} Pa at the time of coating. After coating it was immediately carried to EPMA chamber with a silica gel bearing box so that moisture cannot contaminate the coated sample.

Fig.3.1. Polaron CC7650 Carbon coater in EPMA Lab, WIHG, Dehradun, India.

If it catches moisture it will be charged at the time of electron bombardment and the quality of analyses will be very poor. To remove the carbon coating acetone was used to rub the carbons from the thin section surface. To be sure about carbon coating removal 2 minute polish in BUEHLER POWER HEAD was done.

3.3.2 OPTICAL MICROSCOPE

The optical microscope is used to magnify small samples for its details. Optical microscope is such a system which uses visible light and a network of lenses to magnify small samples. The image from an optical microscope is captured by normal light-sensitive cameras to generate a micrograph. Earlier images were captured by photographic film but modern developments in charge-coupled device (CCD) cameras allow the capture of digital images. In the present research digital microscopes are used which use a CCD camera to examine a sample, showing the resulting image directly on an attached computer screen.

Fig.3.2. Optical microscope for petrography in Fluid Inclusion Lab, WIHG, Dehradun, India.

Optical microscopy was done on thin rock wafers in transmitted and reflected light with Nikon Eclipse LV 100 POL and Nikon Eclipse E600 POL microscopes in Wadia Institute of Himalayan Geology, Dehradun, India (Fig 3.2). Image analyses were done using NIS elements software. These microscopes are equipped with 100X short working distance lenses. The 100X lens was used at the time of small size solid and fluid inclusion petrography. For the present research 64 thin sections are examined and about 2000 photomicrographs are taken with the aid of the microscope.

3.3.3 SCANNING ELECTRON MICROSCOPE

Scanning Electron Microscope (SEM) is used to produce surface topographic images of a specimen in higher magnification. It is a type of electron microscope, in which the sample is bombarded with an electron beam and signals that come from the sample are collected to produce the image. From the surface topography images a rough estimate of composition of sample can be made. SEM is capable to achieve resolution better than 1 nanometer.

All the high resolution surface topographic images are captured in Wadia Institute of Himalayan Geology, Dehradun using a ZEISS EVO 40 model (Fig 3.3). The specimen for study is inserted to the high vacuum sample chamber.

The surface of the sample must be electrically conductive to prevent the accumulation of electrostatic charge at the surface which may produce poor quality of photographs. To make the sample conductive samples are coated by gold and carbon shower. Carbon coating and carbon tape is used in case of polished rock specimen mounted on glass slide. For the rock chip specimen gold coating is used. In all the cases 20 kV accelerating voltage is used. Probe current varies from 71 – 462 pA; but maximum images were captured with 102 pA probe current. The working distance at the time of imaging varied in a range 6.5 – 26 mm. Some instrument conditions (probe current, probe diameter and working distance) are adjusted with due time of analysis depending upon the type of sample and image quality. The images are captured with a wide range of magnification: 83X – 70000X. Total 178 images ultramafics, serpentinites and carbonates were captured with the aid of SEM. Some BSE images (2 photos) were also captured with the SEM attached with EPMA in 15 kV power.

3.4 MINERAL CHEMISTRY

For the in situ studies mineral chemistry is an essential proxy. To generate mineral chemical data EDS and EPMA was carried out. Details of them are discussed here.

3.4.1 ENERGY DISPERSIVE X RAY ATTACHED WITH SEM

Energy dispersive X ray spectroscopy (EDX) is an analytical technique used to determine the chemical composition of a sample. EDS allow identifying what are the particular elements present in a rock sample with their relative proportions (Atomic % for example). It has the ability to produce elemental mapping of selected area of sample. Low energy secondary electrons (in case of SEM), backscattered electrons and X-rays can be generated by primary electron bombardment. The intensity of backscattered electrons can be correlated to the atomic number of the element within the sampling volume.

Hence, some qualitative elemental information can be obtained. SEM, accompanied by X-ray analysis, is considered a relatively rapid, inexpensive, and basically non-destructive approach to surface analysis. It is often used to survey surface analytical problems before proceeding to techniques that are more surface-sensitive and specialized.

Fig. 3.3. SEM with EDS attachment in SEM Lab, WIHG, Dehradun, India.

EDS is being used for line scan, area scan and qualitative chemical composition of a selected area. In the present research SEM/EDS is used for rapid first hand chemical composition of mineral phases. Carbon coated polished rock slides are used for chemical analysis of minerals through SEM/EDS. All the analyses were carried out at WIHG, Dehradun using an EDX -Energy Dispersive X-ray Microanalyser - Bruker LN2 free X-Flash 4010 attached with a ZEISS EVO 40 SEM (Fig 3.3). 20 kV accelerating voltage is used with varying probe current, probe diameter working distance. Roughly 41 area scanning, 43 spots, 10 element mapping and 47 line scan were done by EDS.

But EDS gives a qualitative analysis. Because many elements have overlapping peaks (e.g., Ti K_{β} and V K_{α}, Mn K_{β} and Fe K_{α}) which do not allow to get good results as WDS (Wave length dispersive spectroscopy). Electron Probe Micro Analyzer (EPMA) has four WDS spectrometer and for each spectrometer different diffracting crystals are used. For this EPMA always gives better result.

3.4.2 ELECTRON PROBE MICRO ANALYSES

An Electron Micro Probe (EMP), also known as an Electron Probe Micro Analyser (EPMA) is an analytical tool used to non-destructively determine the chemical composition of small volumes of solid materials. The electron beam is applied on the polished surface of the target specimen cause the emission of characteristic X-rays (as the target atoms absorb and release energy). The X – Rays are then analyzed in a Wavelength Dispersive Spectrometer by a diffracting crystal that focuses each precise wavelength onto a detector, where it is counted. The concentration of each atomic element in the sample is calculated from the intensity of the characteristic X-rays, after making proper matrix corrections. Each atomic element emits specific and identical wavelength of X-rays. EPMA is used for qualitative analysis by which it is possible to detect the presence of elements in the portions of the target sample.

Semi - quantitative analysis through EPMA also can be done which involves the measuring of the intensity of X-ray generated form an unknown sample and compare with suitable standard using identical instrumental condition. EPMA is also capable for capturing SE and BSE imaging. EPMA is also capable to determine chemical or elemental mapping in two dimensions of selected area. EPMA can detect elements efficiently up to 1000 ppm.

Most of the EPMA data was acquired with a “CAMECA SX 100 Microprobe” in Wadia Institute of Himalayan Geology, Dehradun, India (Fig 3.4). The instrument is provided with a gun chamber with tungsten filament for the generation of electrons, a column with condenser and probe lens to de-magnify the electron beam. The vacuum in the EPMA chamber is kept 4×10^{-5} Pa. It is provided with 4 spectrometers (three vertical and one inclined with diffracting crystals like PET, TAP, LIF and some pseudo-crystals for the generation of good resolution X-rays, and a gas proportional counter to measure the intensities.

The standards used for element calibrations were apatite (P), wollastonite (Ca), chromite (Cr), rhodonite (Mn), almandine (Fe), jadeiite (Na), diopside (Mg), kyanite (Al), orthoclase (Si, K) and rutile (Ti). In four spectrometers different elements are selected for analyses – PET (P, Ca), LIF (Cr, Mn, Fe), TAP (Na, Mg, Al, Si) and PET (K, Ti). The instrument is operated using "Peak-Sight Software", which also helps to carry out its various applications.

The instrument is also provided with two rotary pumps, one diffusion pump and an ion pump to maintain good vacuum all along the path of electron beam.

Some EPM Analyses were also carried out by a “JEOL 8900 Microprobe” at Cornell Centre for Materials Research (CCMR), Cornell University, USA.

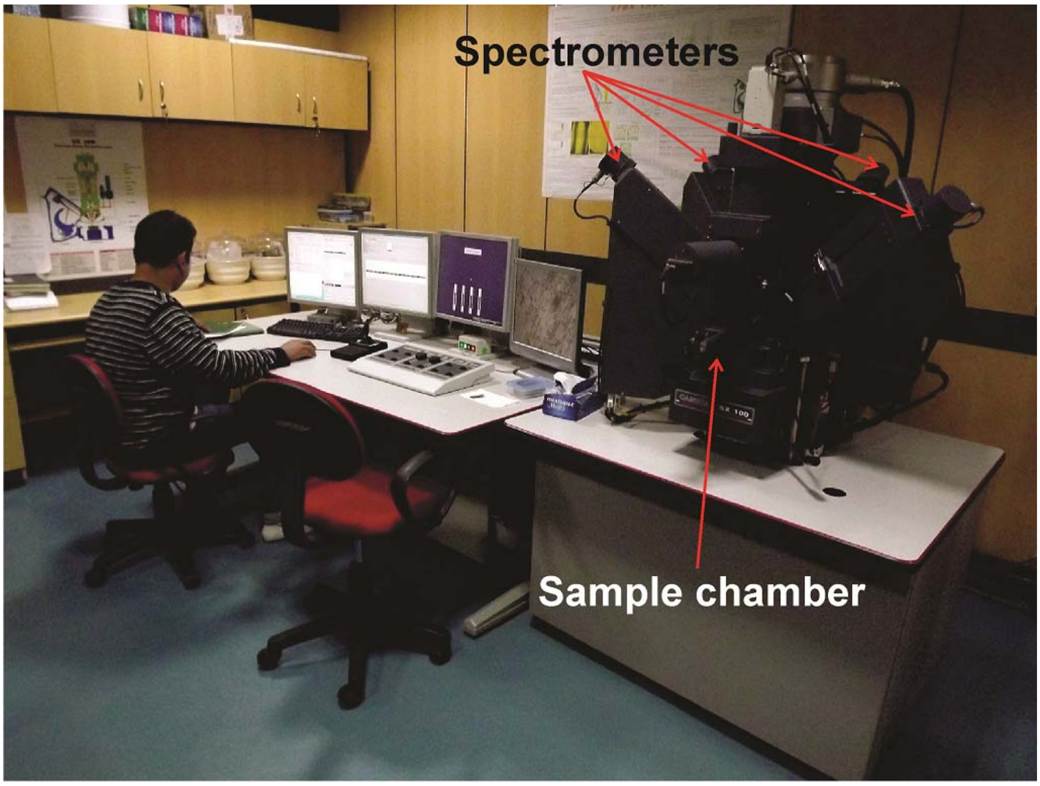

Fig 3.4. CAMECA SX 100 EPMA instrument in EPMA Lab, WIHG, Dehradun, India.

The qualitative and semi quantitative EPM analyses of ultramafic rocks of Nidar ophiolite were carried out on ~ 40 µm thick sections. At the time of analyses excitation voltage was 15 kV and beam current 20 nA. For analyses of alkalis (sodium and potassium) in pyroxenes 15 nA beam current was attempted. The counting times of each element were 10 – 20 s. The diameters of beam at the time of analyses were ~ 3 - 5 µm. The raw data were corrected using the ZAF method. Detection limits were ~ 0.1% and accuracy deviation was less than 5%. In case of ~ 1 - 2 µm thin intergrowth lamellae and some exsolution needles broad beam analyses were attempted and the data was compared with the host mineral. Some cases the experiment was successful to determine the composition of fine lamellas. Total 256 spot analyses were done by EPMA.

3.5 SOLID AND FLUID PHASE CHARATERIZATION

To characterize the solid and fluid phase X Ray Diffractometer (XRD) and Raman Spectroscope were used. XRD was done on rock powders to identify the constituting minerals. For that the rock sample was powdered in an agate mortar with care so that it cannot get contaminated. Raman Spectroscopy was carried out to characterize the micro textures, incipient solid phases and small sized fluid inclusions. Details of XRD and Raman Spectroscopy are discussed below.

3.5.1 X RAY DIFFRACTOMETER

The X-ray Diffraction is a popular technique for identification compounds and minerals. Electrons do not penetrate as deeply into matter as X-rays, hence electron diffraction reveals structure very efficiently. The interaction of X-rays with the spacing of atoms in crystals results in scattering by crystals in such a way that a diffraction grating scatters light. Discrete angles and intensities of scattering can be correlated with the geometric pattern of atoms within a crystal. Examination of the pattern and intensities of scattering from a sample are used to interpret its crystal structure and to identify the mineral or crystalline compound constituting the sample.

Fig 3.5. X-ray diffraction system in XRD Lab, WIHG, Dehradun, India.

The XRD technique is used to characterize the carbonates. The analyses were done using PANalytical, X'pert PRO X-ray diffraction system at Wadia Institute of Himalayan Geology, Dehradun, India (Fig 3.5) and at University of Rochester, Rochester, NY, USA. To obtain the XRD pattern $Cu_{K\alpha}$ excitation was used. At the time of analyses 45 kV power and 40 mA current was used. For data interpretation PANalytical data base was used. Total 8 samples were for XRD analyses.

3.5.2 LASER RAMAN SPECTROSCOPY

Raman spectroscopy is a spectroscopic technique based on inelastic scattering of monochromatic light, usually from a laser source. It is a light scattering technique, and can be thought of in its simplest form as a process where a photon of light interacts with a sample to produce scattered radiation of different wavelengths. Raman spectroscopy is extremely information rich, (useful for chemical identification, characterization of molecular structures, effects of bonding, environment and stress on a sample). The Raman Effect (Raman and Krishnan 1928) occurs when light impinges upon a molecule and interacts with the electron cloud and the bonds of that molecule. For the spontaneous Raman Effect, a photon excites the molecule from the ground state to a virtual energy state. When the molecule relaxes it emits a photon and it returns to a different rotational or vibrational state.

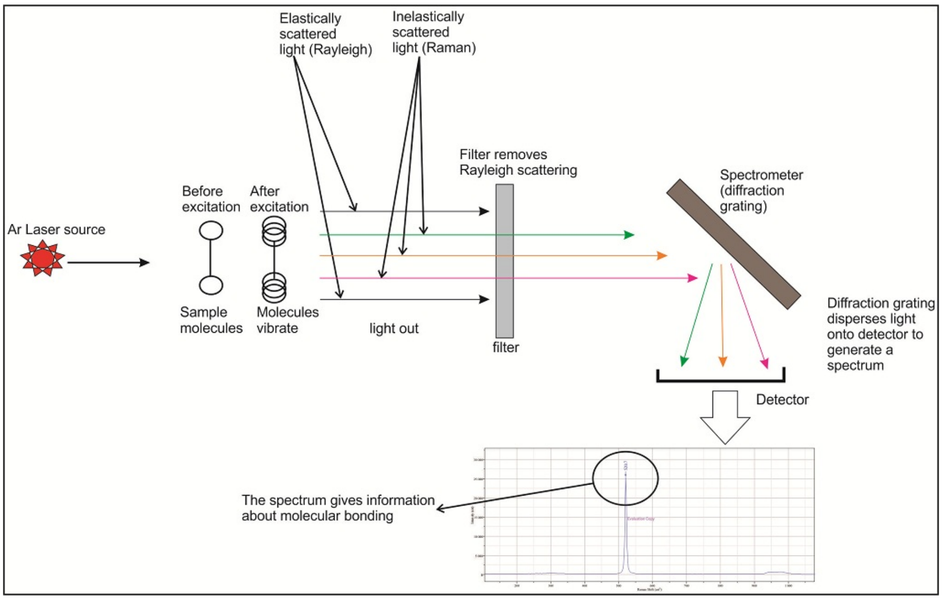

Fig 3.6. The working principle of Raman spectroscope is shown in a schematic diagram.

The difference in energy between the original state and this new state leads to a shift in the emitted photon's frequency away from the excitation wavelength.

A Raman spectroscope system (Fig 3.7) typically consists of four major components:

1. Excitation source (Laser)
2. Sample illumination system and light collection optics
3. Wavelength selector (Filter or Spectrophotometer)
4. Detector (Photodiode array, CCD or PMT)

Raman spectroscopy is a non destructive technique to characterize incipient solid and fluid phases. Importantly, the analyses can be done on very small sized samples.

Most of the Laser Raman spectroscopy was performed using a LabRAM HR - Horiba Jovin Yuvon Instrument at the Wadia Institute of Himalayan Geology, Dehra Dun (India) (Fig 3.7). All of the analyses were done on thin sections of the rock chips. Spectra were excited at room temperature with the 514.5 nm line of a green Ar Laser and detected by a Charged Couple Device (CCD) detector. At the time of analysis at least – 70^0C temperature was maintained for CCD. At the time of data generation OLYMPUS® 50X and 100X objective were used. The laser spot on the surface had a diameter of approximately 2 - 4 μm and a power of ~ 4 – 8 amp and 15 – 33 mW. The 514 laser has generally penetration limit up to 7.62 μm. At the time of analyses the Z axis has been changed to attain the perfect focus according to purpose.

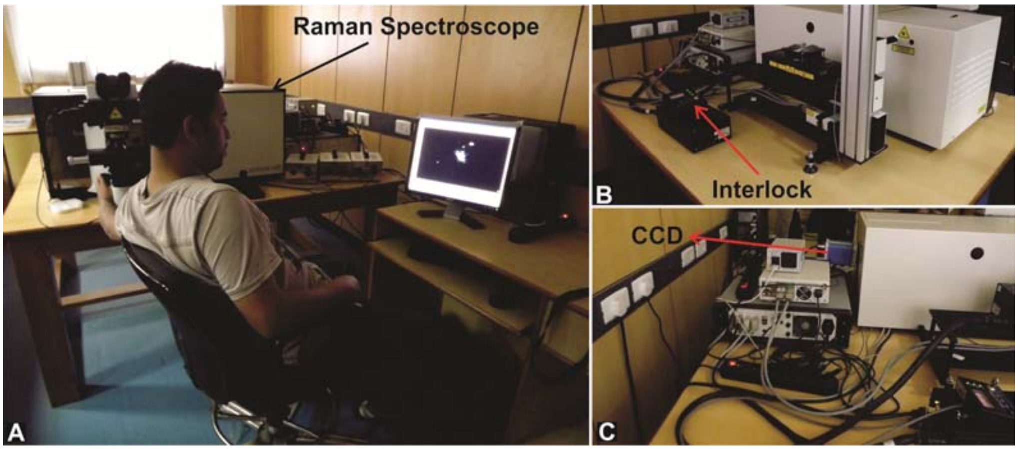

Fig. 3.7.A. Raman Spectroscope in Fluid Inclusion Lab, WIHG, Dehradun, India. B. The interlock system which contraol the laser power. C. The Charge Couple Device (CCD) is shown here which produces digital image of spectrum.

The laser power was controlled by a laser interlock system. Data generation was done with both the holographic grating 600 and 1800 grooves/mm. RTD exposure times for minor mineral phases were selected between 1- 150 s with accumulation number 1 - 30. Spectra are recorded from 0 - 4000 cm $^{-1}$. The Raman was calibrated with synthetic silica standard at 520.5 cm^{-1} and natural olivine from Himalayan ophiolite. The estimated spectral resolution at the time of analyses was 1 – 2 cm^{-1}. Some of the Raman spectra were obtained using Ranishaw in Via Confocal Raman Spectroscope at CCMR, USA, with 488 nm laser through a 50X objective.

To generate spectrum of very tiny solid phases the laser beam diameter was adjusted to 2μm. For that different combination of pinhole and filter was attempted. In case of fluid inclusions and glass phases Laser power and exposure time were kept as low as possible unless the laser may destroy the target specimen. To get better spectrum manually the focus was adjusted at the time of data generation. At time of experiment it is observed that when the exposure time is increased, the individual peaks give more shifts up to 2 - 5 cm^{-1} to the lower value. To avoid this, instrument has been calibrated with synthetic silica standard for every change of exposure time. Some cases it is also noticed when the laser power was increased up to 33 mW the individual peaks show up to 2 cm^{-1} shift to the higher side.

CHAPTER 4

MINERALOGICAL CHARACTERIZATION OF OPHIOLITE ULTRAMAFICS

CHAPTER 4

MINERALOGICAL CHARACTERIZATION OF OPHIOLITE ULTRAMAFICS

4.1 CHAPTER OVERVIEW

Chapter “4” focuses on the basal ultramafic part of Nidar ophiolite. The basal part is important in ophiolite complexes because it provides primary information about spreading center evolution. This chapter contains detail mineralogical description, mineral chemistry and in situ characterization of different mineral phases.

4.2 LITHOLOGICAL DESCRIPTION

By definition a lower ultramafic section is an essential part of a classical ophiolite suite (Dewey and Bird 1971) though it may not be preserved in many ophiolite suites. For that originally Steinmann (1905, 1927) defined – “ophiolite is an association of serpentinite, pillow lava and radiolarian chert disregarding any interpretation of its origin”. The classical display of crust +

mantle part of an ophiolite suite is a rare site in nature but there are some ophiolites which are considered as classical ophiolite suites (example – Oman ophiolite, Trodoos ophiolite). In SE Ladakh long Indus Suture Zone (ISZ) the Nidar ophiolite displays all types of mafic and ultramafic rocks which are expected in a classical ophiolite suite. Importantly the thickness of basal ultramafic part is considerably high (~ 7 km) with compared to other ophiolites throughout the world. The lower most part of ophiolite suite is composed of a ~ 500 m Km thick dunite body concordant with the trend of Indus Suture Zone (NW - SE) trend. From the broad dunite body some conduit like channelized discordant network of the dunite (up to 3 Km long, 50 – 100 m wide; trending NE – SW) emerged, which intrudes into the ultramafic section of ophiolite (Fig 2.7). A well developed foliation is noticed within the dunite channel. Though the channel is composed of uniform yellow coloured rock type (dunite), a significant variation in grain size is noticed (Fig 2.7 B). Coarse grained parts are nearly elliptical shaped porphyroclasts lie within a fine grained matrix and both of them show NE – SW trend which is same with the trend of dunite channel (Fig 2.7 B). The grain size reduction feature suggests a mylonite structure. The nature of the structure infers a plastic flow along the channels from the Ophiolite base which provide a good insight into the melt extraction process in a fossil spreading centre. This feature can be a potential site to understand the relationship between deformations and melt extraction from the upper mantle. Dark coloured spinels are present as disseminated crystals (~ 4 – 6%) in dunite. Many small randomly oriented pyroxenite layers (4 – 6 cm wide) within the dunite are noticed. The pyroxenites are fresh and unaltered (Fig 4.1 B).

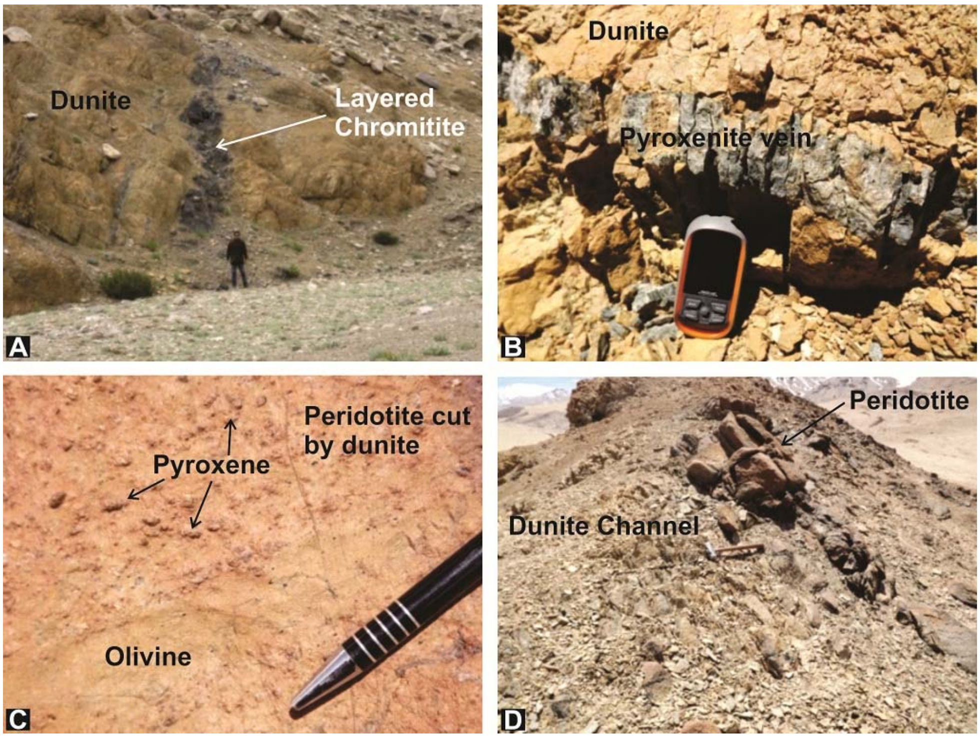

Fig.4.1. Field photographs of different kinds of ultramafic rocks from Nidar valley, SE Ladakh, India. A. A 1.1 m thick chromitite layer in basal dunite. B. Pyroxenite veins in dunite. C. A peridotite, representative of the ultramafics which are cut by dunite. D. A peridotite body caught in discordant dunite.

The serpentinization in dunites varies from 10% - 30% from place to place. Some places the rocks are nearly serpentinized. Serpentinites appear as dark green coloured rock. It has numerous randomly oriented massive dull network of carbonate veins (<1 cm – 10 cm wide) are seen in dunite bodies (Fig 2.8 A, 4.2). These veins are dominantly made of carbonate and display multi generation and disoriented networking. The carbonates are also occurring in patches (Fig 4.2 C) on dunite, apart from their occurrence along veins. The associated peridotites and harzburgite are much less affected by this carbonation process. Carbonates veins with variable thicknesses are found restricted within serpentinites. These veins display complex networking and sometimes their thicknesses go up to a meter (Fig 4.2 D).

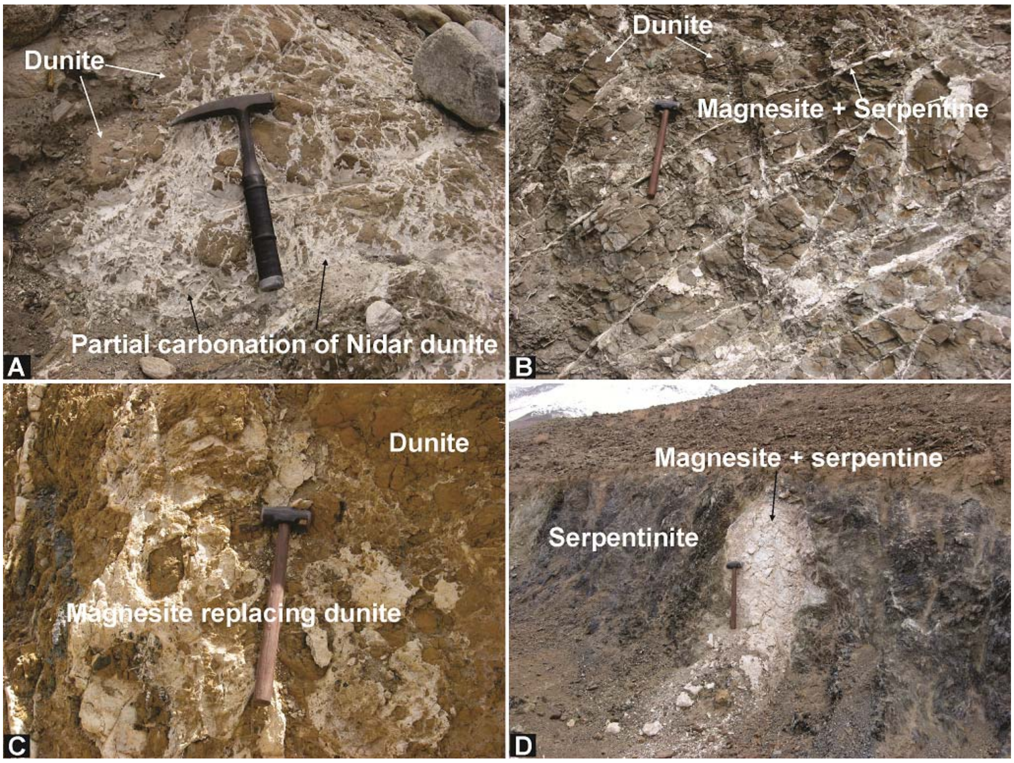

Fig.4.2. Field photographs of carbonate veins in dunite & serpentinites of ultramafic part of Nidar Ophiolite. A. White carbonate veins are weathering out the dunite. B. Different generations of dull white carbonate veins in dunite. C. Patches of carbonate in dunite. It lies on the fresh surface of a dunite body. D, Almost a meter thick carbonate vein (magnesite dominated) within a serpentinites body. This indicates the magnesite veins are formed from serpentinites also.

Mesoscopically, the carbonates are dull white to pale grey sub spherical clasts in some places, whereas in most of the cases it appears as fine powder. Chromitite layers of various thicknesses (few cm to a meter) are identified by black colour, crystalline appearance and very high density (Fig 4.1 A). On the basis of mode of occurrences of the peridotites of Nidar ophiolite are classified in largely three categories – (a) within the discordant dunite channel some peridotite bodies are observed entrapped as large xenoliths; (b) peridotites cut by the dunite channel; (c) the dunite channel and associated chromitites and pyroxenites. These peridotites are reddish and darker with respect to the surrounding dunites. With a close look pyroxene grains with prominent cleavage can be observed. The peridotites have difference in density. Serpentinization in peridotites is very much heterogeneous – almost fresh to serpentinite (5% - 100%). For further characterization petrographic studies were carried out on thin section of these rocks.

4.3 PETROGRAPHY

Petrographic studies were carried out on thin wafers of different ultramafic rocks from ultramafic part of Nidar ophiolite. In this section details of different parts of the basal part of Nidar ophiolite are given. For the Petrographic studies mainly optical microscope and Scanning Electron Microscope are used in detail.

Serpentine and carbonates

The carbonates from veins and patches are studied under scanning electron microscope (SEM). The dominant mineral in these carbonates are magnesite. In naked eye white to pale grey magnesites show botryoidal habit in places, whereas in maximum cases it appear as fine powder. But under SEM the botryoidal habit is seen in almost all carbonate veins and patches (Fig 4.3).

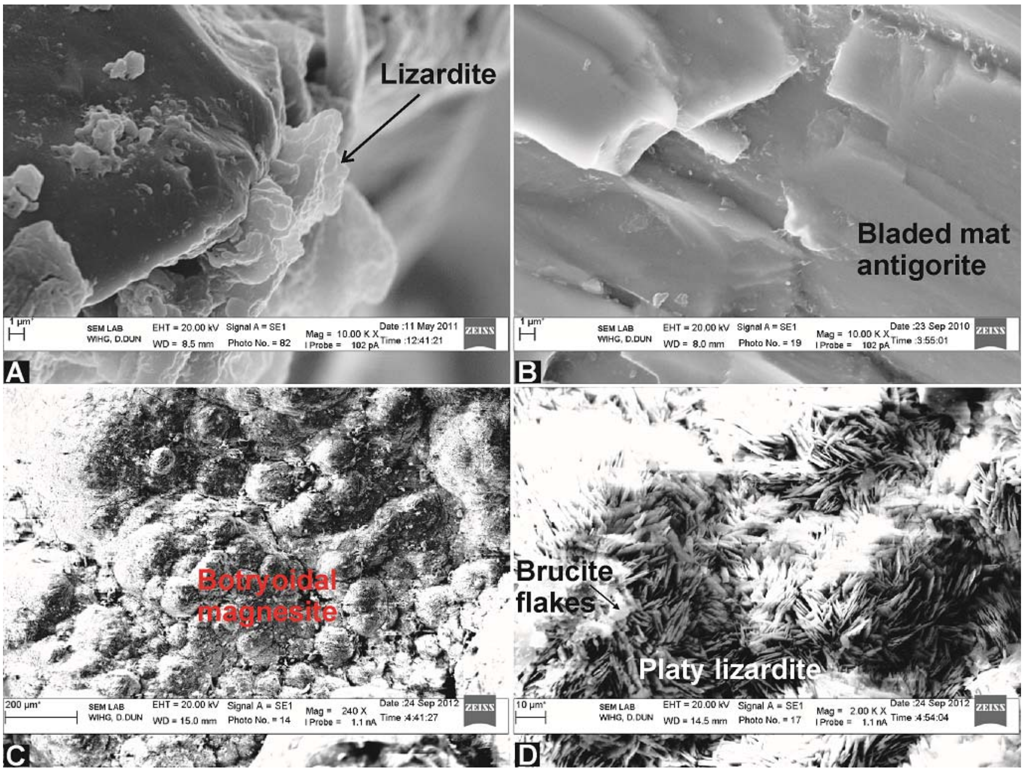

Fig.4.3. SEM images of serpentines and carbonates. A. Growth of lizardite along rim of olivines. B. The bladed mat texture in serpentines indicates presence of antigorite. C. Magnesite shows botryoidal habit. D. Lizardite shows typical platy habit with a few brucite flakes. This image demonstrates dominant serpentine within the vein carbonates is lizardite.

Among the carbonates there are some unusual veins within basal dunite part (Fig 4.4). These carbonates are not fragile like the others. One of these veins incorporates serpentines and part of the host dunite (Fig 4.4 D). These carbonates are mainly composed of calcite and dolomite (confirmed by XRD and Raman spectroscopy) (Fig 4.11).

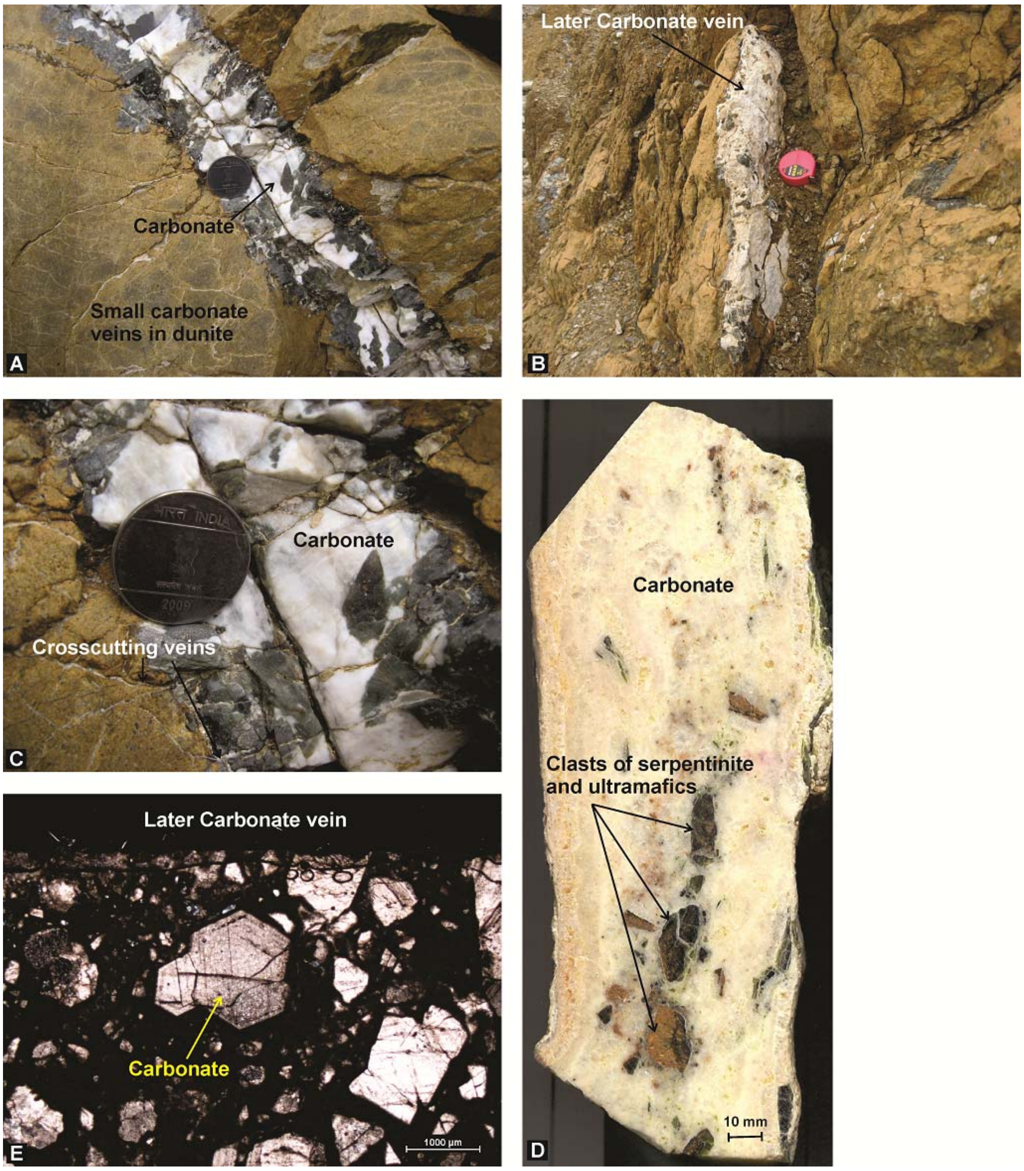

Fig.4.4. A, B, C. Field photographs of the carbonate veins in basal dunite. The vein in photo A & C is cut by the vein in photo B, D. A piece of crosscutting carbonate vein shown in Fig. B. The crosscutting vein bear clasts of serpentines and host ultramafic rock. E. The photomicrograph is showing a euhedral calcite grain.

The serpentinites are enriched in opaque oxides and exhibits different varieties of polymorphs. The lizardite serpentines show mesh texture under microscope. Mesh texture is produced by complex crosscutting veining system due to hydration of ultramafic rocks (Fig 4.5 A). Under SEM lizardite shows fine grained platy and flaky habit (Fig 4.3 A, C, D). Antigorite, a higher order polymorph of serpentine, show bladed mat structure under SEM (Fig 4.3 B). An attempt was made to reveal the different generations of serpentines, which will be discussed in the next chapter.

Dunite

Dunites are composed of olivine (> 90 %) and minor amount of Cr – spinel (~ 4%). Serpentinization varies from 10% - 25%. In some places secondary carbonate veins are also seen. Serpentines create mesh texture which cross cut the olivine and produces isolated islands.

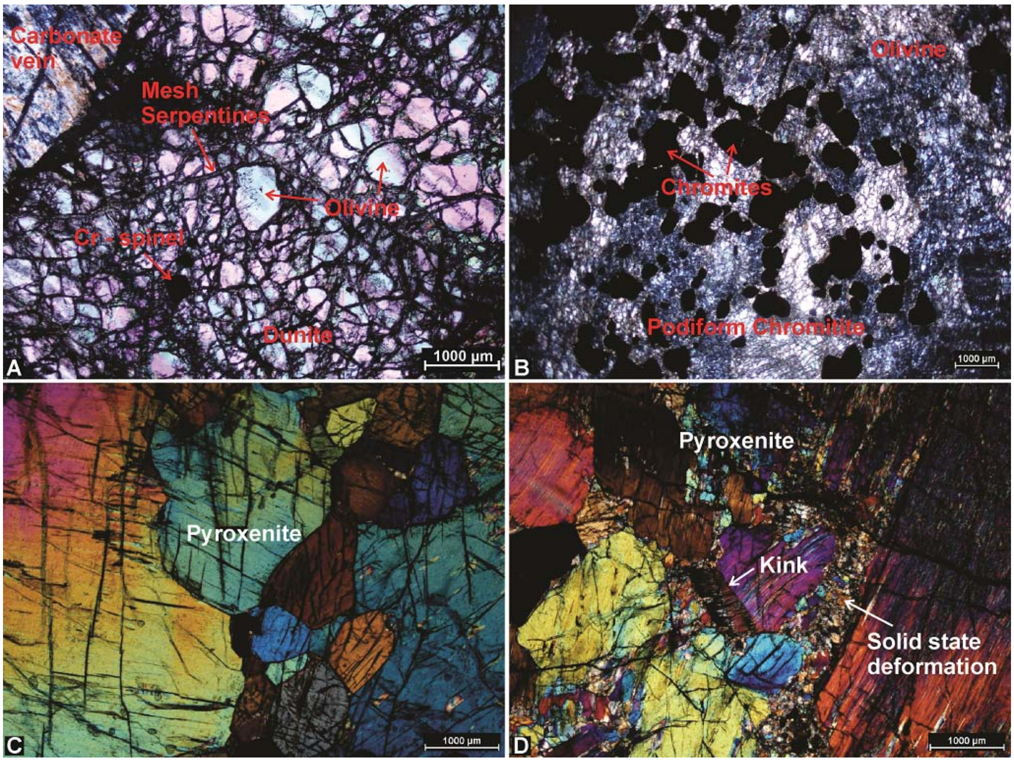

Fig.4.5. A. Photomicrograph of serpentinized dunite from basal part of the ophiolite ultramafics. Dunite is also cut by the secondary carbonate and serpentine veins creating mesh texture. B. Podiform chromitites in the discordant dunite host. C. The pyroxenite vein within basal dunite shows euhedral pyroxenes with sharp boundaries. D. The pyroxenes show kink bands and core – mantle structure which indicate deformation through various mechanisms.

Pyroxenite vein

The pyroxenite vein which is cutting the basal dunite is composed of mainly orthopyroxene and clinopyroxene (Fig 4.5 C). The pyroxenes are some time very coarse grained, but show grain size variation. Pyroxenes also display different types of deformation microstructures like kink bands and core and mantle structure (Fig 4.5 D). The kinking indicates deformation in much plastic condition where as the core and mantle structure generally forms in solid state. So that may be indicative of deformation in higher to lower temperature condition. The euhedral and subhedral pyroxene grains have sharp boundaries and they sometimes create a perfect "Y" (Fig 4.5 C). Many of the pyroxenes bear various types of exsolution lamella which will be shown in chapter "5".

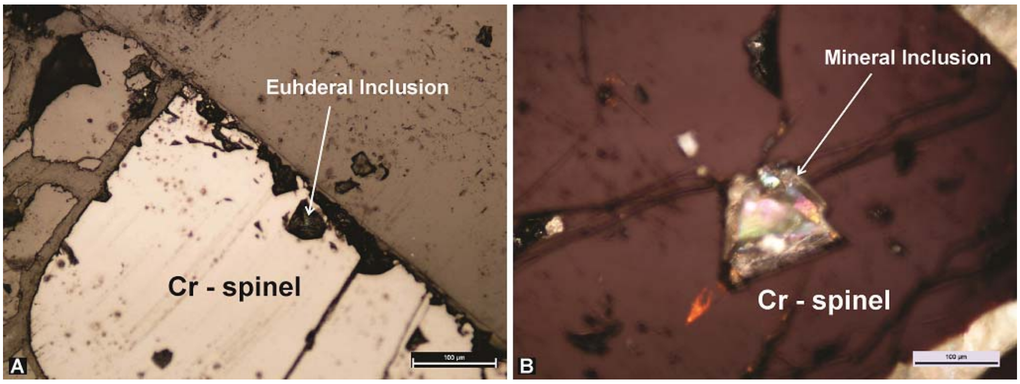

Fig 4.6. The photomicrographs are taken under reflected light as the purpose is to look into the Cr – spinel grains. A. The photomicrograph shows a euhedral inclusion within Cr – spinel. B. Another Cr – spinel contains a euhedral inclusion with optical zoning in it.

Layered chromitite

Layered chromitite is a monomineralic rock entirely composed of black isotropic (under transmitted light) chromite. In reflected light, chromites show high reflectance. The rock shows hypediomorphic texture with almost uniform grain size.

Podiform chromitite

Saccharoidal chromites are present as lens or pods in olivine dominated dunites. The rock is mainly composed of chromites (~ 80%) and olivine (10 – 15%). From place to place serpentinization varies from 5% - 10%. Chromites are isotropic under plane polarised light but for detail observation reflected light was applied. The chromites bear different types of unusual inclusions. Some of them show euhedral, tetrahedral and octahedral shape (Fig 4.6).

Peridotite bodies entrapped within dunite channel

The peridotite xenoliths bodies are variably serpentinized from fresh (~5%) to completely hydrated rocks (~95%). All of the peridotites entrapped within dunite channels are lherzolite. Among them two lherzolites (sample no 1M1 and 1NU27) bear ultra high pressure mineral inclusions and unusual textures which are principal findings of the present thesis. The lherzolite 1M1 is moderately serpentinized (16% - 20%) and composed of olivine (40%), orthopyroxene (25%), clinopyroxene (15%) and chromite (2%).

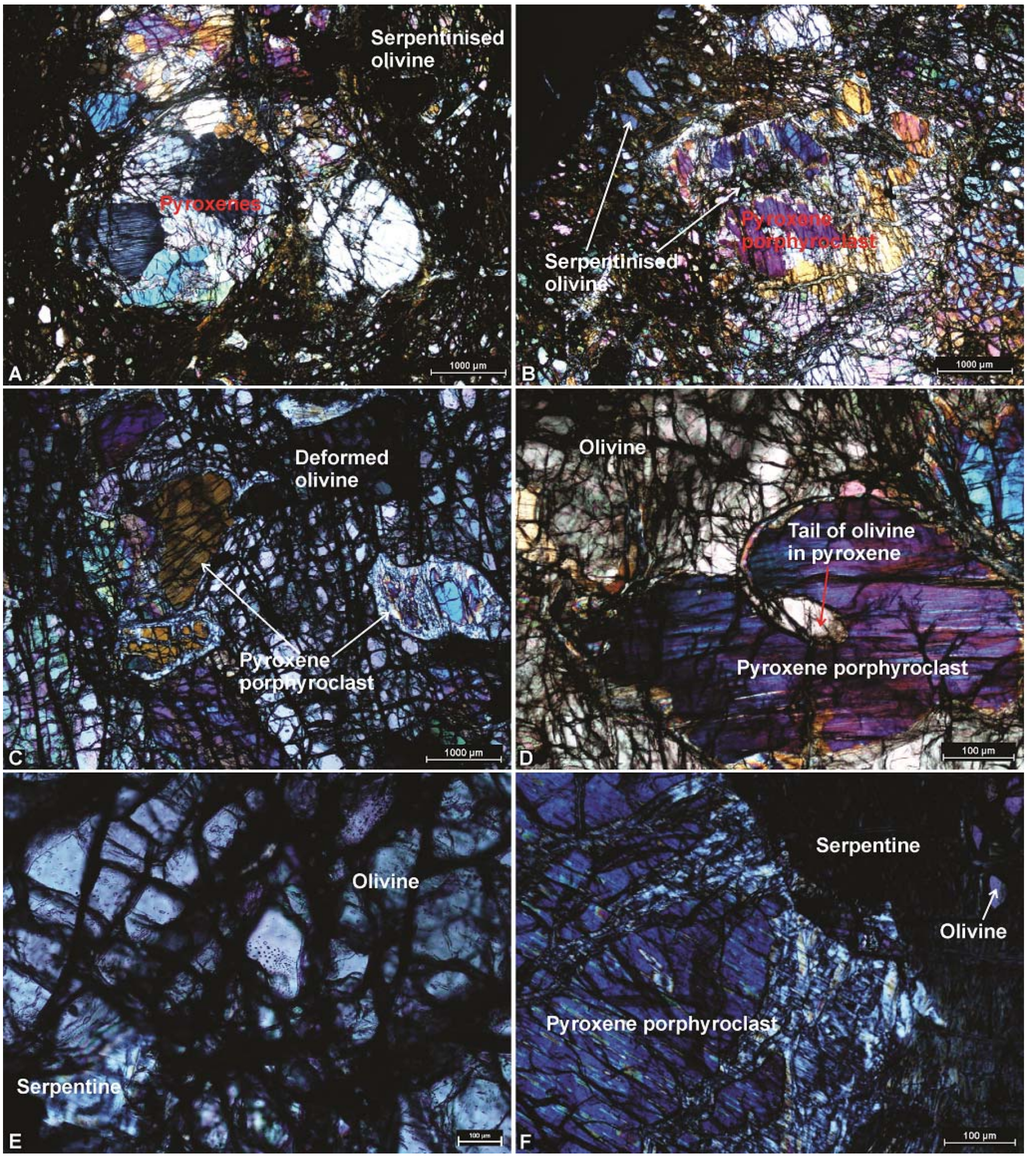

Fig.4.7. Photomicrographs of lherzolites which are entrapped within dunite channel. A. Multiple pyroxene aggregates occur as porphyroclasts within serpentinized olivine ground mass of lherzolite 1M1. B. Serpentinized olivine partially replaces the pyroxene. C. The pyroxenes with alteration rim lie within fresh unaltered olivine ground mass of the lherzolite 1NU27. D. A curved tail of olivine emanating from within the orthopyroxene of lherzolite 1NU27. E. Fresh relatively unaltered olivine rich ground mass of peridotite 1NU27. F. Another xenolith body, where serpentinization is very high showing a pyroxene porphyroclast.

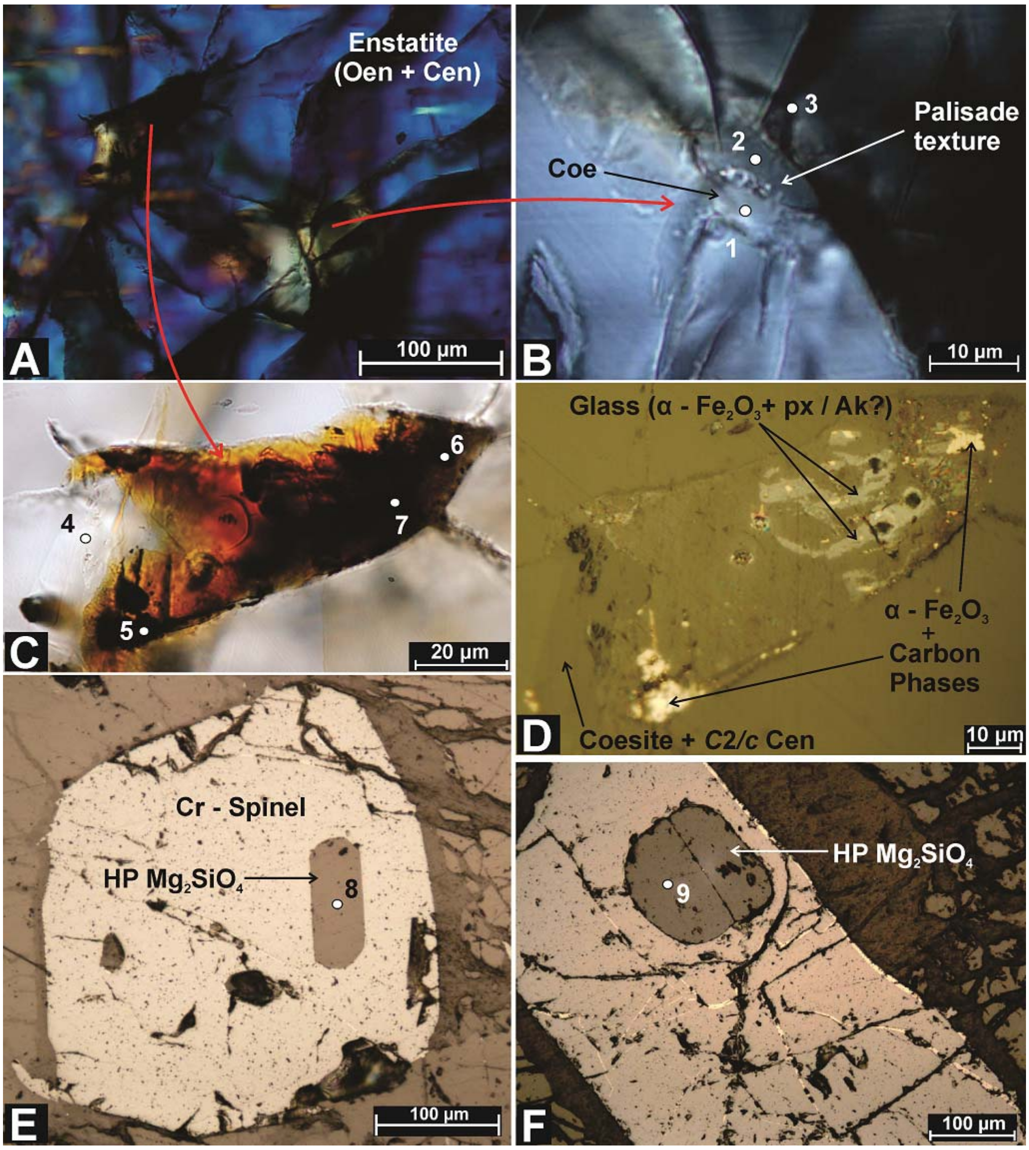

Fig. 4.8. Photomicrographs of high pressure phases recovered from peridotite xenoliths 1M1 and 1NU27. A. Host enstatite (Oen= orthoenstatite and Cen= clinoenstatite) containing high pressure (HP) phase bearing two relict grains both with radiating cracks. B. Palisade texture with foam like high relief coesite in the core. Points 1 – 3 represent analyzed spots for Raman spectra. C. Relict grain in (A) magnified in plane polarized light (PPL). Points 4 – 7 are analyzed spots for Raman spectra. D. Same grain as in C in reflected light showing different reflectance in complex textural relations of HP minerals analyzed by Raman spectroscopy. Dark spots are results of some of the incident Laser beams on glass. E & F. Reflected light view of host spinel, from the lherzolite xenolith 1NU27, with a euhedral inclusion of opaque HP - Mg_2SiO_4. Raman spectral spot marked 8 & 9.

The multiple aggregates of pyroxenes occur as porphyroclast within olivine dominated matrix (Fig 4.7A). Some places they are replaced by olivine partially (Fig 4.7B). The serpentines occur as veins within the olivines and create mesh texture (Fig 4.7C, E). Some of the pyroxenes in the 1M1 lherzolite bear some unusual inclusions. In an orthopyroxene grain some square shaped cleavageless grains with higher relief are noticed (Fig 4.8 A, B). Their boundaries with the host are diffused and not distinct.

In one of them typical palisade texture (Fig 4.8B) is observed. In the elliptical core of that palisade grain colourless foam like crystalline mineral with higher relief is noticed (size - 10 × 5 μm). The rest of the palisade is also colourless and devoid of cleavage but have lower relief than the mineral in core. Radiating fractures are present from the core to rim of the palisade texture. This texture is typical of solid state phase transformations from coesite to quartz and optically the mineral in core display typical character of coesite.

An opaque red coloured relict inclusion is present (~100 x 30 μm in size) which is sharp edged and devoid of any alteration at the rim (Fig 4.8C, D). Parts of the relict exhibit shattered texture and contains fine infuse cracks from its tip. There is also an associated square shaped silica grain. Metallic appearances of the opaques are similar to iron oxide. The dull part (with lower reflectance) indicates another phase (Fig 4.8D). The dark spots are due laser spots when it was probed by laser Raman spectroscopy. The spots may be due to presence of a less robust material such as glass, because at the same condition no such spots are observed in other places. Similar kinds of opaques with radiating fractures are present in the same rock (Fig 4.15). The dull part is also present as vein in one of the opaque (Fig 4.15).

The other lherzolite body (1NU27) is almost not serpentinized (~5%). The rock shows assemblage of olivine (50%), orthopyroxene (25%), clinopyroxene (15%) and Cr spinel (~5%). The ground mass of the lherzolite, which is olivine dominated, nearly unaltered but some of the pyroxenes have alteration and reaction rims (Fig 4.7C). Some places long and curved tail of olivine is noticed surrounded by orthopyroxene (Fig 4.7D). This feature suggests that olivine was more plastic in nature with respect to the pyroxenes. In this lherzolite Cr – spinel grains include some euhedral opaque inclusions (Fig 4.8E, F). They are invisible under transmitted light but prominent under reflected light (Fig 4.8 E, F). Apart from this the olivines and pyroxenes of 1NU27 lherzolite contain some unusual micro textures which will be described in the next chapter.

Peridotite bodies cut by discordant dunite

There are also some parts of ultramafic units cut by the discordant dunite. They include serpentinite, diabase and peridotite as observed (Fig 2.7 A). The diabases, essentially composed of fine grained plagioclase (40%), clinopyroxene (20%), amphibole (20%) and opaque (15%) occupy a large area in the ultramafic parts (Fig 2.3 C, D).

Some places carbonate veins has cut the diabases and the serpentinization is very low (5%). Most of the peridotites cut by the dunite channel are harzburgite which is composed of olivine (55%), orthopyroxene (35%) and spinel (5%). The serpentinization is quite low (5%). The olivine and pyroxenes of these harzburgites unusual exsolution and inclusions are almost absent. Some places within the orthopyroxene inclusions of olivine and serpentines are noticed (Fig 4.9B) which indicates the rock has been evolved through multiple phases. Within the serpentinites one garnet bearing highly serpentinized rock has been observed which is composed of pyroxene (10%), plagioclase (20%), serpentine (40%), amphibole (15%) and Garnet (15%) (Fig 4.9E). The outcrop of the garnet bearing serpentinite is not a continuous one. It occurs as patches within a serpentinized ultramafic body.

In Mahe – Sumdo section apparently the ultramafic part is overlooked by the earlier workers due to similarity of the exposures between gabbro and ultramafics. Some dark brown colour serpentinized peridotite (Fig 4.9 G) is encountered beneath the petrologic Moho part of the Mahe – Sumdo section. Beneath the petrologic Moho diabases are also noticed in this section (Fig 4.9 H).

Among these peridotites in Nidar valley section, cut by the dunite channel, some lherzolites are present which are essentially composed of olivine (40%), orthopyroxene (20%), clinopyroxene (17%) and Cr – spinel (3%). The rock is moderately serpentinized (20%). Clino and ortho pyroxenes of this lherzolite exhibit some rare micro textures (Fig 4.9 C, D) which are discussed in detail in next chapter.

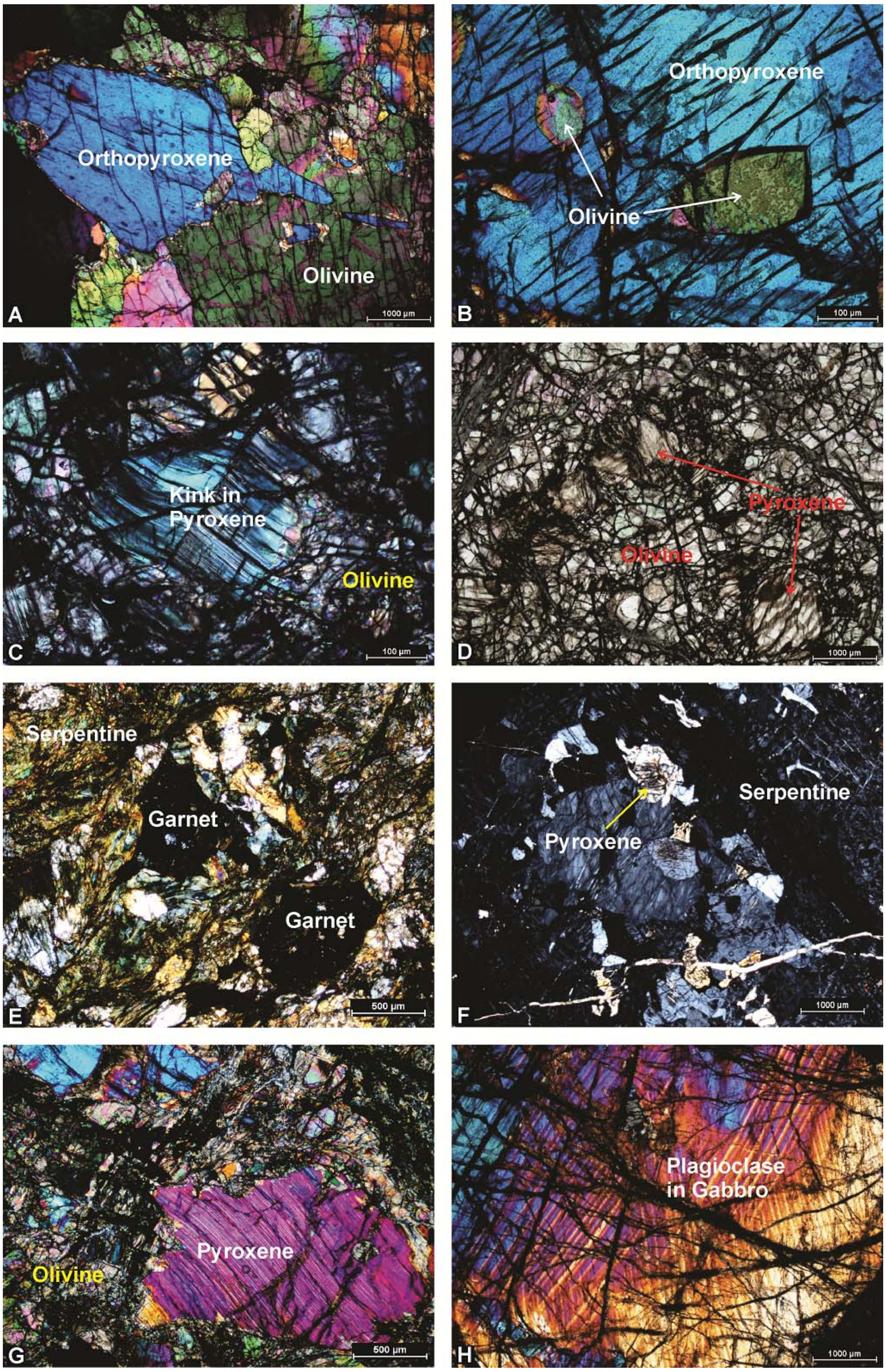

Fig 4.9. A, B. Photomicrographs of harzburgite which are cut by the discordant dunite. Fig B shows inclusions of olivines in an orthopyroxene of harzburgite. C, D. Lherzolites cut by the dunite channel. A pyroxene porphyroclast is deformed by kinking. E. Garnet in serpentinized matrix. F. The rock is entirely serpentinized with some pyroxene relicts. G. A serpentinized peridotite from Mahe – Sumdo section. H. Photomicrograph of a diabase from lower part of the Mahe – Sumdo section.

4.4 MINERAL CHEMISTRY

(Data are at the end of this chapter)

The principal purpose of the present thesis is to investigate the root of ophiolite origin. For that the mineral chemistry of the ultramafic rocks here carried out on the selected rock suites. To compare the compositional variation mineral chemistry data has been recovered from 3 types of ultramafic rocks – (1) the dunite channel (2) ultramafic rocks entrapped within discordant dunite (3) ultramafics cut by dunite channel. Basic comparison of mineral chemical data (using EPMA) shows that the major minerals, olivine, pyroxene and spinel of these ultramafic rocks have a significant difference. Here only representative mineral chemistry data are shown. The olivines of channelized dunite (sample 1NU18) have Fo content 93.34 – 93.57% (Table 4.1, APPENDIX 1). Spinels have Mg# 58.38 – 62.4 % and Cr# 61.94 – 72.3 % (Table 4.1, APPENDIX 1).

Some of the lherzolites caught in discordant dunite show high pressure mineral inclusions and micro textures. Their mineral chemistry is different from the discordant dunite body. In lherzolite 1NU27, olivine have Fo content is around 90.65 – 91.2 %; Mg# of the orthopyroxene ~ 91.13 – 91.34 %. The Mg# numbers of Clinopyroxene are around 95 – 95.17 %. Spinels show Mg# ~ 48.9 – 49.23 % and Cr# ~ 67.9 – 70.3 % (Table 4.2, APPENDIX 1).

The olivines of lherzolite 1M1 show forsterite content 89.9 – 90.5 %. The spinels have Mg# ~ 52.6 – 52.8 % and Cr# of 54.5 – 55.2 %. The Mg# in clinopyroxene varies from 92.5 – 93.3 % (Table 4.3, APPENDIX 1). Across an orthopyroxene, which is similar to the high pressure relict bearing one, 10 points were probed. From core (Mg# ~89.9 %) to rim (Mg# ~91.35 %) (Fig.

4.20, APPENDIX 1) significant variation in Mg# content has been noted (Table 4.4, APPENDIX 1).

The essential minerals of the peridotites (cut by the dunite channel; sample no 3) are also analysed by Electron Probe Micro Analyser. In one representative lherzolite Forsterite content of olivine is ~ 90.06 – 90.37 % (Table 4.5, APPENDIX 1). The Mg# in orthopyroxene and clinopyroxene are 90.83 – 90.86 % and 93.63 – 94.22 % respectively (Table 4.5, APPENDIX 1). In the spinels Mg# and Cr# are 5.46 – 8.1 % and 85.95 – 90.28 % respectively (Table 4.5, APPENDIX 1).

Major minerals of a harzburgite are also analysed, which is cut by the dunite channel. The forsterite content of the olivine is ~ 91.06 – 91.22 % (Table 4.6, APPENDIX 1). The Mg# in orthopyroxene ranges within 91.82 – 92 % (Table 4.6, APPENDIX 1). In spinel, Mg# and Cr# varies from 44.66 - 45.02 % and 21.45 – 21.86 % respectively (Table 4.6, APPENDIX 1).

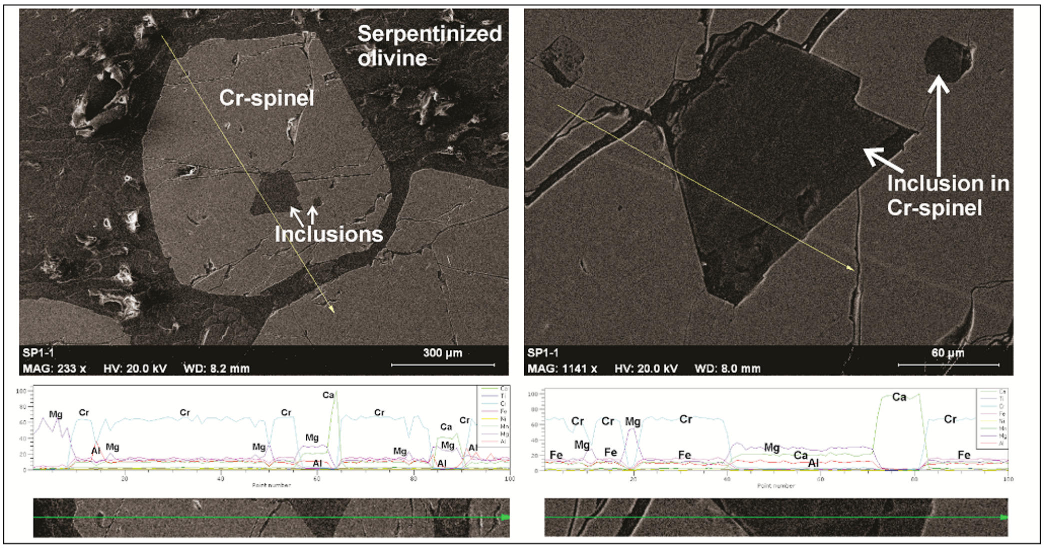

Fig.4.10. Line scan with EDX of a euhedral inclusion in Cr – Spinel (shown in Fig 4.6B) of podiform chromitite part. The core part of the inclusion in Mg – Ca – Al rich and the rim part is Ca rich.

For further characterization a euhedral inclusion (the grain with zoning shown in Fig 4.6B) in Cr – spinel of podiform chromitite part was analysed with the aid of EDX. The line scan (Fig 4.10) reveals that the inclusion has broadly two zones. The part in the core is Mg – Ca – Al rich in decreasing order. The rim part is Ca rich. The serpentine veins also show dominance of Mg but there concentration of Ca and Al are not observed.

4.5 MINERAL PHASE CHARACTERIZATION

Gross mineral phases are characterized by optical microscope. Some of them like serpentines are distinguished (where required) through their habit under optical microscope and Scanning Electron Microscope (SEM). This part of the chapter mainly focuses on the characterization of different types of carbonates and the micro inclusions found in lherzolite 1M1 and 1NU27.

Carbonates

In lower part of the Nidar Ophiolite majority of the carbonates occur as veins and patches in peridotites (especially in dunites) and serpentinites as described earlier (Fig 4.2). They show botryoidal habit under SEM (Fig 4.3 C). XRD analyses revealed that the carbonates shown in Fig 4.2 & 4.3.C are magnesite (Fig 4.11. A). the result is also consistent with the botryoidal nature under SEM. The carbonates occur as veins in lower part of dunite (Fig 4.4) are also characterized by XRD.

The primary vein (1CV15) is composed of mainly magnesite and dolomite (Fig 4.11 B). Some peaks of talc and serpentines are also observed. XRD pattern (Fig 4.11.C) and Raman spectroscopy (4.12) of the carbonate vein 1SCV16 of Fig 4.4.B & Fig 4.4.D shows presence of calcite and dolomite.

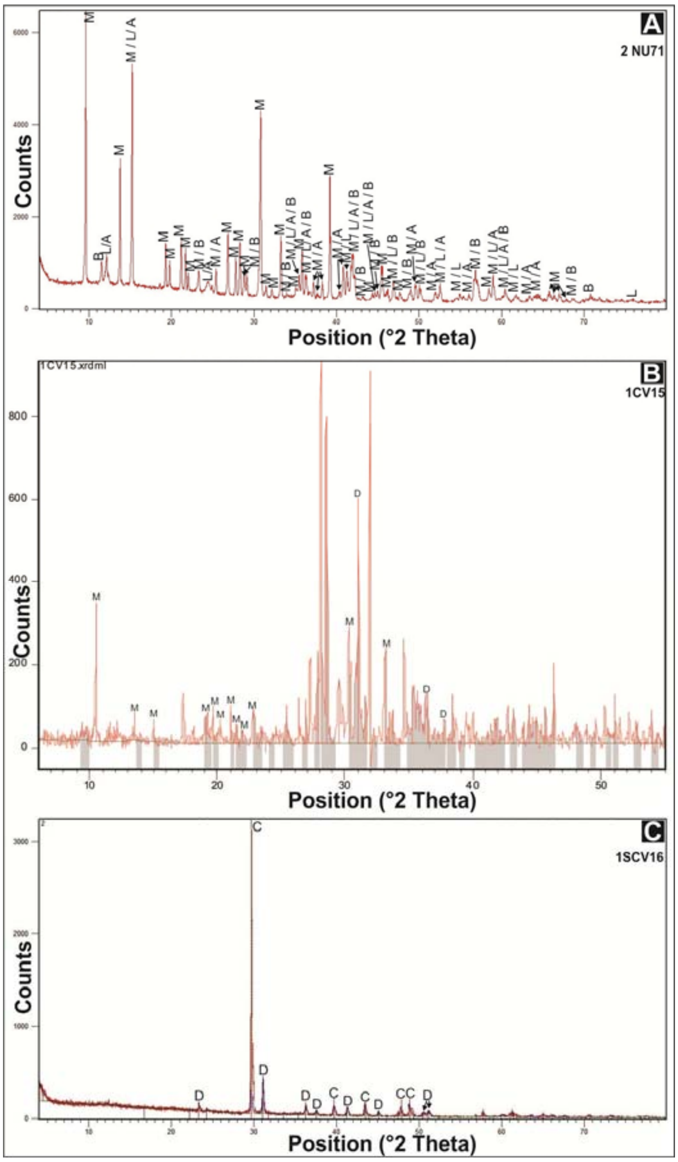

Fig. 4.11. A. XRD pattern of vein carbonate from sample 2NU71 (shown in Fig 4.2 & 4.3.C) obtained using Cu $_{K\alpha}$ excitation. The XRD data indicates dominance of magnesite within the carbonate veins along with some serpentine group of minerals. B. XRD analyses of carbonate vein shown in 4.4 A & C reveal presence of magnesite and dolomite. C. XRD data of the “unusual” carbonate vein (of Fig 4.4.B & D). In the vein both calcite and dolomite are present. (Used abbreviations: Magnesite – M, Antigorite – A, Lizardite – L, Brucite – B, Calcite – C and Dolomite – D).

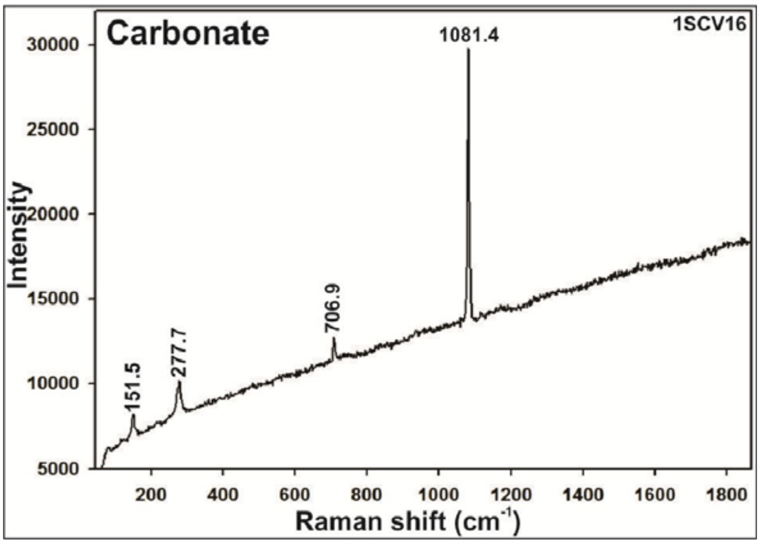

Fig 4.12. Raman spectra of the euhedral carbonate from carbonate vein 1SCV16 (shown in Fig 4.4.E) reveal that the carbonate is calcite. The spectrum shows a shift to the lower value side.

Mineral inclusions from lherzolite 1M1

The unusual mineral phase assemblages from an orthopyroxene porphyroclast of lherzolite 1M1 shown in Fig.4.8 have been characterized by Raman spectroscopy. The spots marked in Fig.4.8 are probed by Raman spectroscope and their corresponding spectra are shown in Fig 4.13. Details descriptions of different spots are given below:

Spot at the palisade core - Fig.4.8 B1

The core of the palisade texture follow trend of coesite (Fig 4.13.B1, APPENDIX 2). But its principle ~ 524 peak is broadened. That could be because of transformation from any other phases (its square shape also suggest possibility of a stishovite pseudo morph). This phenomena also can be interpreted due to exsolution origin of coesite (Zhang et al., 2005). Associated other high pressure phases also support the very high pressure primary condition.

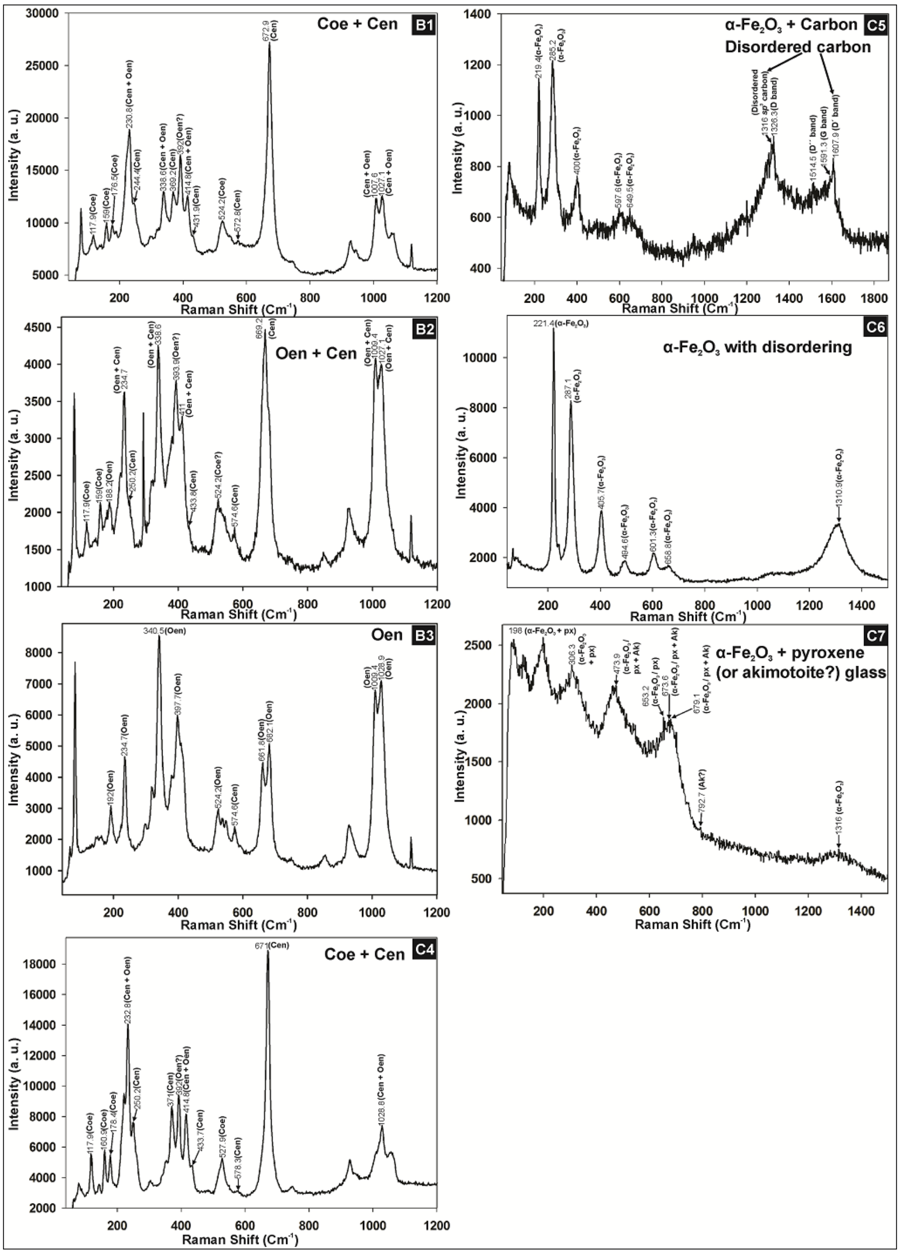

Fig. 4.13. Raman spectra corresponding to the spots 1 - 7 in Fig.4.8: (B1) Raman spectrum reveals coesite and *C2/c* clinoenstatite mineral phases. The principal coesite peak 524cm^{-1} became broad. (B2) Spectrum for mixed ortho and clinoenstatite with weaker coesite peaks. (B3) The spectrum reveals a typical Oen. (C4) This spectrum resembles that in (B1) with coesite and *C2/c* clinoenstatite. (C5) Spectrum indicates α-Fe$_2$O$_3$ with disordered carbonaceous matter. (C6) Spectrum of disordered α-Fe$_2$O$_3$. (C7) Spectrum of glass showing mixed α- Fe$_2$O$_3$, pyroxene (both ortho - and clino) and akimotoite (?) peaks.

The low intensity peaks at 244, 369, 432, 573 cm^{-1} from the core of the palisade texture (with the coesite spectra) indicate towards clinoenstatite (High P Cen or Low P Cen) (Ulmer and Stalder 2001). But the high intensity sharp peak at 673 cm^{-1} indicates presence of a high P Cen (Cholpelas 1999). The splitting of ~ 673 peak from core to rim (Fig 4.14) also suggests transformation from a C centered $MgSiO_3$ to a P centered $MgSiO_3$ (Tribaudino et al 2012). The other peaks are assigned to orthoenstatite. It is observed that, in places where coesite is present signature of *C2/c* clinoenstatite is also obtained from the Raman spectra (Fig 4.14). The low intensity peak at 1027 cm^{-1} and subsequent peaks at 231, 369 and 415 cm^{-1} indicate mixed clino-orthoenstatite.

Spot adjacent to the palisade core – Fig.4.8 B2

Coesite and clinoenstatite peaks are getting weaker. Orthoenstatite peaks are dominating the Raman trend (Fig 4.13.B2, Fig 4.14 and APPENDIX 2).

Spot away from the palisade core – Fig.4.8 B3

The Raman spectra show trend of Oen (Fig 4.13.B3, Fig 4.14 and APPENDIX 2). Coesite peaks are absent. Cen peaks are almost disappeared. Only one peak at 575 can be assigned to Cen.

Spot on the translucent part of the relict - Fig.4.8 C4

The square shaped silica grain with the relict shows Raman trend similar to the B1 (Fig 4.13 C4, APPENDIX 2).

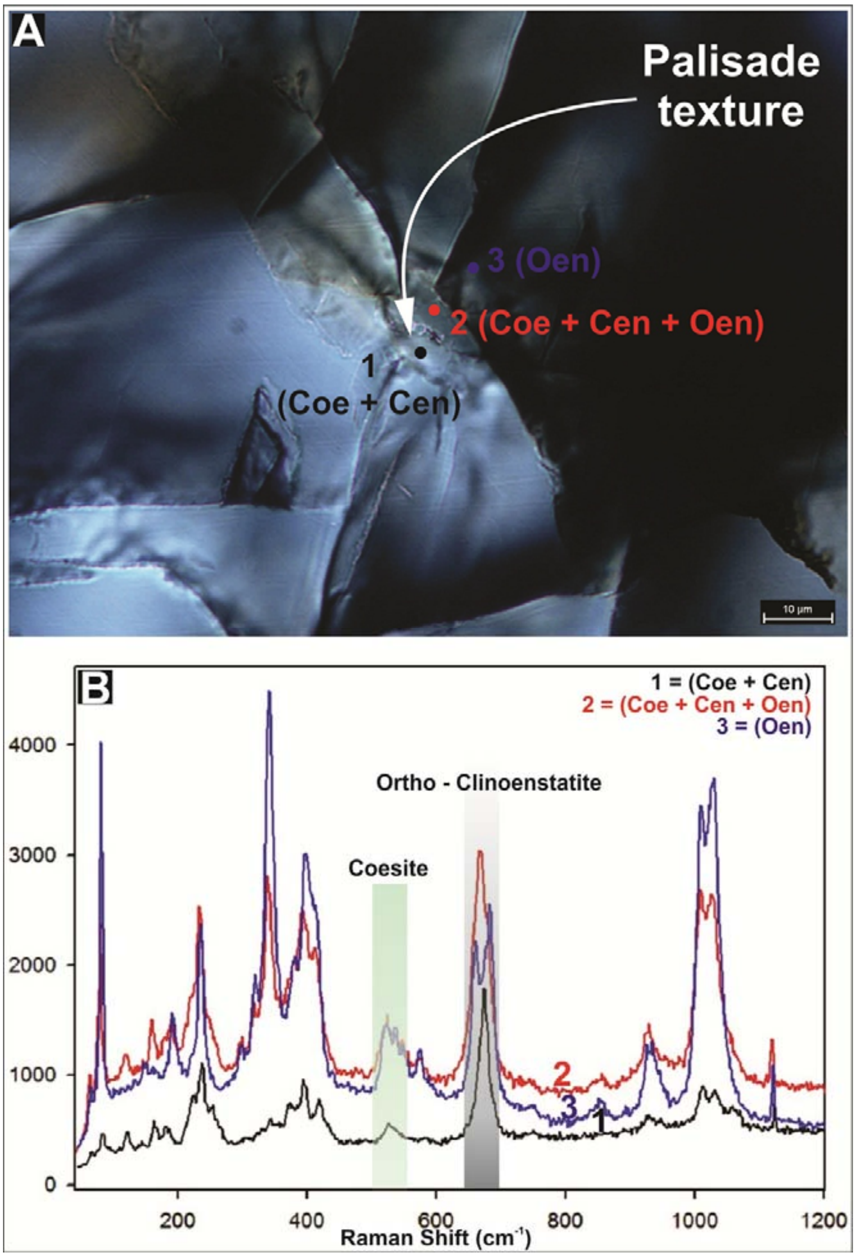

Fig.4.14. A, B. Comparison between Raman spectra of the spots 1 (black), 2 (red) and 3 (blue) in the (A) from core of the palisade texture to the rim. The comparison shows that the coesite and clinoenstatite peaks are getting weak progressively from 1 to 3. The splitting of principal ~ 670 cm^{-1} peak from 1 to 3 indicates transformation of a C centered Cen to Oen.

Spot on the opaque - Fig.4.8 C5

The Raman spectrum for spot 5 (Fig.4.8 C, APPENDIX 2) show characteristic peaks of α - Fe_2O_3 at 219, 285, 400 and 598 cm^{-1} (Fig.4.13 C5, APPENDIX 2), associated with peaks of disordered carbon at 1326 (D), 1514 (D″), 1591 (G) and 1608 cm^{-1} (D′). The sharp 1326 cm^{-1} peak suggests diamond like *sp*^{3} carbon in the absence of ~1350 cm^{-1} D band for graphitic carbon. Additionally, doublet in D band (1316 and 1326.3 cm^{-1}) and dominance of D′ band over the G band indicate a structural disorder in *sp*^{3} carbon (Smith and Godard 2013).

Sometimes it is very difficult to distinguish between synthetic diamonds (cutting or polishing materials) and natural diamonds. Some observations are made on which it can be stated that the inferred diamonds from the lherzolites of the Nidar Ophiolite are not due to contamination during thin section preparation. They are discussed below –

(1) Graphite (G band) is not expected in synthetic diamonds (Perraki et al., 2009).

(2) The Raman spectra of the diamonds in diamond polishers are found to be tightly positioned at 1332 ± 0.5 cm^{-1} (Perraki et al., 2009). But in our case the principal D band is observed at 1326 cm^{-1}. This down shifting in the peak position is likely for natural diamond.

(3) The downshifting of principal diamond band (lower than 1332 cm^{-1}) has been previously observed for natural diamonds (Smith et al., 2011).

(4) The doublets in D band do not support presence of diamond contamination from the thin section polishing materials.

(5) The coexistence of (hematite + diamond) has been reported from natural samples (Vrijmoed et al., 2008) and has been predicted to be stable at ultra high -pressure conditions (Smith et al., 2011).

(6) The associated high -pressure phases in 1M1 lherzolite as described in this study also favour the likely association of nano diamonds in the relict grain of the sample.

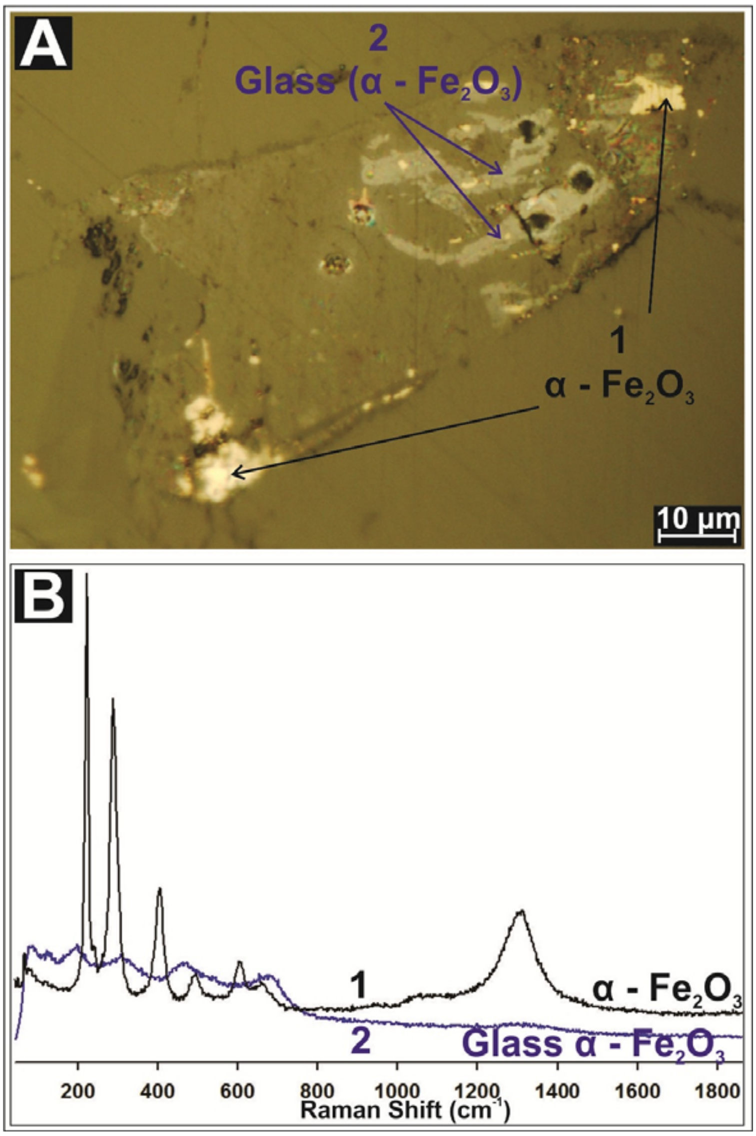

Fig.4.15. Comparison between Raman spectra of the spots 1 (black) and 2 (blue) in the (A). The comparison shows that the Raman trend of glass follows the trend of α-Fe_2O_3.

Spot on the opaque – Fig.4.8 C6

The 221, 287, 406, 495 & 601 cm^{-1} peaks indicate α- Fe_2O_3 phase (Fig.4.13 C6, Fig.4.15 and APPENDIX 2). The occurrence of broad Raman peak at 658 and 1310 cm^{-1} indicates disordering in hematite (Shim and Duffy 2001). This disordering generally takes place at a very high pressure (Shim and Duffy 2001). In the earlier case (C5) the disordering is probably occupied by disordered carbonaceous matter.

Spot on the glass – Fig.4.8 C7

The trend and the broad asymmetric nature of the Raman trend suggest presence of a cooled liquid (glass). The glass contains broad peaks of α- Fe_2O_3 with mixed principal pyroxene (both ortho and clino) peaks (Fig.4.13 C7, Fig.4.15). Some akimotoite ($MgSiO_3$ ilmenite) peaks (285, 474, 674, 679 and the main 793 cm^{-1}) are also noticed in this trend.

Besides these another opaque grain is observed in the 1M1 lherzolite which show radial cracks around it (Fig 4.16.A). In reflected light the opaque shows different reflectance in core and rim (Fig 4.16.B). The texture of the core is also distinguishable from the rim with cross hatched lamella type structure. Some veins of dull material are also noticed within the grain. The veins are essentially restricted within the opaque. From the Raman trend it is interpreted that the grain is α- Fe_2O_3 and the vein is made of entirely α- Fe_2O_3 glass (Fig 4.16.B1, B2). In this case the Raman spectrum of glass shows more convincing signature of α- Fe_2O_3.

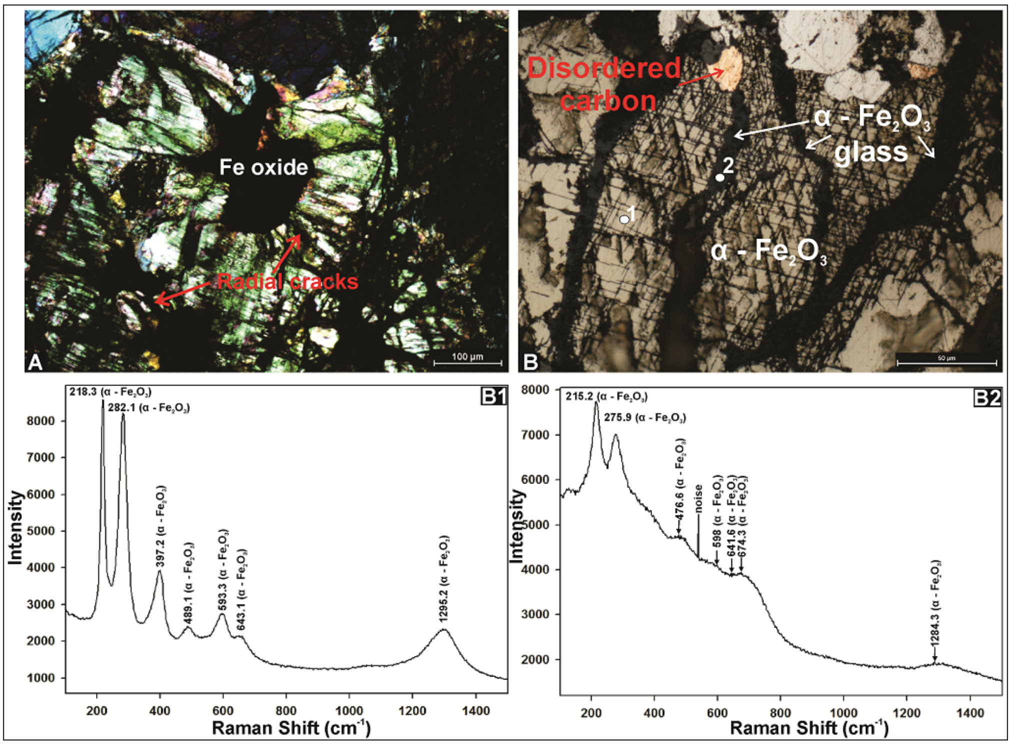

Fig.4.16.A. Photomicrograph of an opaque with radial cracks around it. B. Reflected light shows the core is texturally different from the rim. Some veins with dull material is noticed which are strictly restricted within the opaque. B1. The Raman spectrum displays α- Fe_2O_3 with disordering. B2. Raman spectrum of α- Fe_2O_3 glass from the vein in Fig B.

Mineral inclusions from lherzolite 1NU27

Within some Cr – spinels of the lherzolite 1NU27, euhedral isotropic opaque minerals are observed (Fig.4.8.E & F). The points 8 and 9 correspond to the points in Fig.4.8.E & F. The isotropic opaque phases display Raman spectrum of forsteritic olivine, doublet at 823, 854 with a 961 cm^{-1} peak (Fig 4.17 E8, F9). The peaks nearby 542 and 918 cm^{-1} are also earlier reported from experimentally shocked Balsam gap dunite (Farrell – Turner et al., 2005) at 29.3 GPa. The 918 cm^{-1} is principal wadsleyite peak. The peak near 699 cm^{-1} also may be related to high pressure Mg_2SiO_4 spinelloid. The 372 peak along with 605 cm^{-1} may be assigned to ringwoodite (Mcmillan and Akaogi 1987).

In a sentence the isotropic euhedral grains are dominantly forsteritic olivine but signatures of a pre existing high pr Mg_2SiO_4 spinelloid are present.

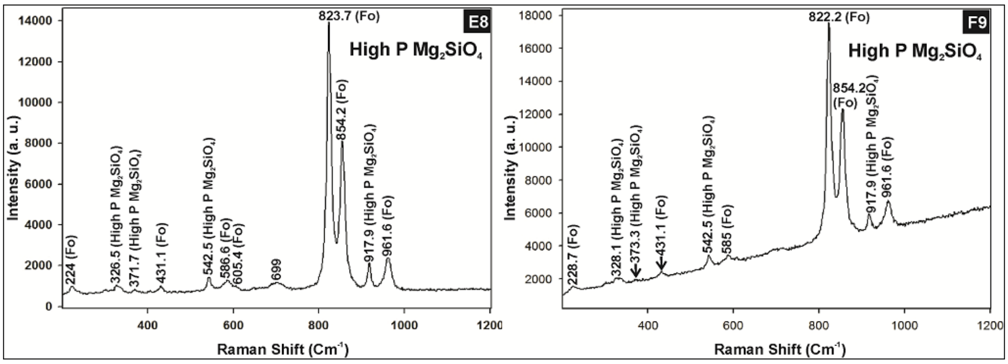

Fig.4.17. Raman spectra of retrogressed high pressure Mg_2SiO_4 spinelloid from Cr – spinels (shown in Fig.3.8.E & F) of 1NU27 lherzolite. E8, E9. Spectra of mixed Mg_2SiO_4 phases with principal wadsleyite peak at 918 cm^{-1}.

The Raman spectra of HP Mg_2SiO_4 shown in Fig.4.17 were generated by a Ranishaw in Via Conofocal Raman Spectroscope through 488 nm laser. To understand the behaviour of peaks of HP Mg_2SiO_4 the same analyses were carried out on different points with the aid of a LabRAM HR-Horiba Jovin Yuvon Instrument with 514.5 nm laser. When the Raman spectrum of HP Mg_2SiO_4 was compared with forsteritic olivine in groundmass of lherzolite 1NU27, an interesting phenomenon is noted (Fig.4.18). The principal olivine doublets in the case of HP Mg_2SiO_4 show inversion with respect to the forsteritic olivine. The doublets of HP Mg_2SiO_4 also show a shift to the higher value.

It is observed in case of a HP Mg_2SiO_4 inclusion in Cr – spinel that some of its part has been transformed into olivine (Fig. 4.19A).

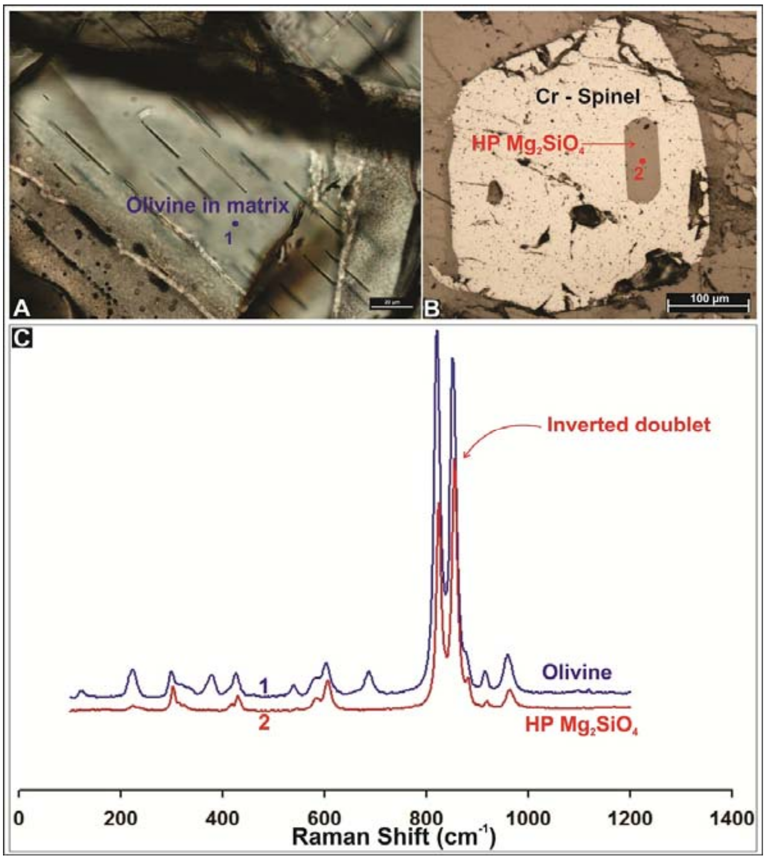

Fig.4.18. Raman spectra of HP Mg_2SiO_4 (red) and forsteritic olivine (blue) of 1NU27 lherzolite matrix are compared. In case of HP Mg_2SiO_4 spectrum doublets show inversion and a slight shift to the higher side with respect to the forsteritic olivine.

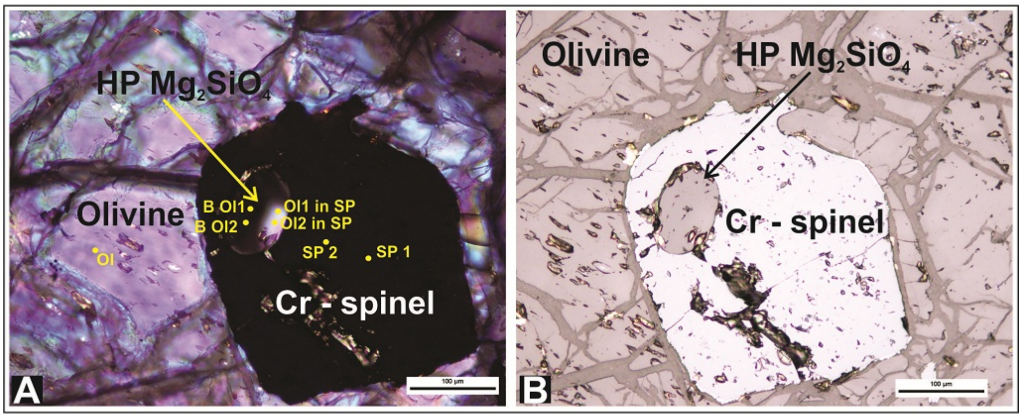

Fig.4.19.A. Another similar kind of HP Mg_2SiO_4 from lherzolite 1NU27 is observed as inclusion in Cr – spinel. This inclusion is probed by EPMA. The analysed spots are marked here and analyses are given in table no. 4.7. B. Reflected light photomicrograph of the same inclusion shown in A.

The inclusion behaves in a same manner under Laser Raman spectroscope like other HP Mg_2SiO_4 grains. Mineral chemical analyses were done on this particular inclusion, its host spinel and compared with the matrix olivine (Table 4.7). As expected from the Raman spectrum the inclusion is Mg_2SiO_4 in composition. The part of inclusion which has transformed into olivine shows similar chemistry like the isotropic one. But the isotropic part is slightly Fe rich. Interestingly the HP Mg_2SiO_4 is Cr rich with respect to the matrix olivine.

4.6 MINERALOGICAL EVOLUTION OF ULTRAMAFIC PART

The studied ultramafics which are both caught and cut by the dunite channel are much enriched in Fe with respect to the dunite. This observation suggests that the peridotites are fertile than the discordant dunite (Kelemen et al., 1995). Structurally both types of ultramafic rocks are also potential to retain the primordial signature of the ophiolite evolution. But detail petrography along with the phase characterizations infer that the lherzolites 1M1 and 1NU27 bear the deepest signature of mantle flow of ophiolite basal section. One lherzolite (3) which is cut by the discordant dunite also have some textural evidence of complex evolution (will be discussed on next chapter).

In orthopyroxene porphyroclast of 1M1 lherzolite, the clinoenstatite (Fig. 4.13. B1 & C4, Fig.4.14) could be any one of the two types of *C2/c* Cen - high T Cen and high P Cen. From Raman spectra it is difficult to decipher the high

P Cen. But high T Cen has a small stability field at P < 1 GPa and T > 1500^0C (Pacalo and Gasparik 1990). The association of coesite (P > 2.7 GPa) with the Cen rules out the high T Cen indicating presence of high P Cen. The phase transition from high P Cen to Oen takes place at minimum ~8 GPa (Gasparik 1990).

The inversion of doublet along with the shift of HP Mg_2SiO_4 peaks with respect to the olivines of 1NU27 (Fig.4.17 & 4.18) lherzolite can also be considered as evidence of decompression from high pressure Mg_2SiO_4 to a forsteritic olivine (Durbin et al., 1993).

The high pressure phases bearing lherzolites are noticed as entrapped bodies within the dunite channel in lower part of the Nidar Ophiolite. It can be concluded that some of the mantle peridotites below the Nidar ophiolite that show evidence of high temperature – pressure recrystallization, plastic deformation and solid state flow began their journey in the mantle transition zone before arriving beneath the ophiolitic volcanic crust at oceanic ridges.

4.7 SIGNIFICANCE OF THE FINDINGS

The assemblage α - Fe_2O_3 + glass (α- Fe_2O_3 + akimotoite?), *C2/c* clinoenstatite and square shaped coesite as a relict inclusion in orthopyroxene porphyroclast of the lherzolite 1M1 infer evidence of beginning of their journey from probably the mantle transition zone (410 – 660 Km). The presence of HP Mg_2SiO_4, which primarily could be a higher pressure polymorph of α -

Mg_2SiO_4, in the lherzolite 1NU27 also supports the evolution from mantle transition zone.

The carbonate patches and veins (Fig. 4.2) are interpreted as evidence of CO_2 mineralogical sequestration in dunite and serpentinites. The observation provides an insight into the CO_2 sequestration process which could be potential solution to green house effect. But the “unusual” carbonate veins (Fig. 4.4) may indicate separate origin as their mineralogy is different from the earlier carbonates.

Table 4.1 Electron microprobe analyses of olivine and spinels of 1NU18 dunite, which represents the discordant dunite.

Elements	Olivine	Olivine	Olivine	Olivine	Spinel	Spinel	Spinel	Spinel
Na_2O	0.01	0	0	0	0.02	0.02	0	0.01
MgO	51.22	50.97	51.22	51.27	13.01	12.31	12.68	13.61
Al_2O_3	0	0	0	0	17.46	14.53	16.06	20.84
SiO_2	41.77	41.98	41.73	41.9	0.04	0.03	0.04	0.08
P_2O_5	0	0	0	0.01	0	0.03	0	0
K_2O	0	0	0.01	0	0	0	0	0
CaO	0.03	0.02	0.04	0.07	0	0.01	0	0.04
TiO_2	0	0.04	0.02	0.03	0.18	0.17	0.18	0.08
MnO	0.17	0.19	0.16	0.12	0.28	0.32	0.3	0.25
FeO	6.29	6.48	6.41	6.35	15.35	15.61	15.21	14.62
Cr_2O_3	0.01	0	0.06	0	52.72	56.53	55.37	50.55
Total	99.5	99.68	99.65	99.76	99.06	99.55	99.85	100.07
Na	0	0	0	0	0.009	0.01	0	0.004
Mg	1.847	1.835	1.846	1.844	4.915	4.705	4.79	5
Al	0	0	0	0	5.217	4.39	4.796	6.054
Si	1.01	1.014	1.009	1.011	0.01	0.006	0.011	0.019
P	0	0	0	0	0	0.006	0	0
K	0	0	0	0	0	0	0	0.001
Ca	0.001	0.001	0.001	0.002	0	0.004	0	0.011
Ti	0	0.001	0	0.001	0.035	0.032	0.034	0.015
Mn	0.003	0.004	0.003	0.002	0.06	0.069	0.064	0.051
Fe	0.127	0.131	0.13	0.128	3.254	3.348	3.223	3.013
Cr	0	0	0.001	0	10.567	11.461	11.092	9.851
Total	2.99	2.985	2.99	2.988	24.067	24.032	24.011	24.017
	(O = 4)	(O = 4)	(O = 4)	(O = 4)	(O = 32)	(O = 32)	(O = 32)	(O = 32)
Mg#	93.57	93.34	93.42	93.51	60.17	58.38	59.78	62.4
Cr#					66.95	72.3	69.81	61.94

Table 4.2 Mineral chemistry data of 1NU27 lherzolite, which is caught in the discordant dunite channel.

Elements	Olivine	Olivine	Olivine	Olivine	Spinel	Spinel	Cpx	Cpx	Opx	Opx
Na_2O	0	0	0	0.016	0	0.031	0.01	0.02	0	0
MgO	49.25	49.27	50.148	50.239	10.5	10.978	17.6	17.94	34.09	34.04
Al_2O_3	0	0.01	0	0.003	15.16	15.276	1	0.8	0.91	0.95
SiO_2	41.63	41.05	41.159	40.807	0.05	0.013	54.34	55.12	57.98	57.74
P_2O_5	0.03	0	-	-	0.02	-	0.01	0	0	0
K_2O	0	0	0.001	0	0	0	0	0	0	0
CaO	0.01	0.01	0	0	0.02	0	24.8	24.06	0.65	0.65
TiO_2	0.02	0.03	0.008	0	0.05	0.031	0.04	0	0	0
Cr_2O_3	0.04	0	0.006	0	53.47	48.166	0.68	0.5	0.37	0.29
MnO	0.19	0.17	0.117	0.108	0.27	0.346	0.08	0.1	0.11	0.17
FeO	9.05	9.04	9.067	8.663	19.28	20.438	1.65	1.64	5.93	5.74
Total	100.24	99.58	100.506	99.836	98.82	95.279	100.22	100.17	100.04	99.58
Cations										
Na	0	0	0	0	0	0.002	0	0.001	0	0
Mg	1.784	1.799	1.815	1.828	0.511	0.555	0.951	0.965	1.746	1.751
Al	0	0	0	0	0.583	0.61	0.043	0.034	0.037	0.039
Si	1.012	1.005	0.999	0.996	0.002	0	1.969	1.99	1.993	1.992
P	0.001	0	-	-	0	-	0	0	0	0
K	0	0	0	0	0	0	0	0	0	0
Ca	0	0	0	0	0	0	0.962	0.93	0.024	0.024
Ti	0	0.001	0	0	0.001	0	0.001	0	0	0
Cr	0.001	0	0	0	1.381	1.291	0.019	0.014	0.01	0.008
Mn	0.004	0.003	0.002	0.002	0.007	0.01	0.003	0.003	0.003	0.005
Fe	0.184	0.185	0.184	0.177	0.527	0.579	0.05	0.049	0.17	0.166
Total	2.986 (O = 4)	2.994 (O = 4)	3 (O = 4)	3.003 (O = 4)	3.012 (O = 4)	3.047 (O = 4)	3.999 (O = 6)	3.987 (O = 6)	3.984 (O = 6)	3.984 (O = 6)
Mg#	90.65	90.67	90.8	91.2	49.23	48.9	95	95.17	91.13	91.34
Cr#					70.3	67.9				

Table 4.3 Mineral chemistry data of 1M1 lherzolite, which is caught in the discordant dunite channel.

Elements	Olivine	Olivine	Olivine	Olivine	Spinel	Spinel	Cpx	Cpx
Na_2O	0.01	0.01	0	0	0	0	0.19	0.16
MgO	48.51	48.41	48.31	48.45	11.57	11.58	16.62	16.69
Al_2O_3	0	0	0	0	23.43	23.32	2.56	2.55
SiO_2	40.88	40.82	40.73	40.53	0.07	0.12	52.61	52.99
P_2O_5	0	0.01	0	0	0.01	0.07	0	0
K_2O	0	0	0	0.01	0	0	0	0.01
CaO	0.03	0.01	0.03	0.01	0.01	0	24.05	23.94
TiO_2	0.01	0	0.06	0.06	0.17	0.11	0.04	0.14
Cr_2O_3	0	0.03	0	0.04	41.8	42.87	1.16	0.27
MnO	0.17	0.12	0.1	0.07	0.38	0.24	0.07	0.03
FeO	9.11	9.58	9.5	9.7	18.6	18.47	2.13	2.4
NiO	0.45	0.47	0.37	0.39	0.07	0.12	0.02	0.01
Total	99.17	99.46	99.1	99.26	96.09	96.89	99.45	99.19
Cations								
Na	0	0.001	0	0	0	0	0.013	0.011
Mg	1.783	1.778	1.779	1.784	0.554	0.55	0.908	0.912
Al	0	0	0	0	0.886	0.875	0.111	0.110
Si	1.008	1.005	1.006	1.001	0.002	0.004	1.928	1.942
P	0	0	0	0	0	0.001	0.000	0.000
K	0	0	0	0	0	0	0.000	0.000
Ca	0.001	0	0.001	0	0	0	0.944	0.940
Ti	0	0	0.001	0.001	0.004	0.003	0.001	0.004
Cr	0	0.001	0	0.001	1.061	1.079	0.034	0.008
Mn	0.004	0.002	0.002	0.001	0.01	0.006	0.002	0.001
Fe	0.188	0.197	0.196	0.2	0.499	0.492	0.065	0.074
Ni	0.009	0.009	0.007	0.008	0.002	0.003	0.001	0.000
Total cation	2.992 (4 oxygen)	2.994 (4 oxygen)	2.993 (4 oxygen)	2.997 (4 oxygen)	3.018 (4 oxygen)	3.013 (4 oxygen)	4.006 (6 oxygen)	4.001 (6 oxygen)
Mg#	90.5	90	90	89.9	52.6	52.8	93.3	92.5
Cr#					54.5	55.2		

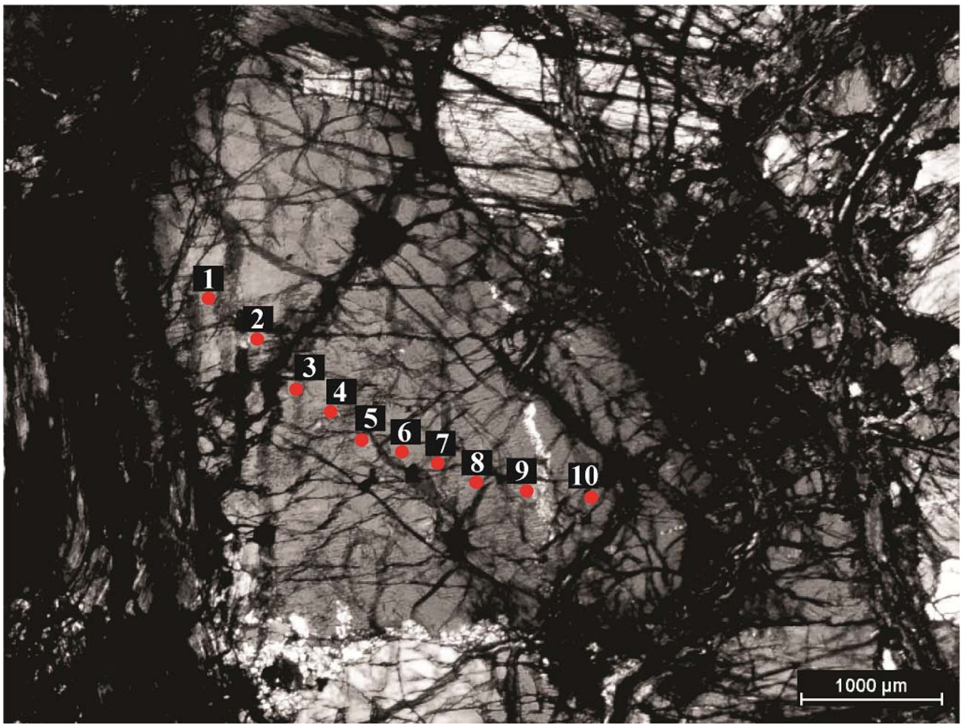

Fig. 4.20. Photomicrograph of an orthopyroxene porphyroclast showing 10 spots for Electron Micro -Probe Analysis. This grain is adjacent and similar to the one containing the relict grains.

Table 4.4 Electron Probe Micro Analyses of points, 1 to 10 across an enstatite grain. The analyzed grain is on the opposite side of the high pressure relict bearing enstatite. The enstatite – ferrosilite solid solution is calculated from 1 – 10 and they are respectively – $En_{91.35}$ $Fs_{8.65}$ (1), $En_{90.6}$ $Fs_{9.4}$ (2), $En_{90.5}$ $Fs_{9.5}$ (3), $En_{90.7}$ $Fs_{9.3}$ (4), $En_{90.7}$ $Fs_{9.3}$ (5), $En_{89.9}$ $Fs_{10.1}$ (6), $En_{91.1}$ $Fs_{8.9}$ (7), $En_{90.6}$ $Fs_{9.4}$ (8), $En_{90.2}$ $Fs_{9.8}$ (9), $En_{90.6}$ $Fs_{9.4}$ (10).

Oxides	1	2	3	4	5	6	7	8	9	10
Na_2O	0	0.01	0.01	0.01	0.04	0.01	0.01	0.01	0.04	0.21
MgO	31.78	33.1	33.01	31.59	31.38	33.1	32.19	33.32	33.26	33.3
Al_2O_3	1.87	2.01	1.99	2.11	2.03	1.93	1.9	1.95	1.96	1.7
SiO_2	56.01	56.29	56.22	55.69	55.72	55.87	55.86	55.72	55.85	56.19
P_2O_5	0	0	0.01	0.02	0.06	0	0.01	0.01	0	0
K_2O	0	0	0	0.02	0	0.01	0	0.02	0.04	0.08
CaO	3.1	0.73	0.79	3.15	3.67	0.73	2.14	0.67	0.61	0.59
TiO_2	0.03	0.02	0	0	0.05	0.01	0.01	0.05	0.08	0.06
Cr_2O_3	0.49	0.52	0.58	0.52	0.67	0.7	0.71	0.59	0.66	0.43
MnO	0.15	0.18	0.14	0.11	0.14	0.15	0.26	0.17	0.21	0.2
FeO	5.36	6.13	6.16	5.81	5.74	6.61	5.6	6.2	6.4	6.12
NiO	0.07	0.08	0.02	0.07	0.16	0.05	0.1	0.08	0.1	0.16
Total	98.86	99.07	98.94	99.11	99.66	99.18	98.79	98.8	99.22	99.03
Na	0	0	0.001	0	0.003	0.001	0.001	0.001	0.003	0.014
Mg	1.659	1.719	1.716	1.65	1.633	1.723	1.682	1.738	1.73	1.732
Al	0.077	0.083	0.082	0.087	0.083	0.08	0.079	0.08	0.081	0.07
Si	1.962	1.961	1.961	1.951	1.946	1.951	1.958	1.949	1.948	1.961
P	0	0	0	0.001	0.002	0	0	0	0	0
K	0	0	0	0.001	0	0	0	0.001	0.002	0.004
Ca	0.116	0.027	0.03	0.118	0.137	0.027	0.08	0.025	0.023	0.022
Ti	0.001	0	0	0	0.001	0	0	0.001	0.002	0.001
Cr	0.014	0.014	0.016	0.014	0.018	0.019	0.02	0.016	0.018	0.012
Mn	0.004	0.005	0.004	0.003	0.004	0.005	0.008	0.005	0.006	0.006
Fe	0.157	0.179	0.18	0.17	0.168	0.193	0.164	0.181	0.187	0.179
Ni	0.002	0.002	0.001	0.002	0.005	0.001	0.003	0.002	0.003	0.004
Total (O = 6)	3.992	3.991	3.99	3.998	4	4	3.993	4.002	4.002	4.005
Mg#	91.35	90.6	90.5	90.7	90.7	89.9	91.1	90.6	90.2	90.6

Table 4.5 EPM analyses of olivine, orthopyroxene, clinopyroxene and spinel in a lherzolite (3) representative of the ultramafics cut by the dunite channel.

Elements	Olivine	Olivine	Opx	Opx	Cpx	Cpx	Spinel	Spinel
Na_2O	0	0.02	0	0	0.1	0.12	0	0.02
MgO	48.95	48.91	33.26	32.87	16.49	16.02	2.28	3.31
Al_2O_3	0	0	3.8	3.97	3.28	3.67	1.25	1.96
SiO_2	41.35	41.44	55.69	55.53	52.33	52.46	1.8	2.7
P_2O_5	0.03	0.02	0.03	0	0	0	0	0
K_2O	0	0.04	0.01	0.02	0	0	0	0
CaO	0	0.02	0.62	0.67	24.91	24.79	0.01	0
TiO_2	0	0.03	0.03	0.06	0.11	0.17	0.26	0.13
MnO	0.15	0.16	0.09	0.18	0.06	0.09	0.31	0.29
FeO	9.3	9.62	5.97	5.88	1.79	1.93	70.42	67
Cr_2O_3	0	0	0.91	0.75	0.9	1.01	17.25	17.91
Total	99.77	100.3	100.4	99.95	99.97	100.26	93.58	93.33
Na	0	0.001	0	0	0.007	0.009	0	0.014
Mg	1.784	1.777	1.704	1.691	0.896	0.868	1.22	1.727
Al	0	0	0.154	0.161	0.141	0.157	0.527	0.809
Si	1.011	1.01	1.914	1.916	1.907	1.906	0.644	0.945
P	0.001	0	0.001	0	0	0	0	0
K	0	0.001	0.001	0.001	0	0	0	0
Ca	0	0.001	0.023	0.025	0.973	0.965	0.003	0
Ti	0	0.001	0.001	0.002	0.003	0.005	0.07	0.035
Mn	0.003	0.003	0.003	0.005	0.002	0.003	0.095	0.086
Fe	0.19	0.196	0.172	0.17	0.055	0.059	21.125	19.584
Cr	0	0	0.025	0.02	0.026	0.029	4.893	4.949
Total	2.988	2.99	3.995	3.992	4.01	4	28.576	28.149
	(O = 4)	(O = 4)	(O = 6)	(O = 6)	(O = 6)	(O = 6)	(O = 32)	(O = 32)
Mg#	90.37	90.06	90.83	90.86	94.22	93.63	5.46	8.1
Cr#							90.28	85.95

Table 4.6 EPM analyses of olivine, orthopyroxene and spinel in a harzburgite (1NU29) representative of the ultramafics cut by the dunite channel.

Elements	Olivine	Olivine	Olivine	Opx	Opx	Opx	Spinel	Spinel
Na_2O	0	0	0	0	0	0.01	0.02	0
MgO	49.33	49.75	49.26	34.55	34.53	34.17	9.38	9.4
Al_2O_3	0.01	0	0	0.67	0.59	0.69	10.76	10.92
SiO_2	41.45	41.46	41.94	58.12	58.49	58.48	0.02	0.05
P_2O_5	0	0.01	0.01	0	0.02	0.01	0.03	0.02
K_2O	0	0.01	0	0	0.01	0	0.04	0
CaO	0.01	0.03	0.01	0.71	0.9	1.33	0.01	0.02
TiO_2	0.03	0.05	0.04	0	0	0.02	0.06	0.1
MnO	0.14	0.03	0.11	0.12	0.05	0.11	0.32	0.38
FeO	8.49	8.67	8.6	5.43	5.36	5.42	20.43	20.75
Cr_2O_3	0.01	0.02	0.08	0.39	0.3	0.39	58.74	58.19
Total	99.47	100	100.1	99.98	100.24	100.6	99.8	99.83
Na	0	0	0	0	0	0	0.009	0
Mg	1.797	1.803	1.783	1.768	1.761	1.74	3.722	3.726
Al	0	0	0	0.027	0.024	0.028	3.375	3.424
Si	1.012	1.008	1.018	1.995	2.001	1.997	0.005	0.013
P	0	0	0	0	0.001	0	0.007	0.005
K	0	0	0	0	0	0	0.013	0
Ca	0	0.001	0	0.026	0.033	0.049	0.002	0.006
Ti	0.001	0.001	0.001	0	0	0.001	0.011	0.02
Mn	0.003	0.001	0.002	0.003	0.001	0.003	0.072	0.085
Fe	0.173	0.176	0.175	0.156	0.153	0.155	4.545	4.616
Cr	0	0	0.002	0.01	0.008	0.011	12.356	12.236
Total	2.987	2.991	2.98	3.986	3.982	3.983	24.118	24.13
	(O = 4)	(O = 4)	(O = 4)	(O = 6)	(O = 6)	(O = 6)	(O = 32)	(O = 32)
Mg#	91.22	91.11	91.06	91.89	92	91.82	45.02	44.66
Cr#							21.45	21.86

Table 4.7 EPM analyses of HP Mg_2SiO_4 and its mineral chemical data is compared with the matrix olivines in the lherzolite 1NU27. The analysed spots are shown in Fig.4.19 A.

	SP 1	SP2	Inc 1	Inc 2	B Ol 1	B Ol2	Ol
MgO	9.25	9.52	49.3	49.39	49.49	49.15	48.21
Al_2O_3	15.13	14.69	0	0	0	0	0
SiO_2	0.03	0.06	41.43	41.46	41.05	41.33	41.35
P_2O_5	0	0.01	0.05	0.05	0	0	0.01
K_2O	0	0.01	0	0	0	0	0
CaO	0.02	0	0.05	0	0.02	0.01	0.02
TiO_2	0.05	0.04	0.01	0.04	0.02	0	0.03
Cr_2O_3	51.26	52.19	**0.43**	**0.48**	**0.64**	**0.44**	**0**
MnO	0.27	0.34	0.21	0.13	0.16	0.13	0.15
FeO	20.57	19.88	6.98	6.99	7.28	7.53	8.72
Total	96.62	96.76	98.47	98.54	98.67	98.58	98.5

CHAPTER 5

MICRO TEXTURES AND VOLATILE PHASES

CHAPTER 5

MICRO TEXTURES AND VOLATILE PHASES

5.1 CHAPTER OVERVIEW

The micro textures and volatile phases preserve valuable information about individual stages of complex evolution of a rock. They retain signature of physicochemical condition of precursor of host rocks. With the help of experimental data those signatures are substantiated to decipher at least the P – T condition. Though there are some textural cases where P – T condition was not determined due to lack of support from experimental data. Extent of such phases and their role in case of evolution of ophiolite ultramafics is not well attempted till date. In this chapter such evidences are elaborated to decode systematic evolution of Nidar ophiolite.

5.2 LITHOLOGICAL DESCRIPTION OF THE STUDIED ROCKS

The micro textures are studied in pyroxenite and two lherzolites. The pyroxenite occur as 4 – 6 cm wide veins in channelized dunite in Nidar valley (Fig 4.1 B). One of the studied lherzolite is entrapped in dunite channel (sample no. 1NU27) (Fig 2.7). The other lherzolite belongs to the group cut by the channelized dunite (Fig 2.7). In the earlier discussed very high pressure lherzolite (Fig 2.7) xenolith bodies (1M1 and 1NU27) hydrocarbon fluid inclusions are obtained as signature of reducing deep mantle. Other volatile phases are studied on serpentinites and ultramafics cut by the dunite channel.

5.3 CHARACTERIZATION OF EXSOLUTION MICRO TEXTURES

In early decades fine scale exsolution micro textures in magmatic rocks were widely interpreted as results decrease in solubility because of cooling (Robinson et al., 1971, Lally et al., 1975). There were some instances where exsolution is thought to take place due to change in oxygen fugacity (Buddington and Lindsley, 1964). Few of them were considered as result of both decompression and cooling (Robinson et al., 1972). But recently there are some electrifying reports claiming that exsolution micro texture preserves signature of decompression (Dobrzhinetskaya et al., 1996, Van Roermond et al., 1998, Katayama et al., 2000) which shifts the paradigm of the exsolution micro texture studies. In the present thesis different types of exsolution micro textures are shown from ultramafic rocks of Nidar ophiolite which indicates complex evolution of ophiolite from a heterogeneous source. Ultramafic rocks from mantle section of the Nidar ophiolite bear diverse varieties of exsolution micro textures; some of them are described according to their occurrence. The details of textures in the pyroxenite vein within dunite channel and two lherzolites (1NU27, entrapped within the dunite channel; another lherzolite cut by the dunite channel) are given here.

Pyroxenite

Many pyroxenite veins (4 – 6 cm wide) are noticed within the channelized dunite body. The veins are mainly composed of orthopyroxene (50%) and clinopyroxene (45%) with more or less no serpentinization (~ 5%).The pyroxenes display different varieties of exsolution. Such as -

(a) Exsolution of Ca – pyroxene in enstatite

Some cleavageless orthopyroxene (enstatite) bear thin rectilinear lamellae (thickness ~2 μm) of Ca – pyroxene in it (Fig5.1 A, Table 5.1). It appears under microscope that the lamellas are parallel to each other. This could be a case of diopside exsolution in enstatite.

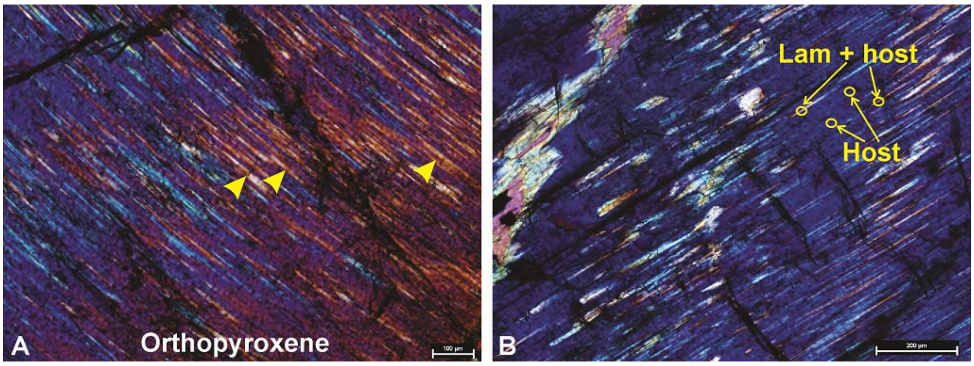

Fig 5.1.A. Exsolution lamellae in pyroxene marked by the yellow coloured arrow. B. The composition of the lamellae and the host pyroxene was determined by the broad beam EPMA technique. The spots are marked here.

	Lam + host	Lam + host	Host	Host
Na_2O	0.013	0.037	0	0.007
SiO_2	55.699	55.604	56.579	56.549
K_2O	0	0	0	0
CaO	5.404	5.822	0.384	0.548
MgO	30.179	29.948	33.911	33.729
Al_2O_3	1.339	1.347	1.154	1.083
MnO	0.156	0.146	0.182	0.189
TiO_2	0.053	0.008	0.017	0
FeO	6.111	6.147	7.557	7.388
Cr_2O_3	0.463	0.454	0.384	0.292
Total	99.417	99.513	100.168	99.785

Table 5.1. EPMA data of exsolution lamellae and host shown in the Fig 5.1.B are shown here. The exsolved pyroxene is Ca rich with respect to the enstatite host.

Broad beam EMPA analyses were carried out on the lamellas (which sometimes give chemistry of lamella + host mineral) and they are compared with the chemistry of host mineral. It is found that the host is enstatite (MgO ~ 33 – 34%) and the lamella is enriched in CaO (5.4 – 5.8%) and deficient of MgO (29 – 30%). The Ca pyroxene exsolution from an enstatite host is generally effect of cooling from a high T condition.

(b) SiO_2 exsolution in enstatite

In an enstatite pyroxene numerous curvilinear SiO_2 exsolution lamellas (20 – 100 μm) are observed (Fig.5.2.A, B) along with some Ca pyroxene. The presence of silica is confirmed by EDX analyses. The exsolution rich part is much richer in Mg and Si according to the given line scan in Fig.5.2.H and Fig.5.2.I. It is also observed that the concentration of K increases with the Si (Fig.5.2.G). The area mapping in Fig.5.2.C also suggests enrichment of Si in exsolution rich zone.

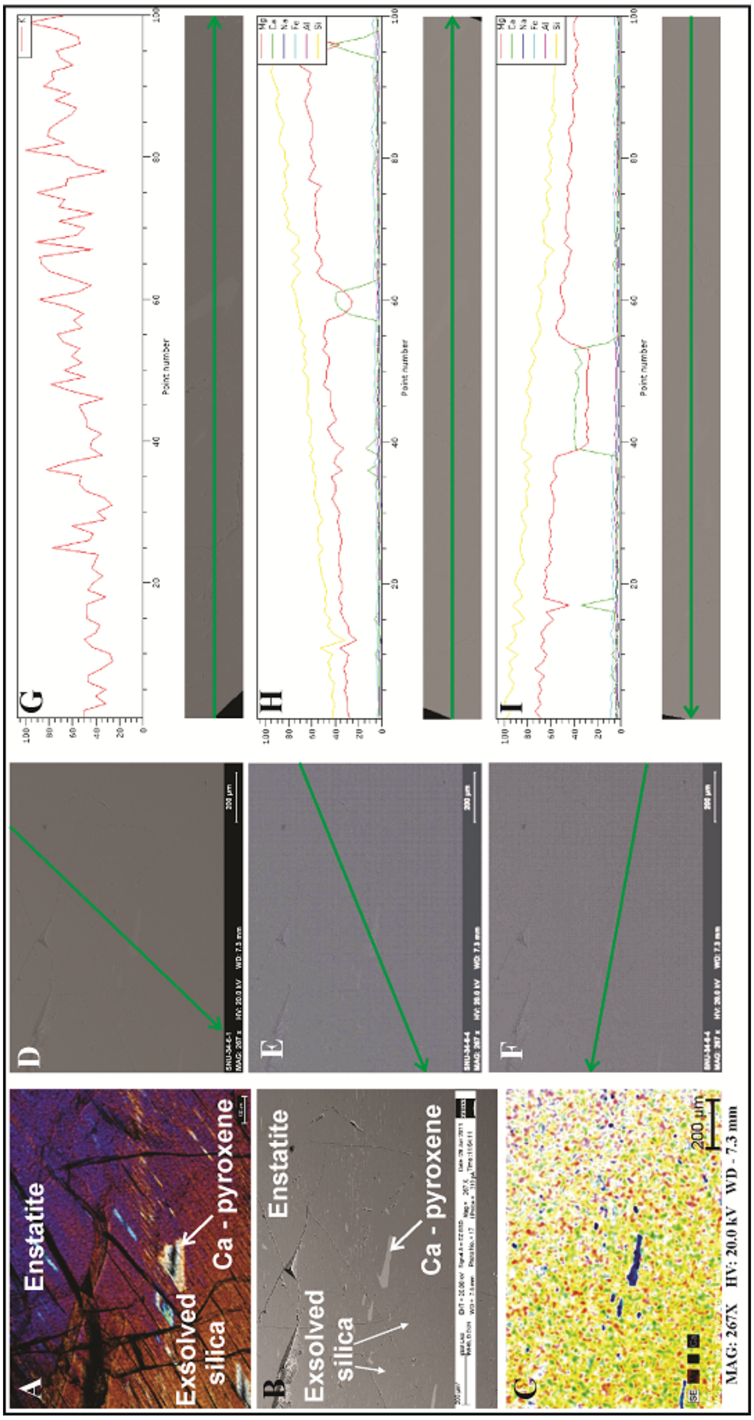

Fig 5.2.A. Photomicrograph of an enstatite with different exsolved phases within it. B. BSE image of the view similar to the A. C. The mapping of three elements Mg (red), Si (green) and Ca (blue) in the given selected area suggests enrichment of Si towards the left portion of the photograph A & B. D & G, Line scan showing increase in concentration of K towards the left part of the selected area shown in A. E – H & F - I, Towards the left part Mg and Si concentration also increase.

Silica exsolution in clinopyroxene is generally explained as decomposition of Ca – Eskola (Ca – E) to Ca – Tschermaks (Ca – T) and free silica. Earlier this exsolution were interpreted as the result of both cooling and decompression (Katayama et al., 2000). But recent studies (Page et al., 2005; Konzett et al., 2008) claim that Ca – E break down is mainly function of temperature and bulk composition. For the lack of other independent high pressure signature the silica exsolution is interpreted as result of cooling.

(c) Ca – pyroxene exsolution needles in two pyroxene

In pyroxenite vein, two pyroxene texture is observed (Fig 5.3.A). The mineral chemistry data (through EPMA) reveals that the one part is diopside (CaO ~ 24%) and another is enstatite (MgO ~ 32%) (Table 5.2). The two pyroxene grain bear numerous rectilinear strongly oriented exsolution lamellae (Fig 5.3.B). The broad beam EMPA data suggests that the exsolved lamellae is Ca – pyroxene (CaO ~ 2%). The high concentration of MgO is due to matrix contamination.

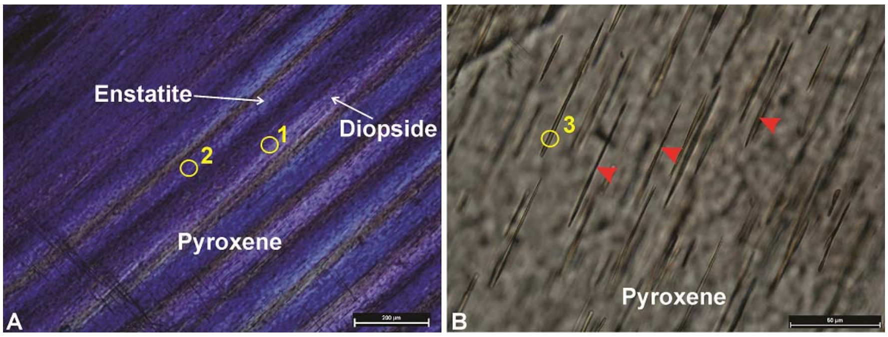

Fig 5.3.A. Photomicrograph of two pyroxene texture. B. Rectilinear strongly oriented exsolution lamellae in the two pyroxene grain. The marked spots are points of EMP analyses.

Element	1	2	3
Na_2O	0.101	0	0
SiO_2	53.895	56.032	56.383
K_2O	0	0	0
CaO	23.99	0.474	1.908
MgO	17.428	32.153	31.618
Al_2O_3	1.028	1.314	0.907
MnO	0.085	0.2	0.199
TiO_2	0.012	0	0.002
FeO	2.548	9.203	9.195
Cr_2O_3	0.512	0.457	0.225
Total	99.599	99.833	100.437

Table 5.2. Mineral chemistry data of two pyroxene and the exsolved lamellae marked in Fig 5.3.

The two pyroxene micro texture and Ca – pyroxene exsolution from it is interpreted as result of temperature fall.

Lherzolite cut by the dunite channel

A lherzolite (sample no. 3; details given in chapter 4) of the part which are cut by the dunite channel also displays some exsolution micro textures in pyroxene. The rock is essentially composed of olivine (40%), orthopyroxene (20%), clinopyroxene (17%) and Cr – spinel (3%). The rock is moderately serpentinized (20%). Two types of exsolution micro textures are observed in pyroxenes. Their details are given here:

(a) Exsolution of clinoenstatite and Al – spinel in diopside

In a pyroxene two types of exsolved phases are found (Fig 5.4). One occur as transparent rods (length 8 – 14 µm; width 3 – 4 µm). The others are opaque (length 8 – 10; width 2 µm) and lie in perpendicular direction of the transparent lamellae. Some places the opaque phases are present in both direction.

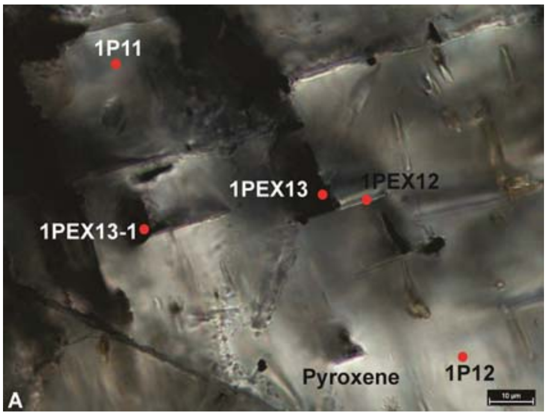

Fig 5.4.A. Photomicrograph of two types of exsolution lamellas in pyroxene. Strongly oriented transparent exsolution rods lie coherently with the opaque exsolution rods. The opaque precipitates show two orientation – one parallel to the transparent lamellas; another perpendicular to them. The marked points are spots of EMPA analyses.

Laser Raman spectroscopy suggests that the transparent lamellas are clinopyroxene and the opaque lamella are probably spinel (Fig 5.5). The mineral chemistry data through EPMA indicate that the transparent lamellas are $MgSiO_3$ pyroxene (Table 5.3).

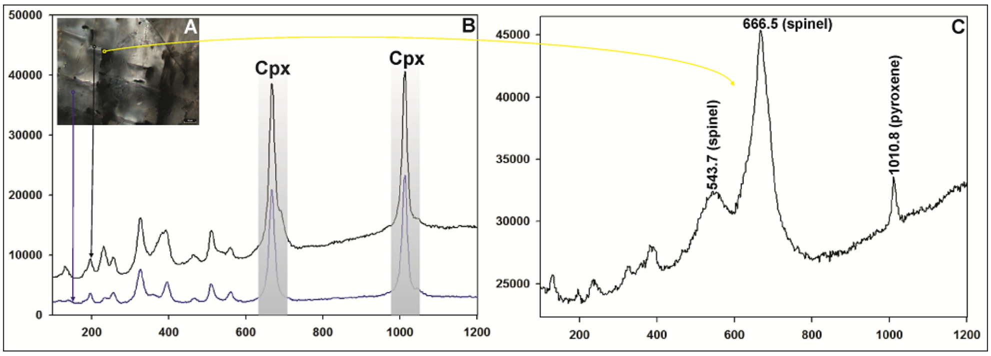

Fig 5.5.A. The inset photomicrograph indicates the analysed spots of Laser Raman spectroscopy. B. The host and the transparent exsolution rods both show clinopyroxene Raman spectrum. C. The opaque lamellas show trend of spinel.

	1P11	1P12	1PEX12	1PEX13	1PEX13-1
Na_2O	0.1	0.12	0.05	0.05	0.04
MgO	16.49	16.02	36.4	30.6	23.44
Al_2O_3	3.28	3.67	3.33	4.18	6.4
SiO_2	52.33	52.46	41.41	42.6	45.34
P_2O_5	0	0	0	0	0
K_2O	0	0	0.04	0	0.01
CaO	24.91	24.79	0.49	5.42	13.06
TiO_2	0.11	0.17	0	0.05	0.1
MnO	0.06	0.09	0	0	0.06
FeO	1.79	1.93	4.4	3.47	3.17
Cr_2O_3	0.9	1.01	1.04	1.55	1.09
Total	99.97	100.26	87.16	87.92	92.72

Table 5.3. EPMA data of spots on host pyroxene and the exsolved lamellas corresponding to the Fig 5.4.

Hence they are clinoenstatite. The suspected spinel lamellas are enriched in Al (Table 5.3). The clinoenstatite could be either high P

Cen or low P Cen. It cannot be characterized because of paucity of high pressure evidences. But exsolution of high valence cations may require high pressure condition to incorporate Al – spinel in clinopyroxene. That case the clinoenstatite could be likely high P Cen.

(b) Clinoenstatite in diopside

In another pyroxene of the same lherzolite 2 set of lamellar inclusions are observed (Fig 5.6 A). The lamellas occupy the core of the pyroxene. The length and width of the lamellas are > 100 – 200 µm and 4 – 6 µm respectively.

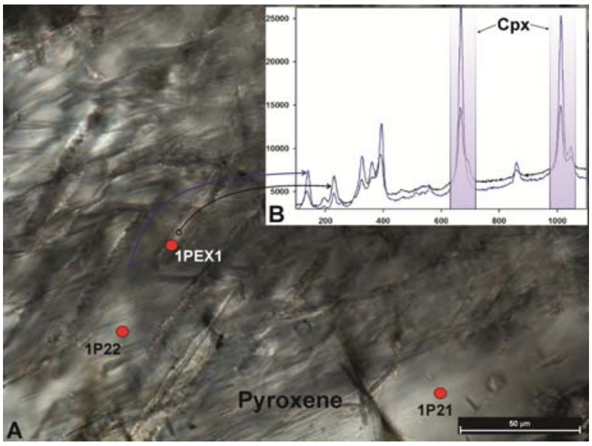

Fig 5.6.A. The photomicrograph shows two sets of lamellae in a pyroxene grain. The analysed EPMA spots are marked as 1P21, 1P22 and 1PEX1. B. The inset shows Raman spectra of host pyroxene and the lamellae. From Raman trend it can be inferred that both the host and the lamellas are clinopyroxene.

	1P21	1P22	1PEX1
Na_2O	0.12	0.13	0.05
MgO	16.39	16.33	33.74
Al_2O_3	3.32	3.79	3.39
SiO_2	52.92	52.35	42.29
P_2O_5	0	0.03	0
K_2O	0.01	0	0
CaO	24.67	24.33	3.27
TiO_2	0.14	0.15	0.05
MnO	0.11	0.13	0.03
FeO	2.1	2.05	3.65
Cr_2O_3	0.93	0.79	0.9
Total	100.71	100.08	87.37

Table 5.4. EPMA data of spots on host pyroxene and the lamellas corresponding to the Fig 5.6.

Raman spectra of lamellas follow trend of a clinopyroxene (Fig 5.6 B). The host also shows Raman spectra of clinopyroxene. Mineral chemical data obtained through EPMA suggests the host is diopsidic clinopyroxene (CaO ~ 24%; MgO ~ 16%). Broad beam EMPA data infer the lamellas are enstatite (MgO ~ 33%; CaO ~ 3%) in composition. Combined mineral chemistry and Raman spectral analyses indicate that the lamellas are clinoenstatite within a diopsidic clinopyroxene host. In this case also it is hard to characterize the clinoenstatite as high P or low P independently. But presence of Al – spinel exsolution in diopside in the same rock advocate for a high P clinoenstatite.

Lherzolite entrapped in the dunite channel

Some lherzolites, which are entrapped within the dunite channel, bear signatures of the deep mantle origin as discussed in the earlier chapter. One of them (1NU27) shows unusual exsolution and precipitation micro textures. The lherzolite (1NU27) is almost not serpentinized (~5%) and shows assemblage of olivine (50%), orthopyroxene (25%), clinopyroxene (15%) and Cr spinel (~5%). The studied micro textures are described below:

(a) Cr – spinel exsolution needles in olivine

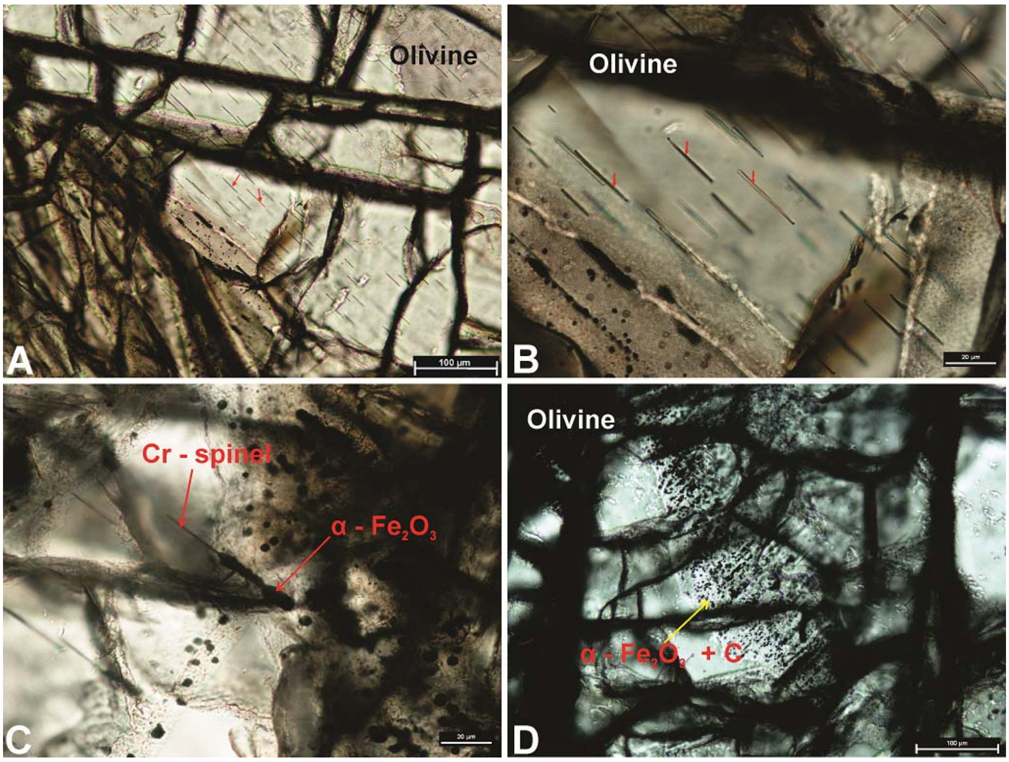

Fig 5.7.A, B. The photomicrographs show strongly oriented needles (marked by red arrow) in olivine. C. The Cr – spinel needle is attached with the $\alpha - Fe_2O_3$ phase. D. Precipitation micro texture of $\alpha - Fe_2O_3$ in olivine.

In the lherzolite strongly oriented rectilinear needles (length 12 – 30 μm; width 1 μm) are found in olivine (Fig 5.7 A, B, 5.8). The needles are translucent and have higher relief. From the polished surface of the thin sections and calculating with “Nikon” software the area occupancy of the needles is about 0.3% by volume, and locally up to 0.7%. Laser Raman spectroscopy and EPMA were employed to characterize the tiny needle. In the case of needles the spot size was ~ 2 μm while width of the needles is ~ 1 μm (Fig 5.8). For this the spectrum bear peak of host olivine as background. The deducted Raman spectra of needles show characteristic peaks of Cr - spinel at 659.3 and 701.7 cm^{-1} (Fig 5.8). Besides the 601.8 cm^{-1} band gets intensified which is close to the 607 cm^{-1} olivine band (Fig 5.8).

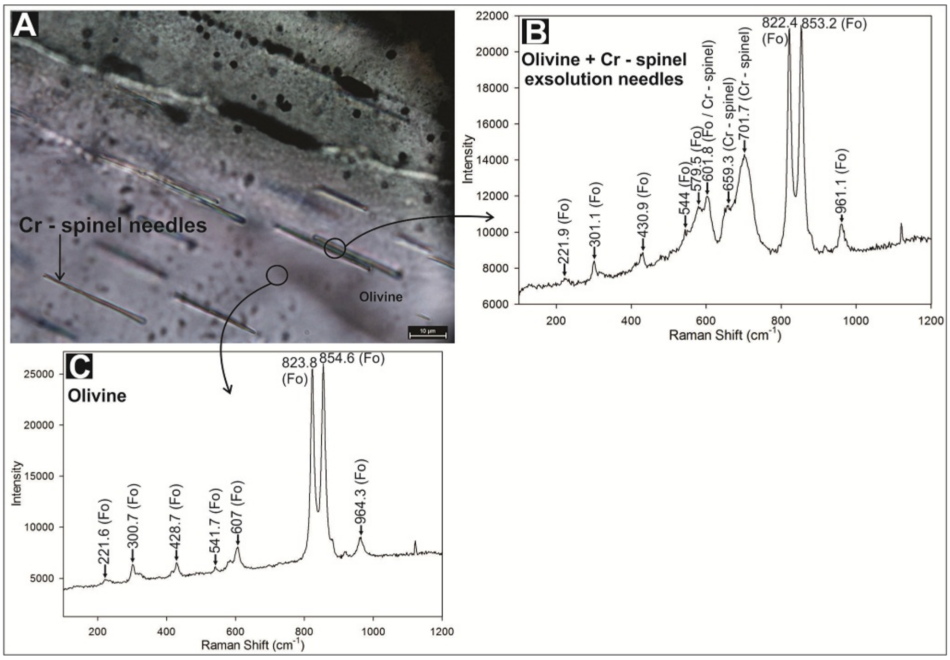

Fig 5.8.A. Strongly oriented needles in olivine are probed by Raman spectroscope. The analysed spots are marked here. B. The Raman trend suggests presence of Cr – spinel + olivine. C. Raman trend of olivine to deduct the peaks of the needle from Fig B.

	Olivine + needle	Olivine + needle	Olivine + needle	Olivine
MgO	46.59	46.75	46.47	48.21
Al_2O_3	**0.69**	**0.55**	**0.85**	**0**
SiO_2	39.4	39.8	39.27	41.35
P_2O_5	0	0	0	0.01
K_2O	0	0	0	0
CaO	0.02	0.04	0.02	0.02
TiO_2	0	0.04	0.01	0.03
Cr_2O_3	**2.05**	**1.93**	**2.34**	**0**
MnO	0.12	0.1	0.14	0.15
FeO	**9.19**	**9.4**	**9.24**	**8.72**
Total	98.06	98.62	98.34	98.5

Table 5.5. Mineral chemical composition of the exsolution needles are deducted from comparison between broad beam EPM analyses of needle + olivine and olivine.

The needles are also analysed by broad beam EPMA technique (Table 5.5). Comparing the data with the host olivine the composition of Cr – spinel was confirmed. The exsolution of Cr – spinel may be due to decompression from a very high pressure condition as reported by early workers (Dobrzhinetskaya et al., 1996) and the primary phase could be β - Mg_2SiO_4. But possibility of a primary β - Mg_2SiO_4 was discarded soon (Hacker et al., 1997) because of lack of supporting evidences for mantle transition zone condition (~ 410 – 660 km depth). In the same lherzolite HP - Mg_2SiO_4 is found as inclusion in Cr – spinel (chapter 4). From mineral chemistry data it is also observed that the HP - Mg_2SiO_4 is Cr rich with respect to the matrix olivine (Fig 4.19, Table 4.7). So it can be correlated that decompression from mantle transition depth resulted in break down of HP - Mg_2SiO_4 (β - Mg_2SiO_4?) and produces Cr – spinel exsolution needles in olivine.

(b) $\alpha - Fe_2O_3$ precipitation in olivine

Some Cr - spinel exsolution needles in olivines of 1NU27 peridotite bear opaque attachments. These opaque attachments are irregular lamellar shaped (length up to 35 µm; width up to 8 µm) (Fig 5.7 C). The opaques are also occurring devoid of needles and they show a large population (Fig 5.7 D). Apart from the lamellar patches they are seen as saccharoidal grains (~ 5 – 15 µm) in olivine (Fig 5.7 D). In rare places the patches individually show orientation in one direction (Fig 5.7 D).

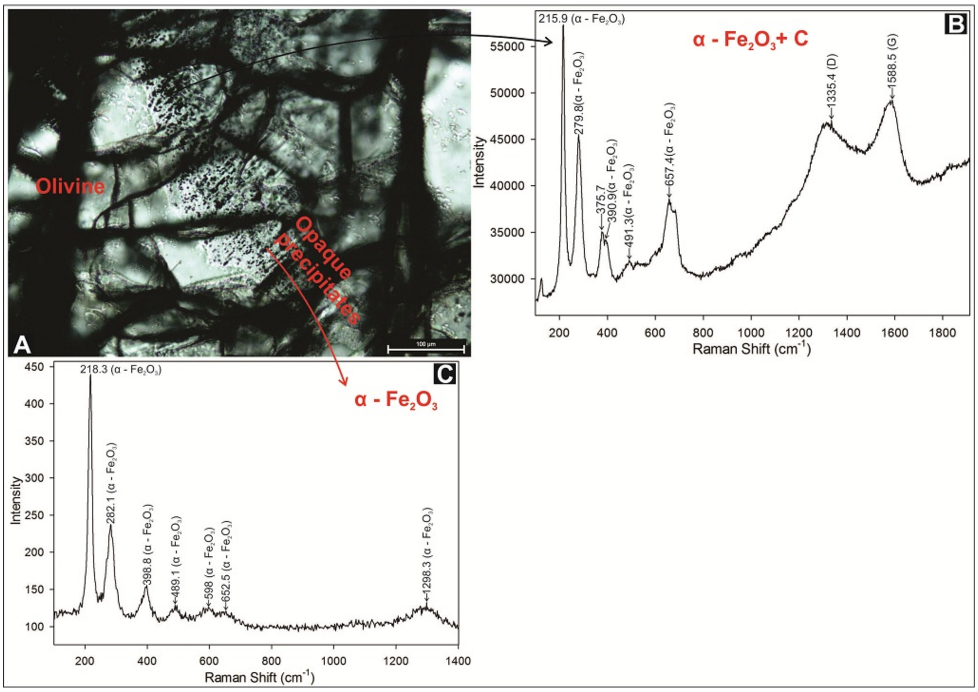

Fig 5.9.A. Opaque precipitates in olivine are analysed by Raman spectroscope. The analysed spots are marked here. B. The Raman trend shows presence of $\alpha – Fe_2O_3$ + C. C. Raman trend of opaque precipitates indicate that they are $\alpha – Fe_2O_3$.

The saccharoidal grains generally occur as scattered manner (Fig 5.7 C). The opaque patches occupy locally up to about 4% area in olivine. Sometimes the opaques are noticed in vein of pyroxene grains (Fig 5.10 A, B). They are essentially restricted within veins (Fig 5.10 A, B). The opaque inclusions show higher reflectance under reflected light (Fig 5.10 B). Through Laser Raman spectroscope the opaque phases in olivine and vein within the pyroxene with high reflectance are identified as $\alpha - Fe_2O_3$ (Fig 5.9 B, C). The characteristic peaks are at 214 – 218.3, 279.8 – 282.1, 394.7 – 398.8, 489.1 - 489.4 and 592.4 - 598 respectively (Fig 5.9 C). The trend shows a 12 – 20 cm^{-1} shift to the lower side with respect to the classical $\alpha - Fe_2O_3$ trend. The calibration at the time of analyses was not higher than 1 cm^{-1}. That could be because of the distortion of the normal structure. The probable reason may be due to precipitation origin of $\alpha - Fe_2O_3$. The occurrence of broad Raman peak at 652.5 – 659.2 and 1295.9 – 1298.3 cm^{-1} indicates disordering in $\alpha - Fe_2O_3$ (Fig 5.9 C) and the disordering is due to high pressure condition (Shim and Duffy 2001).

Some cases $\alpha - Fe_2O_3$ Raman spectrum shows broad peaks of disordered carbons in place of $\alpha - Fe_2O_3$ disordering. The 1335.4 cm^{-1} Raman peak indicate D band and 1588.5 cm^{-1} peak infer G band of the carbon allotropes. The spectrum indicates presence of a coupled $\alpha - Fe_2O_3 + C$ phase (Fig 5.9 B).

Precipitation of $\alpha - Fe_2O_3$ from olivine can be correlated with Cr – spinel exsolution due to P – T fall from mantle transition zone condition.

5.4 CHARACTERIZATION OF MICRO INCLISUIONS

The olivine and pyroxene of high pressure lherzolites of Nidar Ophiolite bear varieties of solid and fluid inclusions which indicate complex evolution of ultramafic rocks of Nidar Ophiolite. They are described here –

(a) Lamellar clinoenstatite inclusion in orthoenstatite

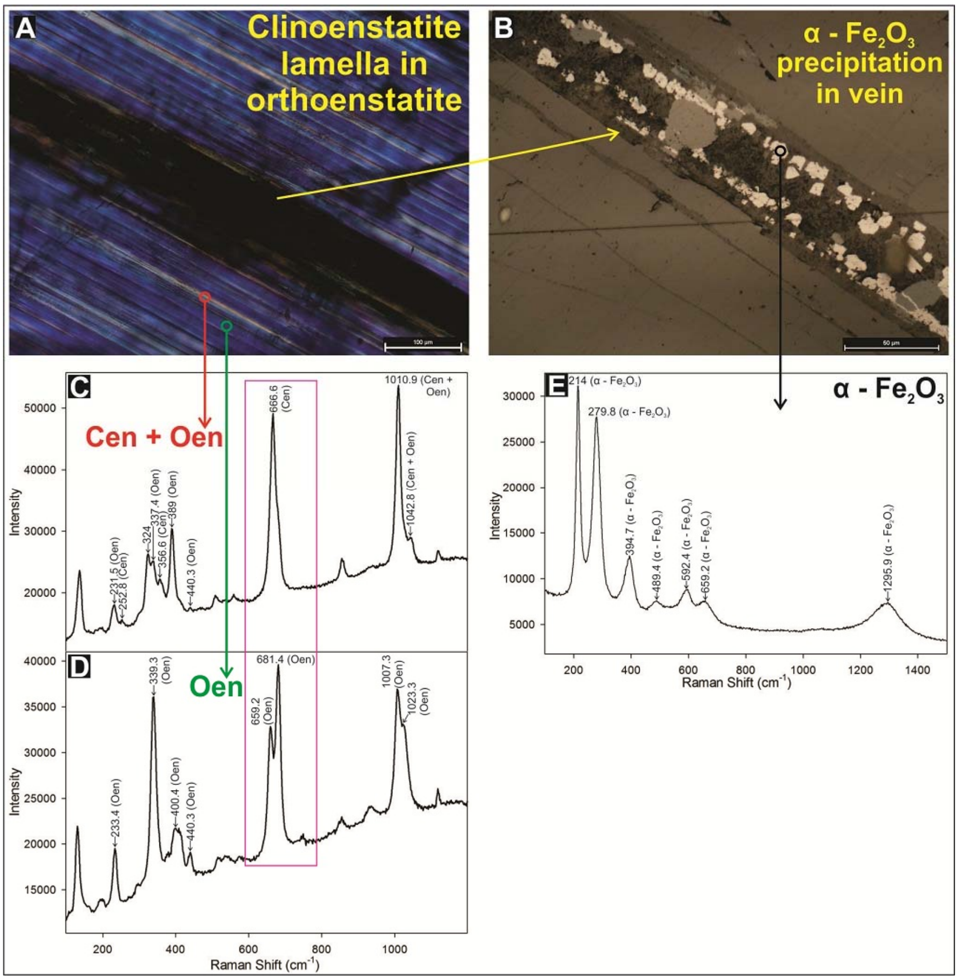

Fig 5.10.A. Photomicrograph of coherent lamellar inclusions of clinoenstatite in orthoenstatite. B. Reflected photomicrograph of saccharoidal α – Fe_2O_3 bearing vein in the same grain. C. Raman spectrum of α – Fe_2O_3 in the vein. D. Raman spectrum of lamellae indicates a clinopyroxene phase. E. Raman spectrum of host pyroxene infer an orthopyroxene phase.

In the previously discussed lherzolite 1NU27, some cleavageless orthopyroxene of lherzolite display rare long (several hundred microns; up to 700 µm) and thin (1 – 2 µm) coherent lamellar inclusions (Fig 5.10 A). Under crossed nicole of an optical microscope the lamella can be easily distinguished (Fig 5.10 A). In plane polarized light the lamellas show higher relief. The lamellas are characterized by combined Raman spectroscopy and EMP analyses.

The closely spaced lamellar inclusions in pyroxene are analysed by EMPA (Table 5.6). At the time of broad bam analyses spot size was ~ 4 - 5 µm and the width of the lamellas are < 2 µm. It is found that there is no marked difference in Ca content between lamella and host enstatite (Table 5.6). It can be said that the lamellas are also $MgSiO_3$ pyroxene (Table 5.6). The lamellas are slightly enriched in Ti with respect to host enstatite.

The lamellar inclusions show a clinopyroxene spectrum where as the host display orthopyroxene Raman band (Fig 5.10.D, E). From the EMP analyses it is clear that both the pyroxenes are $MgSiO_3$. It can be said that the host is orthoenstatite (Oen) and the lamellae phase indicate a mixed clinoenstatite (Cen) and orthoenstatite phase. The splitting of the 666.6 peak into a 659.2, 681.4 doublet from lamellae to host infer a C centered to P centered pyroxene structure (Tribaudino et al., 2012) (Fig5.10 D, E).

Elements	Cen + Oen	Cen + Oen	Oen	Oen
Na_2O	0	0	0	0.01
MgO	33.64	33.85	33.5	33.31
Al_2O_3	1.02	1.04	0.98	1.05
SiO_2	57.54	57.45	57.37	57.48
P_2O_5	0	0	0.01	0.03
K_2O	0	0	0	0
CaO	1	0.63	0.55	0.89
TiO_2	0.05	0.01	0	0
MnO	0.16	0.18	0.15	0.11
FeO	5.75	5.91	5.96	5.57
Cr_2O_3	0.39	0.43	0.56	0.47
Total	99.56	99.5	99.09	98.93

Table 5.6. Mineral chemical composition of the lamellar inclusion are compared with the host enstatite. The lamellas are also $MgSiO_3$ pyroxene.

There are some subtle differences between Cen + Oen lamellae and host Oen in 324 – 389 cm^{-1} region (Fig 5.10 D, E). The 252.8 and 356.6 peaks appeared in lamellae which may be assigned to clinoenstatite (Ulmer and Stalder 2001) (Fig 5.10 D, E). But C centered clinoenstatite may be either low P or high P. But in this case presence of other high P phases indicate the clinoenstatite is of high pressure origin as high T clinoenstatite cannot remain stable > 1 GPa (Pacalo and Gasparik 1990).

(b) Carbon inclusions in olivine

The olivines of the lherzolite 1NU27 bear rare euhedral inclusions of disordered carbons (Fig 5.12 A, B). The hexagonal (Fig 5.11 C) carbon (probably graphite) inclusions are observed in rare places of the olivine of lherzolite 1NU27. Graphitic carbon is interpreted from Raman spectroscopic data. The D band at 1355.9 cm^{-1} and the G band at 1601.8 cm^{-1} confirms the presence of graphitic carbon in olivine. Presence of carbon in very high pressure rock indicates high reducing environment in deep mantle probably in transition zone (410 – 660 km).

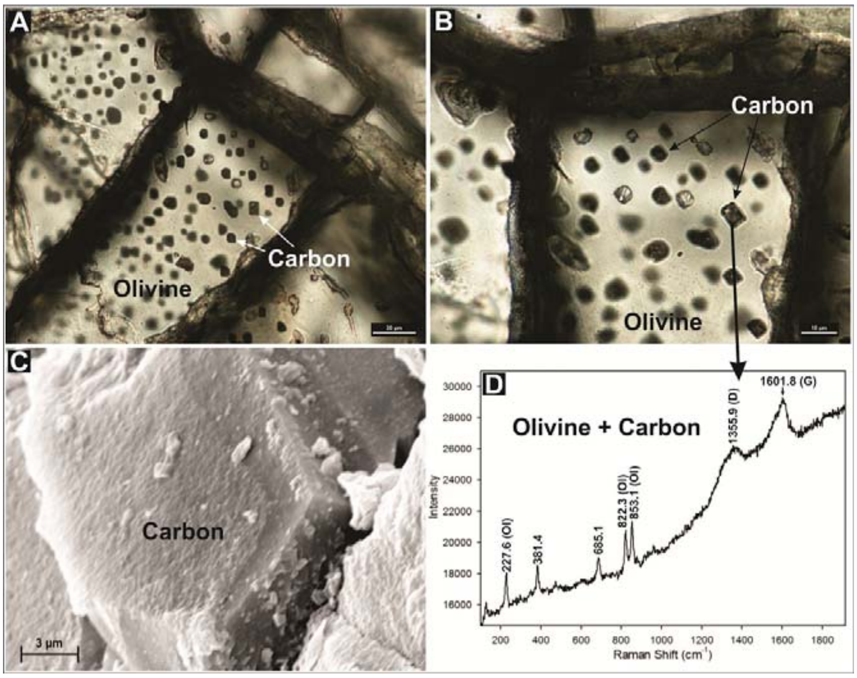

Fig 5.11.A, B. Photomicrograph of euhedral saccharoidal inclusions of graphitic carbon in olivine. C. BSE image of euhedral carbons show hexagonal shape. D. Raman spectrum of the inclusions indicates presence of graphitic carbon phase in olivine. The background olivine peaks suggests that the inclusions are beneath the surface.

5.5 VOLATILE PHASES

Volatile phases play very important role the deep earth processes. They often bear important information regarding the initiation melting, sometimes the primitive condition. In this thesis some rare volatile phases are shown through fluid inclusion study from the mantle transition zone (410 – 660 Km deep). An attempt was also made through characterization of different generations of serpentinization through mineral inclusion study so that events of hydration and dehydrations can be decoded. Different generations of volatile phases are characterized by their presence in the respective rock bodies. Relatively primary and secondary events are further classified by their crosscutting relationship and texture of their host minerals. In very high pressure rock bodies hydrocarbon fluid inclusions are found indicative of a reducing deep mantle. From other ultramafics signature of other primary volatile phases are also obtained which are discussed here.

(a) Aliphatic hydrocarbon

In an olivine of high pressure peridotite 1NU27, a primary fluid inclusion is observed along with the graphitic carbon inclusions (Fig 5.12 A). The fluid inclusion is two – phase (vapour + liquid) and the bubble has no movement, which also indicates the dense nature of that particular fluid inclusion. The composition has been characterised by Laser Raman Spectroscopy. The peaks at 2906 and 2955.7 cm^{-1} are indicative of aliphatic hydrocarbon group (Fig 5.12 B; Krishnan 1961).

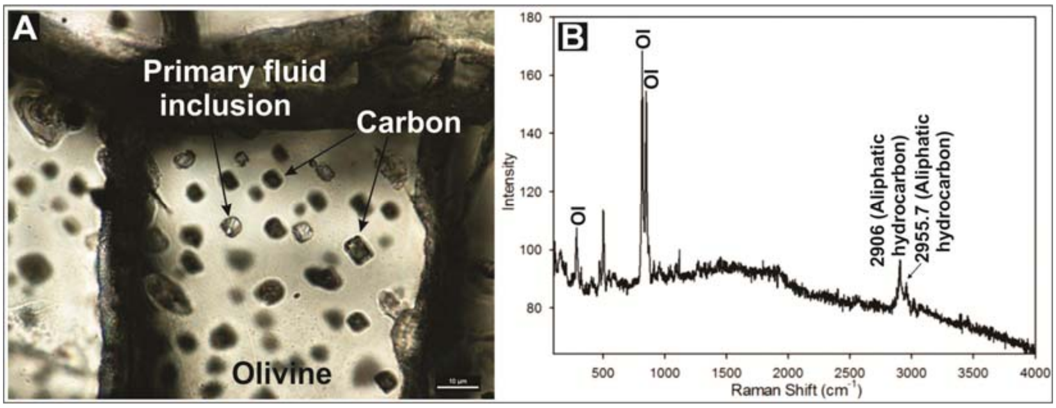

Fig 5.12.A. The photomicrograph shows a dense two phase (fluid + gas) primary fluid inclusion trapped in an olivine. That part of the olivine also contains inclusions of graphitic carbon. B. The Raman spectrum of marked fluid inclusion corresponds to aliphatic hydrocarbon stretching features.

(b) Methane

In lherzolite 1M1, an orthopyroxene found with inclusions of coesite, clinoenstatite and α – Fe_2O_3 (solid + glass) (Fig 4.8). Among the same inclusions some α – Fe_2O_3 inclusions are observed with inclusions of other phases (Fig 5.13 A). Laser Raman spectroscopy suggests that the phases are clinopyroxene (Fig 5.13 B). These clinopyroxene phases sometimes show characteristic peak of methane (CH_4) at ~2915 cm^{-1} (Fig 5.13 B). This methane is primitive with respect to their occurrence within iron oxide inclusion.

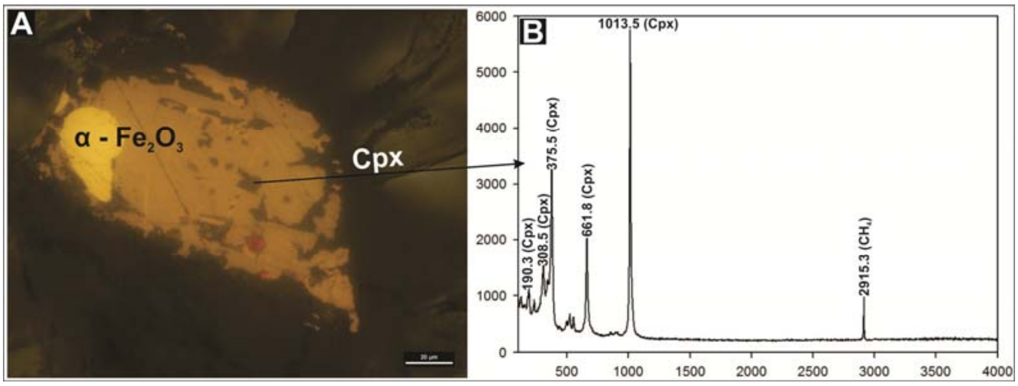

Fig 5.13.A. The α – Fe_2O_3 includes different mineral phases. B. The Raman spectrum of those portions suggests presence of methane with clinopyroxene.

(c) Different generations of hydration and dehydration

The most prominent serpentinization is observed as dominant serpentines in ultramafic rocks of the Nidar ophiolite. But detail study revealed there are multiple generations of hydration. Through petrographic studies of serpentine veins three generations of veining are characterised on the basis of cross cutting relationship in deformed plagioclase peridotite (Fig 5.14 A, B). The plagioclase peridotite is among them which are cut by the dunite channel. Quenched melt is observed as evidence of partial melting that peridotite (Fig 5.14 C). Sometimes the quenched melt contains laths of plagioclase feldspar.

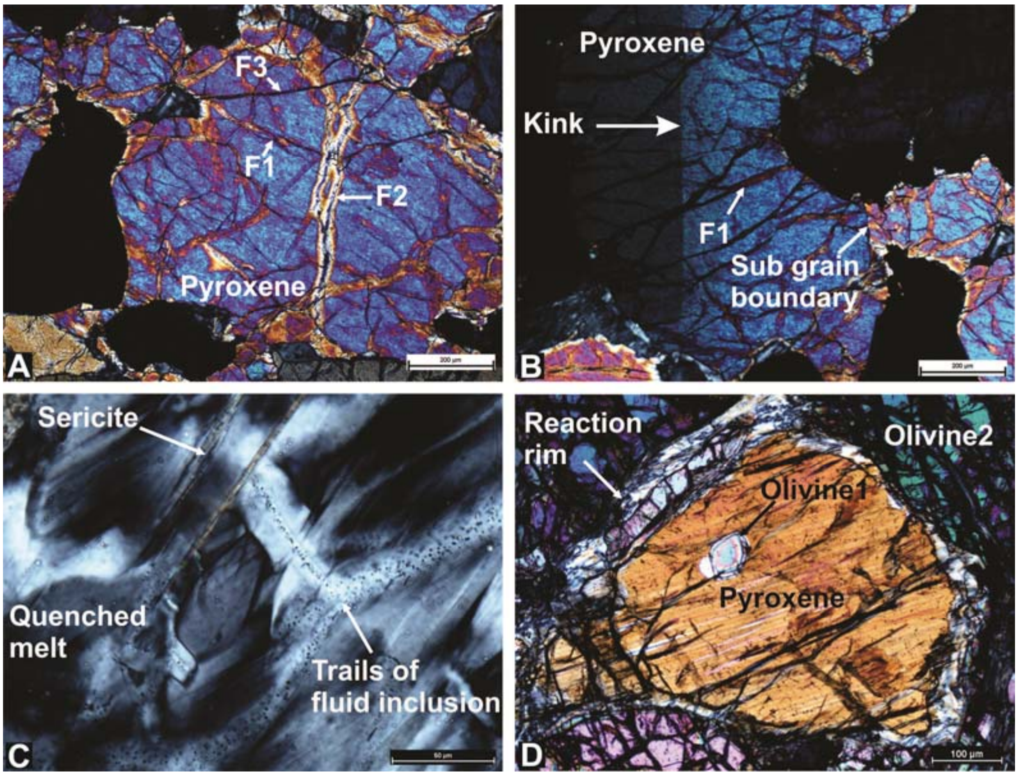

Fig 5.14.A. Three generations of serpentinization is marked as F1, F2 & F3. B. B. In this photomicrograph, Fi veining cut the kink and was cut by the sub grain. This indicates two deformation events prior and after the F1 veining. C. The trail bound fluid inclusions in quenched glass. D. Bimodal occurrence of olivine - (1) As inclusion in orthopyroxene (2) In ground mass of the peridotite. D. Inclusion of olivine in pyroxenes of harzburgite of the Nidar Ophiolite.

Some orthopyroxenes of harzburgite part shows multiple inclusions of olivine indicating secondary origin of the orthopyroxene (Fig.5.14 D). The olivines display bimodal occurrence – (1) as inclusions in orthopyroxene and (2) in matrix. The plagioclase peridotites occasionally show primary inclusions of serpentines in pyroxenes and quenched melt (Fig 5.15). It is observed that the serpentine grains are rimmed by the quenched melt in plagioclase peridotite.

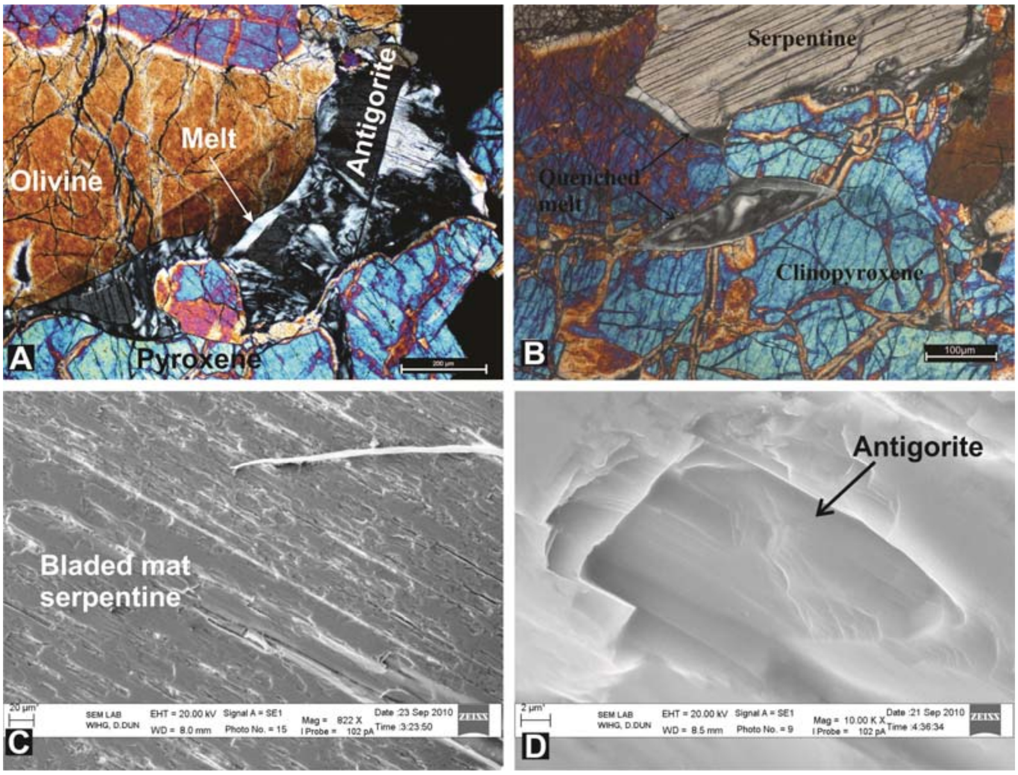

Fig 5.15.A, B. Primary serpentines are rimmed by quenched melt in peridotite. C, D. BSE image shows that the serpentines are bladed mat antigorite.

SEM study reveals bladed mat habit of the serpentines indicating that they are antigorite. In a serpentinite rock two modes of serpentines are noticed – (1) inclusion of serpentines in orthopyroxene and (2) the matrix serpentines. This infer that the orthopyroxene could product of serpentine break down (Fig 5.16 A). Within the peridotites which are cut by the dunite channel a garnet bearing serpentinite is noticed (Fig 5.16 B). The rock occur as patches within serpentinized plagioclase bearing peridotite. The rock contains pyroxene (20%), plagioclase (10%), serpentine (35 - 40%), amphibole (10 - 15%) and garnet (20%). Some garnets bear inclusions of serpentines (Fig 5.16 B). The occurrence of serpentine as inclusions within the ultramafic rocks cut by the dunite channel infer that some of the peridotites may have formed from serpentine break down process. This process is capable to release a high volume of water in mantle wedge through metamorphic dehydration (Ulmer and Trommsdorff 1995). The water can play a great role in melting of mantle wedge.

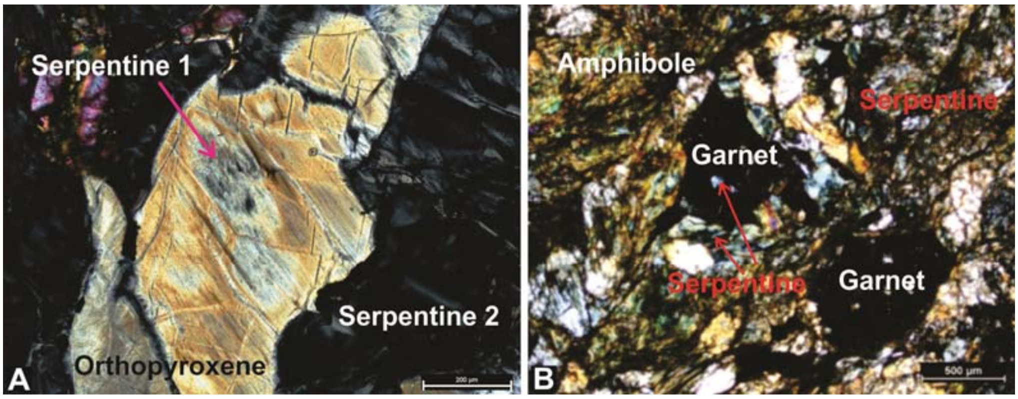

Fig 5.16.A. Photomicrograph from serpentinite of Nidar ophiolite reveals two generations of serpentines – (a) as inclusions in orthopyroxene (2) in matrix. B. A garnet bearing serpentinite rock is found within the serpentinized peridotites of Nidar ophiolite.

5.6 EVOLUTION OF MICROTEXTURES AND VOLATILE PHASES

The micro texture and volatile phase study reveal that peridotites of Nidar Ophiolite has a complex origin. These textures and volatiles indicate progressive change in P – T and other conditions which ultimately have implication to their emplacement on to the surface. A brief explanation is given here which will be discussed in detail in chapter 6.

The uniform shape, orientation of the Cr - spinel needles in the olivine (Fig 5.7A, B) of lherzolite 1NU27 suggest that needles are exsolution or precipitation products from a primary unusual condition. The origin of the Cr – spinel needles in olivine can takes place from the HP Mg_2SiO_4 grain included within Cr – spinels (Fig 4.19). Comparison of the mineral chemistry data of olivines with HP Mg_2SiO_4 shows that the HP Mg_2SiO_4 inclusions are more enriched in Cr (Table 4.7). So with the pressure fall the high pressure polymorph of olivine can produce Cr – spinel exsolution in olivine.

Some places the needles bear disordered α – Fe_2O_3 as attachment with or without disordered carbonaceous phases with it. The α – Fe_2O_3 + carbon phase assemblage indicate evolution from zone of metal saturation (> 250 Km) where highly reduced environment exists due to carbon – iron coupling (Rohrbach and Schmidt 2011). The triggering cause behind this precipitation may not be only decompression. It can be that existing iron was not released with the exsolved needles. Iron oxide precipitated separately. The higher fayalite component (Fe# ~ 9.5 %) in olivine than the host dunite (Table 4.2) gives hint for evolution from deeper part where $\alpha \rightarrow \beta$ Mg2SiO4 is favoured in the presence of additional Fe (Irfune and Isshiki, 1998).

The same lherzolite bear lamellar Cen inclusions (Fig). There are two possibilities regarding the *C2/c* Cen - (1) High T Cen (2) high P Cen. From Raman data it is difficult to state directly that the Cen is high P. But high T Cen has a small domain of stability field at P < 1 GPa and T > 1500^0C (Pacalo and Gasparik 1990). Our additional high pressure signature (HP Mg_2SiO_4 and Cr – spinel needles in olivine) rules out the possibility of high T Cen and indicate presence of pre-existing high P Cen. The phase transition from high P Cen to Oen takes place minimum at ~ 240 Km depth (P > 8 GPa, T ~ 900^0C; Gasparik 1990).

Another peridotite (sample no. 3) of ultramafic suit also bear clinoenstatite in diopside (Fig 5.4, 5.6). But there are no additional high pressure signatures which can give a hint whether the Cen is high temp or high pr. The pyroxenes of pyroxenite vein bear varieties of exsolution (Fig 5.1, 5.2, 5.3). But they all indicate cooling from a high temp environment.

The presence of carbon and hydrocarbons in olivine of lherzolite 1NU27 with iron oxide infer a highly reduced primary environment. Presence of methane with clinopyroxene in α – Fe_2O_3 of 1M1 lherzolite also supports the redox state. These evidences are unequivocal natural evidences of reduced (hydrocarbon and carbon rich) mantle transition zone. Additionally the metal oxides and the free carbon also can trigger redox melting (Cottrell and Kelley 2013) to produce magmas at spreading center.

The primary serpentine in orthopyroxene and garnet suggests that some part of the peridotites may be of metamorphic origin. Dehydration of antigorite type of serpentine may produce olivine and orthopyroxene. Presence of garnet in a serpentinite indicates that the subduction of serpentinites possibly attained the sub arc depth. The signature of serpentine break down from ophiolite ultramafics provides an insight into the transport mechanism of water to the deep mantle (Ulmer and Trommsdorff 1995). This fluid in the mantle wedge brings peridotitic rocks below wet solidus temperature and triggers partial melting. Besides introduction of these fluids into mantle wedge play very critical role in subduction dynamics which promote hydration and other physical and chemical modifications of rocks overlying subducting slab. The advent of water into mantle wedge may generate earthquake (Peacock, 2001; Dobson et al., 2002). Altogether in context of Himalayan geodynamics the primary serpentine may be representative of subducted oceanic (Tethyan) lithosphere beneath Asia.

CHAPTER 6

DISCUSSION AND MODEL RECONSTRUCTION

CHAPTER 6

DISCUSSION AND MODEL RECONSTRUCTION

6.1 CHAPTER OVERVIEW

Ophiolite is segment of former oceanic crust and mantle pieces which is tectonically exposed on the Earth surface. It display complex internal structure and preserve wide range of chemical heterogeneity. The mantle part of Nidar Ophiolite Complex (NOC) have the thickest (~7 km) best known exposure of ultramafics. These mantle rocks show unique internal structures and wide range of mineralogy. The aim of the present thesis was to characterize the complete mineralogy from basal part of NOC ultramafic section. The outcome of this thesis demonstrates conclusively that the NOC ultramafics retains signature of mantle transition zone (410 – 660 km). This deep mantle rocks are potential to study the nature of upper mantle convection. Besides, ophiolite also bear signature of steep and deep subduction of oceanic (Tethys) slab beneath Asia which has a great significance in Himalayan geodynamics. The evidences for sudden release of water in deep mantle may also put a significant effect in orogenic processes. This thesis work also recognizes first identification zone of natural CO_2 sequestration in the Himalaya.

6.2 RESEARCH SUMMARY

On the basis of in situ micro inclusion and texture, present research suggests ultra-deep origin for the some portions of peridotites of the Nidar Ophiolite Complex of the Indus Suture Zone (ISZ) in western Indian Himalaya (Fig 2.3). The reported systematic mineral phase transitions are yet-to-be recognized in terrestrial rocks as it may be considered originating from the 410 - 660 km deep mantle transition zone.

Detail mapping of Nidar ophiolite (Indus suture zone, SE Ladakh, India) reveals, it is one of the thickest ophiolite suits across the globe. In Nidar valley it is at least 10 km thick and some places it may increase. The ophiolite is consists of three units from top to bottom – pillow lava with volcanics and chert, gabbroic middle part and lower most ultramafic unit. The ultramafic unit (~ 7 km thick) is composed of various types of peridotites (for detail – see chapter 2; Fig 2.3). Such thick mantle section of the basal part of Nidar ophiolite is unique of its own as compare to the other ophiolite suite.

On the basis of field occurrence, petrography and mineral chemistry data relatively primary rock bodies of the mantle section of Nidar ophiolite have been identified. From field occurrences, the ultramafic rocks of Nidar ophiolites can be divided into three types – (1) the dunite channel which cut the mantle section of Nidar ophiolite (2) the ultramafics carried by the dunite channel (3) ultramafics cut by the channelized dunite (Fig 2.7). After comparing mineral chemistry data of essential minerals (olivine, pyroxene and spinel) of three types of ultramafic rocks show significant differences with the channelized dunite. It is found that the chemistry of essential minerals of dunite body is significantly different from the ultramafics carried by the dunite channel and the ultramafics cut by the dunite channel. In the dunite the Mg# of olivine is ~ 93.5%, Mg# and Cr# of spinel is ~ 62.4 – 68.66% and 48.38 – 61.34% respectively (Table 4.1). The lherzolites cut by the channelized dunite show Mg# of olivine is ~ 90 – 90.3%, Mg# & Cr# of spinel is ~ 5.46 – 8.1% & ~ 85.95 – 90.28 % respectively (Table 4.5). The harzburgites cut by the channelized dunite have Mg# of olivine is ~ 91 – 91.22%, Mg# & Cr# of spinel is ~ 44.66 – 45.02% & ~ 21.45 – 21.86 % respectively (Table 4.6). The lherzolites carried by the dunite channel display Mg# of olivine is 90 – 91%, Mg# and Cr# of spinel is 48.9 – 52.8% and 54.5 – 70.3 % respectively (Table 4.2, 4.3, 4.4). In a word it can be said that Mg# of olivine and spinels of the dunites are much higher than the other ultramafics of the Nidar Ophiolite. This implies the ultramafics may be much more primitive than the dunite (Kelemen 1995). Within the two groups of ultramafics (group 2 – ultramafics carried by the dunite channel and group 3 – ultramafics cut by the dunite channel) further classification is made on the basis of petrographic studies. Some rock bodies from both groups of ultramafics bear unusual micro textures and inclusions which could be indicative of primitive signatures.

In an enstatite of group 2 (xenolith – carried by the dunite channel) lherzolite (sample no – 1M1) the primary relict is discovered which show unique co-existence of square shaped coesite + *C2/c* clinoenstatite + disordered Fe_2O_3 + disordered carbon and Fe_2O_3 glass (Fig 4.8). All the phases are characterised by Laser Raman spectroscopy and Electron Probe Micro analyser. In another lherzolite body (1NU27; adjacent to the 1M1 lherzolite) lamellar *C2/c* clinoenstatite inclusions in orthoenstatite (Fig 5.10), Cr – spinel exsolution needles in olivine (Fig 5.8) and high pressure Mg_2SiO_4 (retrogressed wadsleyite) in Cr – spinel (Fig 4.8 E, F, 4.18, 4.19) are discovered. Presence of Cr – spinel exsolution needles in olivine of high pressure rocks has been earlier interpreted as result of decompression of β-Mg_2SiO_4 (Dobrzhinetskaya et al., 1996). However this interpretation was questioned very soon (Hacker et al., 1997). In the present work the presence of high pressure Mg_2SiO_4 and *C2/c* clinoenstatite confirm the original pressure could be as high as mantle transition depth (410 – 660 km; 14 – 22 GPa). Though high pressure mineralogical evidences have been reported from other ophiolites (Robinson et al., 2004; Yang et al., 2007; Yamamoto et al., 2009; Trumbull et al., 2009) but these evidences suggest a systematic mineral phase transition from mantle transition zone and thus infer a progressive upwelling in a spreading center. The given evidences in this thesis advocate for ultra – deep origin of relict mineral phases in the lower ultramafics of the NOC and their P-T stability relations (Fig. 6.1) allow a tentative exhumation pathway of these mineral phases. For the system MgO – FeO - SiO_2, this pathway, the adiabat, terminates beneath the mid-ocean-ridge basalt eruption temperatures of ~1200^0 C. Data suggest this pathway originates from mantle transition zone depths, passes through the stability fields of wadsleyite, continuing successively through high-pressure clinoenstatite field, the stability field of coesite, and finally terminates in the orthoenstatite field (Fig. 6.1, 6.2).

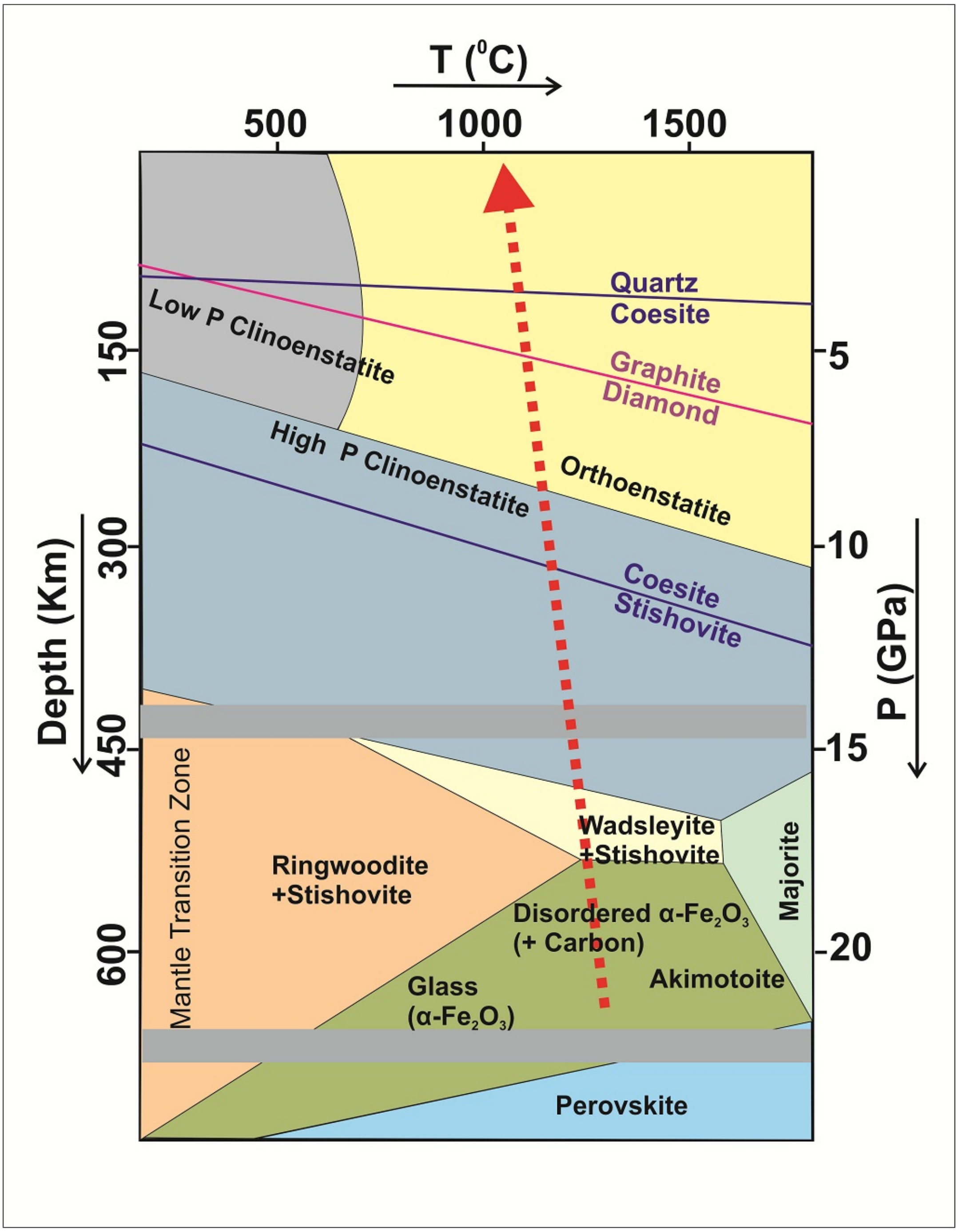

Fig. 6. 1. The P - T path of the relict grains' journey from place of origin to final emplacement in the peridotitic host beneath the ophiolitic volcanic crust. Inferred adiabat as functions of pressure (P) and temperature (T) for the system MgO – FeO - SiO_2 starts from mantle transition zone, ending at oceanic spreading center. The representative phase diagrams are adapted from Pacalo and Gasparik 1990, Gasparik 1990 Shim and Duffy 2001 and Presnall and Gasparik 1990. Forsterite (α) – Wadsleyite (β) – Ringwoodite (γ) Mg_2SiO_4 phase boundaries are adapted from Katsura and Ito 1989, Kirby et al., 1991 and Akaogi et al., 1989.

It can be concluded that some of the mantle peridotites below the Nidar ophiolite show evidence of high temperature – pressure recrystallization, plastic deformation and solid state flow began their journey in the mantle transition zone depths of 410 – 660 km before arriving beneath the ophiolitic volcanic crust at oceanic ridges.

This study has obvious implications for the nature of upper mantle flow and sources of ocean-ridge basalts in a spreading center (Fig 6.2). Several studies related to this study previously reported ultra-high-pressure minerals, such as diamonds, coesite, high-pressure form of TiO_2 and other minerals in chromitites of a Tibetan ophiolite (Robinson et al., 2004; Yang et al., 2007; Yamamoto et al., 2009; Dobrzhinetskaya et al., 2009) and more recently the high-pressure polymorph of olivine, ringwoodite, found as inclusions in diamond of a Brazilian kimberlite (Pearson et al., 2014). Another group of micro-mineralogical studies in peridotites from continental collision zones has established exhumation of the host peridotites from 300 - 400 km depths in the mantle (e.g. Dobrzhinetskaya et al., 1996, Liou et al., 2007). The current study, however, can be distinguished from previous work by the discovery of a unique set of ultra-high-pressure mineral assemblages that demonstrate contiguity in their pressure- temperature stability space, linking the mantle transition zone to the ocean ridge-formed basaltic crust (Fig 6.2). Unlike previous studies that reported minerals of high- pressure origin in similar rocks, the report here a set of minerals; some newly discovered that shows a continuous pathway from the mantle transition zone to the uppermost mantle region. These minerals began their journey from the transition zone upwards by solid -state flow, arriving below the ophiolite's volcanic crust at ocean ridges (Fig 6.2).

The observed orthoenstatite – *C2/c* clinoenstatite mineral phase transition has implications on sampling the "X – discontinuity" because the phase transformation of (Mg,Fe)SiO_3 pyroxene from orthorhombic (Oen) to monoclinic (HCen) structure due to compression (for a typical composition with Fe# ~ 10%; Woodland 1998) takes place at a depth of 240 Km (P > 8 GPa, T ~ 900^0C; Gasparik 1990).

Presence of aliphatic hydrocarbon as fluid inclusions and volatiles along with carbons in ultra-deep lherzolites indicate a highly reducing environment in mantle transition zone depth (Fig 5.11, 5.12, 5.13). Textural evidences also infer that Fe_2O_3 and its glass is also present as primitive material in 1M1 lherzolite (Fig 4.15, 4.16). It has been shown by experimental studies that at > 250 km depth mantle is metal enriched (Rohrbach et al., 2007). But there was lack of evidences in nature. Present study shows dominance of iron oxide in mantle rocks which is deeper than X discontinuity depth (220 – 250 km).

Signature of serpentine dehydration is observed in peridotites which are cut by the dunite channel. The reaction textures reveal prograde transition from serpentine to olivine + orthopyroxene assemblage occurs in ultramafic rocks of Nidar Ophiolite. In serpentinite primary phase obtained as relict serpentine included in an orthopyroxene showing diffusing margin with host (Fig 5.16 A). The serpentinized matrix around that orthopyroxene grain indicates later hydration event.

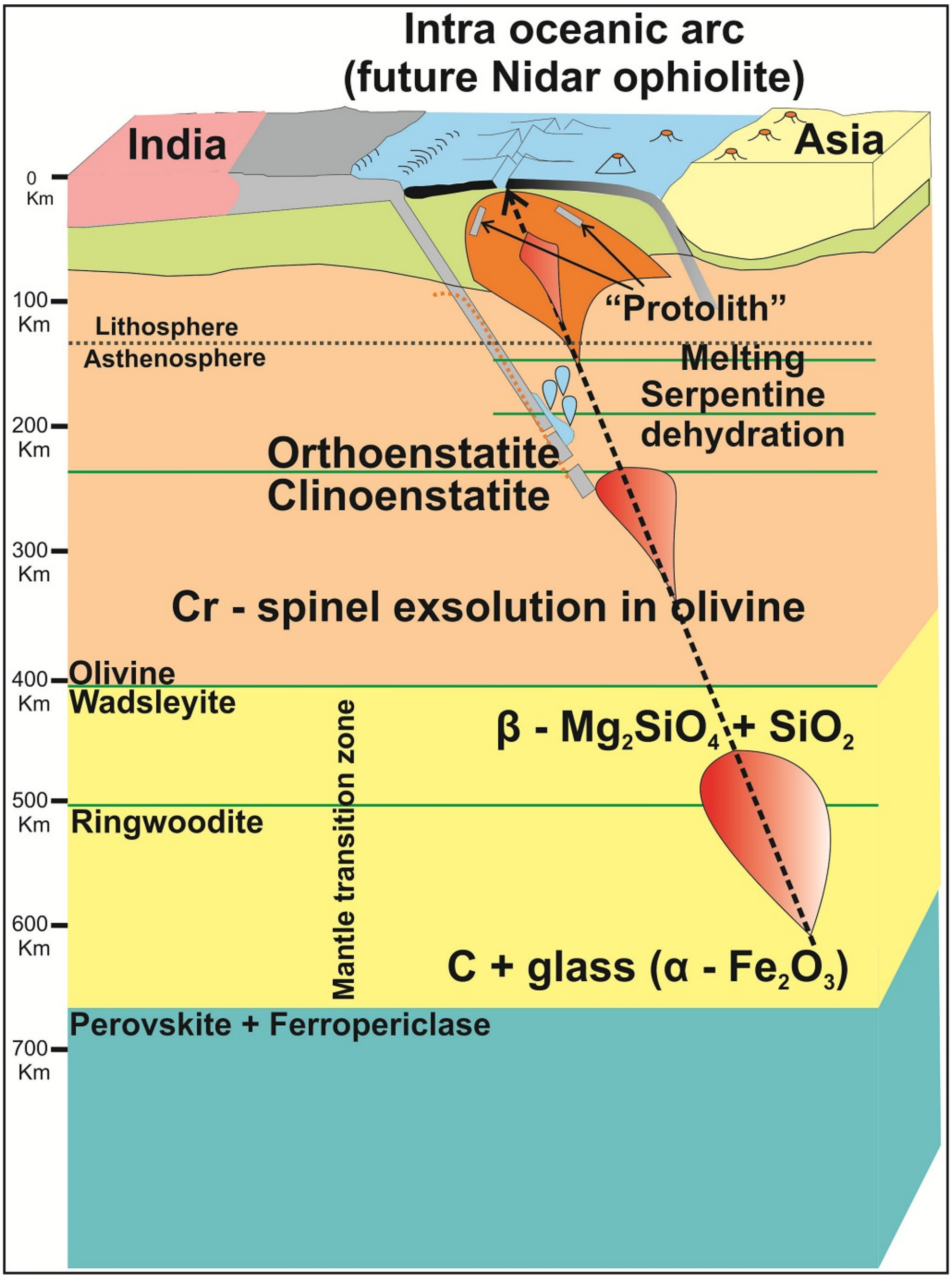

Fig. 6.2. Probably in an ancient intra oceanic arc the process was initiated by a deep oceanic subduction followed by dehydration of serpentines released a huge amount of free water. The water was responsible for melting in mantle wedge. This process created a vacuum in mantle which attracted the regular mantle flow towards the open "window" in the pre Himalayan intra oceanic arc where the deep Earth phases are emplaced on to the surface. The flow began its journey from the transition zone upwards by solid – state flow, arrived below the ophiolite's volcanic crust at spreading center in an intra-oceanic arc.

In the fresh (~20% serpentinized) peridotites, bladed mat serpentines rimmed by quenched melt (?) are characterized as primary serpentine occurring within olivines and pyroxenes (Fig 5.15). The secondary serpentines occur along veins and exhibit mesh texture. The chronological sequence (primary serpentine olivine + orthopyroxene assemblage secondary serpentine) infer serpentine break down to produce olivine + orthopyroxene and release water at mantle depths during subduction of serpentinized oceanic lithosphere. These fluids ascend into the overlying mantle wedge which may be responsible for the hydration and melting. In peridotites two stages of hydration before melting is obtained and it is characterized by crosscutting relationship of veins and their different morphology (Fig 5.14). Different stages of olivine and orthopyroxene are obtained which are characterized on the basis of relict polyphase olivine inclusions in orthopyroxene and vise versa (Fig 5.14 D). These melting and metasomatism events advocate for fluid release from a subducting slab into the overlying mantle wedge and serpentines are possibly the principle source of fluids and volatiles. Within the peridotites which are cut by the dunite channel a garnet bearing serpentinite is noticed (Fig 5.16 B). Some places the garnets bear includes serpentines. This suggests for deep subduction of serpentinites to release water at higher mantle depth (~ 6 GPa). The mineralogical evidences advocate for probably a steep and deep oceanic subduction in early stages of Himalayan orogeny. Geochemical signatures from ophiolite earlier suggested an intra-oceanic arc origin for Indus suture zone ophiolites (Maheo et al., 2004) at around 140 Ma (Ahmed et al., 2008). The dehydration reaction produced high volume of water in overlying mantle wedge result in melting and ascent of the buoyant mantle to create the crustal part and some portions of the mantle part of the Nidar ophiolite in an intra-oceanic setting.

The dunite body in the NOC is ~ 3 km thick and covers 10s of km^2 surface area and the outcrop surface underwent carbonation of serpentine. The outer surfaces of dunite body have been modified by heavy alteration process. It has abundant magnesium silicate (olivine), hydrated silicates (serpentine) and carbonates (magnesite). This dunite has been through a series of deformation and alteration process. The degree of alteration is less dense and penetrative in the deeper part of the dunite body (Fig 4.2). However, the alteration and vein formation is seen dramatically increased at the shallow level of dunite (Fig 4.2). This alteration process controls the conversion reaction of dunite (forsterite rich olivine) to serpentine (lizardite and amount antigorite). This conversion is a slow geological process, which is manifest by low temperature condition: 330 to 440^o C (Khalepp and Burd 1985), would suggests the reaction of hydrothermal fluids with olivine rich dunite at depth. In contrast, the newly formed carbonate veins in shallow weathering zone of dunite show young and brecciated massive in character. These 1-10 cm thick young massive veins are characterized by magnesite, brucite and low temperature lizardite. Eventually, thin veins of carbonate on the dunite erode continuously and subsequently renew by alteration. Serpentine to carbonate conversion is driven by carbonation reaction by near surface CO_2 and dissolved CO_2 in the rain and snow melt water and this reaction progresses preferably at low temperature condition (Power et al 2007, Kelemen 2011). At places, a crystalline carbonate vein has also been recognized as dolomite and magnesite. The veins eroded less effect and formed at moderately higher temperature and deeper depth. Oxygen isotopes analyses have been applied on those crystalline veins to constrain the indirect interpretation on the initial temperature of carbonation reaction on the altered dunite for CO_2 capture and storage. The same approach was taken by Kelemen and Matter (2008). Assuming that, the crystalline veins may establish isotopic exchange equilibrium with infiltrate fluids. The higher $\delta^{18}0$ 17.3‰ values signify alteration of magnesite and Ca-Mg dolomite formed from serpentine relatively at lower temperature (as per Chako and Denies 2008). It is also noticed elsewhere, the rate of carbonation is much faster when serpentine formed at low temperature condition. It attributed isotopes fractionation during diffusive CO_2 uptake from atmosphere condition (Hammer et al 2005). This result matches with carbonation of Oman peridotite (Kelemen 2008). With above data set and oxygen isotopes value on altered ultramafic (dunite) of NOC, it can be inferred that the rate of the carbonation of altered dunite is controlled by low temperature with the sequestration of atmospheric CO_2.

6.3 MAJOR CONTRIBUTIONS FROM THE PRESENT STUDY

The results obtained from this thesis can be compiled in following points –

- Details mapping reveals that NOC is the one of thickest known ophiolite section on Earth surface.
- The plan view of Nidar valley is an "eye" shaped which is the main reason for this abnormal high thickness.
- The ultramafic part is ~7 km thick in Nidar valley section which is probably the thickest among known ophiolites.
- In Nidar valley a deformed dunite channel (3 km long) is observed which crosscuts the ultramafics of ophiolite. The structure has implications to the melt extraction processes in a spreading center.
- Within dunite channel some entrapped lherzolite xenolith bodies are observed. Some of them bear evidences of unusual high pressure origin.
- In an orthopyroxene porphyroclast of "xenolith" lherzolite 1M1 coesite + high pressure *C2/c* clinoenstatite assemblage has been discovered (Fig 4.14). This evidence challenge the conventional idea of "origin of ophiolite peridotites in a spinel lherzolite stability field" (Coleman 1977). The presence of high P clinoenstatite indicate the origin of host rock at >240 km (> 8 GPa; Gasparik 1990) depth.

- In the lherzolite 1M1 some α – Fe_2O_3 grain is recovered with disordered carbon and glass inclusion in it (Fig 4.15, 4.16). Laser Raman spectroscopy reveals that the glass follow the trend of α – Fe_2O_3. The glass and carbon in high pressure peridotite infer a high reducing environment in deep mantle.

- In another lherzolite xenolith (sample 1NU27) entrapped within dunite channel, some orthopyroxene porphyroclasts are noticed with lamellar inclusions of clinoenstatite (*C*2/*c*) (Fig 5.10). The olivines bear strongly oriented exsolution needles of Cr – spinel and α – Fe_2O_3 precipitations (Fig 5.8, 5.9). They indicate a pre-existing deep mantle environment. From that lherzolite high pressure Mg_2SiO_4 (β - Mg_2SiO_4?) is discovered as inclusions in Cr – spinel (Fig 4.8, 4.13, 4.17, 4.18, 4.19). It has been concluded that mantle flow in spreading center originates from transition zone (410 – 660 km).

- Many other micro textures are also reported in this thesis from pyroxenite and peridotites cut by the dunite channels. Most of the textures infer late stage temperature fall from a high T conditions. Among them some micro textures are suspected as evidence in favour of high pressure origin especially within a lherzolite which is cut by the dunite channel.

- In the lherzolite 1NU27 where mantle transition zone (410 – 660 km depth) signature is recovered unusual disordered carbon inclusions are noticed within olivine (Fig 5.11). Along with them primary aliphatic fluid inclusion is also present (Fig 5.12). In the other high P lherzolite xenolith methane has been detected by Laser Raman spectroscopy (Fig 5.13) with the $\alpha - Fe_2O_3$. These evidences strongly infer a high reducing environment in lower part of upper mantle. This is the rare natural evidence of highly reducing environment in transition zone. From only experimental studies we know that deeper part of the upper mantle is reduced, metal rich (Rohrbach et al., 2007) and these metal and carbon is potential to trigger melting (Dasgupta et al., 2013) at depths $\geq$ 250 km. This study shows rare natural signature which infer that metal, carbon and hydrocarbons are present in mantle transition zone (410 – 660 km) which result in a highly reducing and metal rich base of upper mantle.

- The signatures of serpentine dehydration and formation of garnet bearing serpentinite (Fig 5.14, 5.15, 5.16) infer deep and steep subduction of primary oceanic lithosphere which releases free high volume of water (~13%) in sub arc depth (Ulmer and Trommsdorff 1995). This phenomena facilitate melting at the overlying mantle wedge and potential of volcanism in intra oceanic arc. Additionally due to dehydration and ascent of magma a sudden vacuum can be formed in mantle wedge which may trigger upwelling from mantle transition depth (410 – 660 km). Thus subduction induced mantle flow may create the ‘geodynamo’ which initiated the Himalaya building process.

- The upper skin of the dunite and serpentines are intensely affected by carbonation in many places. The carbonations preserve evidence of natural CO_2 sequestration.

6.4 SCOPE OF THE FUTURE WORK

The origin of Earth from accretion of chondritic bodies and nature of the pristine Earth is still an unfolded mystery. After studying many extra-terrestrial bodies it has been found that only reliable way to determine the nature of the early Earth is by sampling the primitive lower mantle. For that first it is required to sample the deep Earth. Present study suggests systematic mineral phase transitions from at least base of the upper mantle. Thus deep Earth relicts could be a great opportunity to study the hints of primitive mantle and from that the evolution of mantle can be attempted.

After sampling the transition zone rocks it can be further studied about the mechanism of formation of different discontinuities which are probably results of mineral phase transition. From these samples the nature of mantle convection, which passes through different discontinuity planes, also can be studied in detail.

It is very little known from the redox state and metal concentration of deep mantle. Only some speculations can be made on the basis of experimental studies. The signatures of reduced and metal rich mantle transition zone provide a unique opportunity to further substantiate the redox state of the deep mantle at least up to mantle transition zone.

BIBLIOGRAPHY

BIBLIOGRAPHY

Ahmad, T. et al. (2008), Geochemical and isotopic constraints on the age and origin of the Nidar Ophiolitic Complex, Ladakh, India: Implications for the Neo-Tethyan subduction along the Indus suture zone, Tectonophysics, Vol. 451, pp. 206 – 224.

Akaogi, M., Ito, E. and Navrotsky, A. (1989), Olivine-modified spinel–spinel transitions in the system Mg_2SiO_4–Fe_2SiO_4: calorimetric measurements, thermochemical calculation, and geophysical application, Journal of Geophysical Research, Vol. 94, pp. 15671–15685.

Anonymous, M. (1972), Penrose field conference on ophiolites. Geotimes, Vol. 17, pp. 24–25.

Arai, S. (2013), Conversion of low – pressure chromitites to ultra-high pressure chromitites by deep recycling: A good inference, Earth and Planetary Science Letters, Vol. 379, pp. 81–87.

Arita, K. (1983), Origin of the inverted metamorphism of the Lower Himalayas, central Nepal, Tectonophysics, Vol. 95, pp. 43-60.

Baker M. B. and Beckett J. R. (1999),The origin of abyssal peridotites: a reinterpretation of constraints based on primary bulk compositions. Earth and Planetary Science Letters, Vol. 171, pp. 49–61.

Beaumont, C., Jamieson, R.A., Nguyen, M.H. and Lee, B. (2001), Himalayan tectonics explained by extrusionof a low-viscosity crustal channel coupled to focused surface denudation, Nature, Vol. 414, pp. 738–742.

Berthelsen, A. (1953), On the geology of the Rupshu District, N.W. Himalaya, Medd. Dan. Geol. Foren., Vol. 12, pp. 350– 415.

Bilham, R., Larson, K., Freymueller, J., and Project Idylhim members (1997), GPS measurements of present-day convergence across the Nepal Himalaya: Nature, Vol. 386, pp. 61–64.

Bodinier, J. L., Vasseur, G., Vernie`res, J., Dupuy, C., and Fabrie`s, J. (1990), Mechanism of mantle metasomatism: geochemical evidence from the Lherz orogenic peridotite. Journal of Petrology, Vol. 31, pp. 597–628.

Buddington, A.F. and Lindsley, D.H. (1964), Iron–titanium oxide minerals and synthetic equivalents, Journal of Petrology, Vol. 5, pp. 310–357.

Burkhard D. J. M. and O'Neil J. R. (1988), Contrasting serpentinization processes in the eastern Central Alps.Contribution to Mineralogy and Petrology, Vol. 99, pp. 498–506.

Cannat, M. and Mascle, G. (1990), Re´union extraordinaire de la socie´te´ ge´ologique de France en Himalaya du Ladakh, Bull. Soc. Ge´ol. Fr.,Vol. 4, pp. 553–582.

Chacko T, Deines P (2008), Theoretical calculation of oxygen isotope fractionation factors in carbonate systems. Geochimica Cosmochimica Acta, Vol. 72, pp. 3642-3660.

Chopelas, A. (1999), Estimates of mantle relevant Clapeyron slopes in the $MgSiO_3$ system from high-pressure spectroscopic data, American Mineralogist,Vol. 84, pp. 233 – 244.

Clark, M.K., Schoenbohm, L.M., Royden, L.H., Whipple, K.X., Burchfiel, B.C., Zhang, X., Tang, W., Wang, E. and Chen, L. (2004), Surface uplift, tectonics and erosion of eastern Tibet from large-scale drainage patterns, Tectonics, Vol. 23, TC1006.

Clift, P.D., Degnan, P.J., Hannigan, R. and Blusztajn, J. (2000), Sedimentary and geochemical evolution of the Drasforearc basin, Indus Suture, Ladakh Himalaya, India, Geological Society of America Bulletin, Vol. 112, pp. 450–466.

Coleman, R.G., (1971), Plate tectonic emplacement of upper mantle peridotites along continental edges, Journal of Geophysical Research, Vol. 76, pp. 1212–1222.

Coleman, R.G., (1977), Ophiolites: New York, Springer – Verlag, pp. 220.

Corfield, R., Searle, M. and Green, O. (1999), Photang thrust sheet, an accretionary complex structurally below the Spontang ophiolite constraining timing and tectonic environment of ophiolite obduction, Ladakh Himalaya, NW India, Journalof Geological Society, London, Vol. 156, pp. 1031– 1044.

Corfield, R., Searle, M. and Pedersen, R.B.(2001), Tectonic setting and obduction history of the Spontang ophiolite, Ladakh Himalaya, NW India, Journal of Geology, Vol. 109, pp. 715–736.

Cottrell, E. and Kelley, K. A. (2013), Redox Heterogeneity in Mid-Ocean Ridge Basalts as a Function of Mantle Source, Science, Vol. 340, pp. 1314 – 1317.

Dasgupta, R., Mallik, A., Tsuno, K., Withers, A. C., Hirth, G. and Hirschmann, M. (2013), Carbon – dioxide – rich silicate melts in the Earth's upper mantle. Nature, Vol. 493, pp. 211 – 215.

DeCelles, P.G., Robinson, D.M. and Zandt, G. (2002), Implications of shortening in the Himalayan fold-thrust belt for uplift of the Tibetan Plateau, Tectonics, Vol. 21, No. 6, pp. 1062–1087.

De Sigoyer, J. et al., (2000), Dating the Indian continental subduction and collisional thickening in the northwest Himalaya: multichronology of the Tso Morarieclogites, Geology, Vol. 28, pp. 487 – 490.

Dietrich, V.J., Frank, W. and Honegger, K. (1983), A Jurassic– Cretaceous island arc in the Ladakh– Himalaya, Journal of volcanology and geothermal research, Vol. 18, pp. 405– 433.

DeMets, C., Gordon, R.G., Argus, D.F. and Stein, S. (1994), Effect of recent revisions to the geomagnetic reversal time scale on estimates of current plate motions, Geophysical Research Letters, Vol. 21, pp. 2191–2194.

Dewey, J. F. and Bird, J. M. (1970), Mountain belts and the new global tectonics, Journal of Geophysical Research, Vol. 75, pp. 2625–2647.

Dewey, J.F., and Bird, J.M., (1971), The origin and emplacement of the ophiolite suite: Appalachian ophiolites in Newfoundland, Journal of Geophysical Research, Vol. 76, pp. 3179–3206.

Dewey, J.F., Cande, S. and Pitman, W.C. (1989), Tectonic evolution of the India–Eurasia collision zone, Eclogae Geologicae Helvetiae,Vol. 82, pp. 717–734.

DeSigoyer, J. (1998),Me´canismesd’exhumation des roches de haute pressionbassetempe´rature, en contexte de convergence continentale (Tso Morari, NO Himalaya), The`se Univ. Claude Bernard, Lyon, pp. 236.

Dilek, Y. and Furnes, H. (2011) Ophiolite genesis and global tectonics: Geochemical and tectonic fingerprinting of ancient oceanic lithosphere. Geological Society of America Bulletin Vol. 123, pp. 387-411.

Dilek, Y. and Furnes, H. (2011), Ophiolites and their origins, Elements, Vol. 10, pp. 93–100.

Dobson, D. P., Meredith, P. G. and Boon, S. A. (2002), Simulation of subduction zone seismicity by dehydration of serpentine, Science, Vol. 298, pp. 1407 – 1410.

Dobrzhinetskaya, L. F., Green, H. W. and Wang, S. (1996), Alpe Arami: A Peridotite Massif from depths of more than 300 Km, Science, Vol. 271, No. 5257, pp. 1841–1845.

Dobrzhinetskaya, L. F. et al. (2009), High-pressure highly reduced nitrides and oxides from chromitite of a Tibetan ophiolite, Proceedings of National Academy of Sciences USA, Vol.106, pp. 19233 – 19238.

Durbin, D. J., Mcmillan, P. F. and Wolf, G II. (1993), Raman study of the high pressure behavior of forsterite (Mg_2SiO_4) crystal and glass, American Mineralogist, Vol. 78, pp. 1143 – 1148.

Ewart, A. (1982), In: Andesite, R.S., Thorpe, R.L. (Eds.), The Mineralogy and Petrology of Tertiary – Recent Orogenic Volcanic Rocks with Special Reference to the Andesitic–Basaltic Compositional Range. Wiley, New York, pp. 25–95.

Farell – Turner, S., Reimold, W. U., Nieuwoudt, M. and Erasmus, R. M. (2005),Raman spectroscopy of olivine in dunite experimentally shocked to pressures between 5 and 59 GPa,Meteoritic and planetary science, Vol.40, pp. 1311 – 1327.

Fuchs, G. and Linner, M. (1996), On the geology of the Suture Zone and Tso Morari Dome in Eastern Ladakh (Himalaya), Jb. Geol. B., Vol. 139, pp. 191– 207.

Gansser, A. (1964), Geology of the Himalayas, Willey Inter science Publishers, London.

Gass, I.G. (1968), Is the Troodos massif of Cyprus a fragment of Mesozoic ocean floor? Nature, Vol. 220, pp. 39–42.

Gass I. G., et al. (1975), Comments on ‘The Troodos ophiolitic complex was probably formed in an island arc’, by A. Miyashiro and subsequent correspondence by A. Hynes and A. Miyashiro. Earth and Planetary Science Letters, Vol. 25, pp. 236–238.

Gasparik, T. (1990), Phase relations in the transition zone,Journal of Geophysical Research, Vol.95, pp. 15751–15769.

Grujic, D., Coutand, I., Bookhagen, B., Bonnet, S., Blythe, A. and Duncan, C. (2006), Climatic forcing of erosion,landscape and tectonics in the Bhutan Himalaya, Geology, Vol. 34, pp. 801–804.

Gruijc, D., Hollister, L.S. and Parrish, R. (2002), Himalayan metamorphic sequence as an orogenic channel: insight from Bhutan, Earth and Planetary Science Letters, Vol. 198, pp. 177 – 191.

Grujic, D., Casey, M., Davidson, C., Hollister,L. S., Kundig, R., Pavlis, T. & Schmid, S. (1996),Ductile extrusion of the Higher Himalayan Crystalline in Bhutan: evidence from quartz microfabrics, Tectonophysics, Vol. 260, pp. 21– 43.

Guivel, C.et al., (1999), New geochemical constraints for the origin of ridge-subduction-related plutonic and volcanic suites from the Chile Triple Junction (Taitao Peninsula and Site 862, LEG ODP141 on the Taitao Ridge), Tectonophysics, Vol. 311, pp. 83-111.

Guillot, S., De Sigoyer, J.,Lardeaux, J. M. and Mascle, G. (1997), Eclogitic metasediments from the Tso Morari area (Ladakh, Himalaya): evidence for continental subduction during India–Asia convergence, Contribution to Mineralogy and Petrology, Vol. 128, pp. 197– 212.

Hacker, B. R., Sharp, T., Zhang, R. Y., et al., (1997), Determining the Origin of Ultrahigh-Pressure Lherzolites (Discussion), Science, Vol. 278, No. 5338, pp. 701–707.

Hallet, B. and Molnar, P. (2001),Distorted drainage basins as markers of crustal strain east of the Himalaya, Journal of Geophysical Research,Vol. 106, pp. 13697–13709.

Hammer O, Jamtveit B, Benning LG et al. (2005), Evolution of fluid chemistry during travertine formation in the Troll thermal springs, Svalbard, Norway. Geofluids, Vol. 5, pp. 140 – 150.

Harrison, T.M., Ryerson, F.J., LeFort, P., Yin, A., Lovera, O. andCatlos, E.J.(1997),A late Miocene–Pliocene origin for the central Himalayan inverted metamorphism, Earth and Planetary Science Letters, Vol. 146, pp. E1–E7.

Harrison, T.M. (2006), Did the Himalayan Crystallines extrude partially molten from beneath the Tibetan Plateau? In: Law, R.D., Searle, M. & Godin, L.(eds) Channel Flow, Ductile Extrusion and Exhumation in Continental Collision Zones. Geological Society, London, Special Publications, Vol. 268, pp. 237–254.

Hauck, M.L., Nelson, K.D., Brown, W., Zhao, W. and Ross, A.R. (1998), Crustal structure of the Himalayan orogenat ~90°E longitude from Project INDEPTH deep reflection profiles, Tectonics, Vol. 17, pp. 481–500.

Heim, A., and Gansser, A. (1939), Central Himalaya: Geological observations of the Swiss expedition, 1936: Memoirs of the Swiss Society of Natural Sciences, Vol. 73,pp. 245.

Henry, P., LePichon X. and Goffe, B. (1997), Kinematic, thermal and petrological model of the Himalayas: Constraints related to metamorphism within the underthrust Indian crust and topographic elevation, Tectonophysics, Vol. 273, pp. 57–76.

Hodges, K.V. (2006), A synthesis of the channel flow-extrusion hypothesis as developed for the Himalayan–Tibetan orogenic system. In: Law, R.D., Searle, M.P. & Godin, L. (eds) Channel Flow, Ductile Extrusion and Exhumation in Continental Collision Zones. Geological Society, London, Special Publications, Vol. 268, pp. 71–90.

Hodges, K. V., Parrish, R. and Searle, M. P. (1996), Tectonic evolution of the central Annapurna Range, Nepalese Himalayas, Tectonics, Vol. 15, 1264–1291.

Hodges, K.V. (2000), Tectonics of the Himalaya and southern Tibet from two perspectives: Geological Society of America Bulletin, Vol. 112, pp. 324–350.

Honegger, K., Dietrich, V., Frank, W., Gansser, A., Tho¨ni, M. and Trommsdorff, V. (1982), Magmatism and metamorphism in the Ladakh Himalayas (the Indus – Tsangpo suture zone), Earth and Planetary Science Letters, Vol. 60, pp. 253–292.

Hubbard, M. S. and Harrison TM. (1989), 40Ar/39Ar age constraints on deformation and metamorphism in the MCT Zone and Tibetan Slab, Eastern Nepal Himalaya, Tectonics, Vol. 8, pp. 865–880.

Irfune, T. and Isshiki, M. (1998), Iron partitioning in a pyrolite mantle and the nature of the 410-km seismic discontinuity, Nature, Vol. 392, pp. 702 – 705.

Ishizuka, O. et al., (2006), Early stages in the evolution of Izu – Bonin arc volcanism: New age, chemical and isotopic constraints, Earth and Planetary Science Letters, Vol. 250, pp. 385 – 401.

Jain, A.K. and Manickvasagam, R. M. (1993) Inverted metamorphism in the intracontinental ductile shear zone during Himalayan collision tectonics. Geology, Vol.21, pp.407-410.

Katsura, T. and Ito, E. (1989), The system Mg_2SiO_4 - Fe_2SiO_4 at high pressures and temperatures: Precise determination of stabilities of olivine, modified spinel, and spinel, Journal of Geophysical Research, Vol. 94, pp. 15663 – 15670.

Katayama, I., Parkinson, C.D., Okamoto, K., Nakajima, Y. and Maruyama, S. (2000), Supersilicic clinopyroxene and silica exsolution in UHPM eclogitic and pelitic gneiss from the Kokchetav massif, Kazakhstan, American Mineralogist, Vol. 85, pp. 1368 – 1374.

Kelemen, P. B., Shimizu, N., Salters, and Vincent, J. M. (1995), Extraction of mid-ocean-ridge basalt from the upwelling mantle by focused flow of melt in dunite channels, Nature (London), Vol. 375, pp. 747–753.

Kelemen, P. B. and Matter, J. (2008), In situ carbonation of peridotite for CO_2 storage, Proceedings of National Academy of Sciences USA, Vol. 105, pp. 17295 – 17300.

Kelemen PB, Matter J, Streit EE et al. (2011) Rates and Mechanisms of Mineral Carbonation in Peridotite: Natural Processes and Recipes for Enhanced, in situ CO2 Capture and Storage. Ann. Rev. Earth Planet. Sci., Vol 39, pp. 545–576.

Khalepp, L. V. & Burd, G. I. (1985), Temperature of formation of serpentine minerals. International Geology Review, Vol. 27, pp. 109-112.

Kirby, S. H., Durham, W. B. and Stern, L. A. (1991), Mantle phase changes and deep-earthquake faulting in subducting lithosphere, Science, Vol. 252, pp. 216–225.

Konzett, J., Frost, D. J., Proyer, A., and Ulmer, P. (2008), The Ca-Eskola component in eclogitic clinopyroxene as a function of pressure, temperature, and bulk composition: an experimental study to 15 GPa with possible implications for the formation of oriented SiO_2-inclusions in omphacite. Contributions to Mineralogy and Petrology, Vol. 155, pp. 215 – 228.

Krishnan, K. (1961), The Raman spectra of organic compounds, Proceedings of Indian Academy of Sciences, Vol. 53, No. 3, pp. 151 – 167.

Langmuir, C. H., Klein, E. M. and Plank, T. (1992), Petrological systematics of mid-ocean ridge basalts: constraints on melt generation beneath ocean ridges, AGU Geophysical Monograph Series, Vol. 71, pp. 183-280.

Langmuir, C. H., Bezos, A., Escrig, S., Parman, S. W. (2006), Chemical systematics and hydrous melting of the mantle in back-arc basins, AGU Geophysical Monograph Series, Vol. 166, pp. 87 – 145.

Larson, K.M., Burgmann, R., Bilham, R. and Freymueller, J.T. (1999), Kinematics of the India-Eurasia collision zone from GPS measurements, Journal of Geophysical Research, Vol. 104, pp. 1077–1093.

Lave, J. and Avouac, J.P. (2000), Active folding of fluvial terraces across the Siwaliks Hills, Himalayas of central Nepal: Journal of Geophysical Research, Vol. 105, No. 3, pp. 5735–5770.

Lally, J.S., Heuer, A.H., Nord Jr. G.L. and Christie, J.M. (1975), Sub solidus reactions in lunar pyroxenes: an electron petrographic study, Contribution to Mineralogy and Petrology, Vol. 51, pp. 263 – 282.

Leech, M.L., Singh, S., Jain, A.K., Klemperer, S.L. and Manickavasagam, R.M. (2005), The onset of India – Asia continental collision: Early, steep subduction required by the timing of UHP metamorphism in the western Himalaya, Earth and Planetary Science Letters, Vol. 234, pp. 83–97.

Le Fort, P. (1975), Himalayas: the collided range. Present knowledge of the continental arc. American Journal of Science, Vol. 275, pp. 1 – 44.

Le Pichon, X., Fournier, M. and Jolivet, J.(1992), Kinematics, topography, shortening and extrusion in the India –Asia collision, Tectonics,Vol. 11, pp. 1085– 1098.

Lenoir, X., Garrido, C. J., Bodinier, J.-L., Dautria, J.-L. and Gervilla, F. (2001), The recrystallization front of the Ronda peridotite: evidence for melting and thermal erosion of subcontinental lithospheric mantle beneath the Alboran basin, Journal of Petrology, Vol. 42, pp. 141–158.

Liou, J. G., Zhang, R. Y. and Ernst, G. W. (2007), Very high –pressure orogenic garnet peridotites, Proceedings of National Academy of Science, USA, Vol. 104, pp. 9116 – 9121.

Liu, X-W., Jin, Z-M. and Green, H. W. (2007), Clinoenstatite exsolution in diopsidic augite of Dabieshan: Garnet peridotite from depth of 300 km, American Mineralogist, Vol. 92, pp. 546 – 552.

Macfarlane, A. M. (1995), An evaluation of the invertedmetamorphic gradient at Langtang National Park, CentralNepal Himalaya. Journal of Metamorphic Geology, Vol. 13, pp. 595–612.

Mahe´o, G., Bertrand, H., Guillot, S., Mascle, G., Peˆcher, A., Picard, C. and de Sigoyer, J.(2000),Te´moins d’un arc immature te´thysiendans les ophiolites du Sud Ladakh (NW Himalaya, Inde). C. R. Acad. Sci. Ser. II 330, pp. 289– 295.

Mahéo, G., Berttrand, H., Guillot, S., Villa, I.M., Keller, F. and Capiez, P. (2004),The South Ladakh Ophiolites (NW Himalaya, India): an intra-oceanic tholeiitic arc origin with implications for the closure of the Neo-Tethys, Chemical Geology,Vol. 203, pp. 273–303.

Mallet, F. R. (1875),On the geology and mineral resources of the Darjiling District and the Western Duars; Mem. Geol. Surv. India, Vol.11, pp. 1–50.

Malpas, J. (1978), Magma generation in the upper mantle, field evidence from ophiolite suites, application to the generation of oceanic lithosphere. Philosophical Transactions of the Royal Society of London, Vol. 288A, pp. 527– 546.

Mattauer, M. (1986), Intra continental subduction, crust mantle décollement and crustal-stacking wedge in the Himalayas and other collision belts, *in* Coward, M.P., and Ries, A.C., eds., Collisional tectonics: Geological Society of America Special Publication, Vol. 19, pp. 37–50.

Mcmillan, P. and Akaogi, M. (1987), Raman spectra of beta - Mg_2SiO_4 (modified spinel) and gamma - Mg_2SiO_4 (spinel), American Mineralogist,Vol. 72, pp. 361-364.

Menzies, M.A.(1973), Mineralogy, partial melt textures within an ultra-mafic body, Greece. Contribution to Mineralogy and Petrology, Vol. 42, pp. 273– 285.

Miyashiro, A. (1973), The Troodos ophiolitic complex was probably formed in an island arc. Earth and Planetary Science Letters, Vol. 19, pp. 218– 224.

Miyashiro, A., 1975, Classification, characteristics, and origin of ophiolites: The Journal of Geology, Vol. 83, pp. 249–281.

Mohan, A., Windley, B. F. and Searle, M. P. (1989) Geothermobarometry and development of inverted metamorphism in the Darjeeling–Sikkim region of the eastern Himalaya, Journal of Metamorphic Geology, Vol.7, pp. 95–110.

Molnar, P. (1988), A review of geophysical constraints on the deepstructure of the Tibetan plateau, the Himalaya, and the Karakoram,and their implications. Philosophical Transactions of theRoyal Society, London, Vol. A 326, pp. 33– 88.

Moores, E.M. and Vine, F.J. (1971), The Troodos massif, Cyprus, and other ophiolites as oceanic crust: Evaluation and implications: Philosophical Transactions of the Royal Society of London, Vol. 268A, pp. 443–466.

Mugnier, J.L., Huyghe, P., Leturmy, P. and Jouanne, F. (2003), Episodicity and rates of thrust sheet motion in Himalaya (western Nepal), *in* McClay, K.R., ed., Thrust Tectonics and Hydrocarbon Systems: American Association of Petroleum Geologists Memoir 82, pp. 1–24.

Mukherjee, B.K. and Sachan, H.K. (2001), Discovery of coesite from Indian Himalaya: A record of ultra-high pressure metamorphism in Indian continental crust, Current Science, Vol. 81, pp. 1358–1361.

Mukherjee, B.K. and Sachan, H.K. (2005), Garnet response diamond pressure metamorphism from Tso-Morari region, Ladakh, India, Himalayan Journal of Science, Vol. 2, No. 4, pp. 209.

Murphy, M.A. and Yin, A. (2003), Structural evolution and sequence of thrusting in the Tethyan fold-thrust belt and Indus-Yalu suture zone, southwest Tibet, Geological Society of America Bulletin, Vol. 115, No. 1, pp. 21–34.

Nelson, K.D. et al. (1996), Partially molten middle crust beneath southern Tibet: A synthesis of Project INDEPTH results, Science, Vol. 274, pp. 1684–1688.

Nicolas A. (1989) Structure of Ophiolites and Dynamics of Oceanic Lithosphere. Kluwer Academic Press, Dordrecht, Boston, London.

O’Reilly S. Y., Griffin, W. L., Poudjom-Djomani, Y. H. and Morgan P. (2001), Are lithospheres forever? GSA Today,Vol. 11, pp. 4–10.

O’Leary, J. A., Gaetani, G. A. and Hauri, E. H. (2010), The effect of tetrahedral Al31 on the partitioning of water between clinopyroxene and silicate melt. Earth and Planetary Science Letters, Vol. 297, pp. 111–120.

Pacalo, R. E. G. and Gasparik, T. (1990), Reversal of the orthoenstatite-clinoenstatite transition at high pressure and high temperatures,Journal of Geophysical Research,Vol. 95, pp. 15853–15858.

Page F. Z., Essene E. J. & Mukasa S. B. (1990), Quartz exsolution in clinopyroxene is not proof of ultrahigh pressures: Evidence from eclogites from the Eastern Blue Ridge, Southern Appalachians, U.S.A., Vol 90, no. 7, pp. 1092 – 1099.

Patriat, P. and Achache, J. (1984), India-Eurasia collision chronology has implications for crustal shortening and driving mechanism of plates, Nature, Vol. 311, pp. 615–621.

Peacock, S. M. (2001), Are the lower planes of double seismic zones caused by serpentine dehydration in subducting oceanic lithosphere? Geology, Vol. 29, pp. 299–302.

Pearce, J.A.(1975), Basalt geochemistry used to investigate past tectonic environments on Cyprus, Tectonophysics, Vol. 25, pp. 41–67.

Pecher, A. (1989), The metamorphism in the central Himalaya. Journal of Metamorphic Geology, Vol. 7, pp. 31 – 41.

Pedersen, R.B., Searle, M.P. and Corfield, R.I. (2001), U–Pb zircon ages from the Spontang Ophiolite, Ladakh Himalaya, Journal of Geological Society, London,Vol. 158, pp. 513–520.

Perraki, M., Korsakov, A. V., Smith, D. C. and Mposkos, E. (2009), Raman spectroscopic and microscopic criteria for the distinction of microdiamonds in ultrahigh-pressure metamorphic rocks from diamonds in sample preparation materials, American Mineralogist, Vol. 94, pp. 546 – 556.

Powell, C.M. and Conaghan, P.J. (1973), Plate tectonics and the Himalayas, Earth and Planetary Science Letters, Vol. 20, pp. 1–12.

Power IM, Wilson SA, Thom JM et al. (2007) Biologically induced mineralization of dypingite by cyanobacteria from an alkaline wetland near Atlin, British Columbia, Canada. Geochem. Trans. Vol. 8, pp. 13.

Presnall, D. C. and Gasparik, T. (1990), Melting of enstatite ($MgSiO_3$) from 10 to 16.5 GPa and the forsterite (Mg_2SiO_4) -majorite ($MgSiO_3$) eutectic at 16.5 GPa: Implications for the origin of the mantle, Journal of Geophysical Research, Vol. 95, pp. 15771 – 15777.

Raman, C. V. and Krishnan, K. S. (1928), A new type of secondary radiation, Nature, Vol. 121, pp. 501 – 502.

Rampone, E., Piccardo, G. B., Vannucci, R., Bottazzi, P., and Ottolini, L. (1993), Sub solidus reactions monitored by trace element partitioning: the spinel- to plagioclase-facies transition in mantle peridotites. Contribution to Mineralogy and Petrology, Vol. 115, pp. 1–17.

Ravikant, V., Pal, T. and Das, D. (2004), Chromites from the Nidar ophiolite and Karzok complex, Transhimalaya, Eastern Ladakh: their magmatic evolution, Journal of Asian Earth Sciences, Vol. 24, pp. 177 – 184.

Reagan, M. K. et al., (2010), Fore arc basalts and subduction initiation in the Izu-Bonin-Mariana system. Geochemistry, Geophysics, Geosystems, Vol. 11.

Reuber, I., Colchen, M. and Mevel, C. (1987),The geodynamic evolution of the South – Tethyan margin in Zanskar, NW Himalaya, as revealed by the Spontang ophiolitic melange, Geodin. Acta, Vol. 1, pp. 283– 296.

Reuber, I. (1989), The Dras arc, two successive volcanic events on eroded oceanic crust, Tectonophysics,Vol. 161, pp. 93–106.

Robinson, P., Jaffe, H.W., Ross, M. and Klein Jr., C. (1971), Orientation of exsolution lamellae in clinopyroxenes and clinoamphiboles: consideration of optimal phase boundary, American Mineralogist, Vol. 56, pp. 909 – 939.

Robinson, P., Ross, M., Nord Jr., G.L., Smyth, J.R. and Jaffe, H.W. (1972), Exsolution lamellae in augite and pigeonite: fossil indicators of lattice parameters at high temperature and pressure, American Mineralogist, Vol. 62, pp. 857 – 873.

Robinson, P.T., Bai, W.-J., Malpas, J., Yang, J.-S., Zhou, M.-F., Fang, Q.-S., Hu, X.-F., and Cameron, S. (2004), Ultra-high pressure minerals in the Luobusa ophiolite, Tibet and their tectonic implications, in Malpas, J., Fletcher, C.J.N., Ali, J.R., and

Aitchison, J.C., eds., Aspects of the tectonic evolution of China: Geological Society [London] Special Publication Vol. 226, pp. 247–271.

Robinson, D.M., DeCelles, P.G. and Copeland, P.(2006),Tectonic evolution of the Himalayan thrust belt inwestern Nepal: Implications for channel flow models: Geological Society of America Bulletin, Vol. 118, pp. 865–885.

Rohrbach, A., Ballhaus, C., Golla-Schindler, U., Ulmer, P., Kamenetsky, V. S. and Kuzmin, D. V. (2007), Metal saturation in the upper mantle, Nature, Vol. 449, pp. 456-458.

Rohrbach, A. and Schmidt, M. W. (2011), Redox freezing and melting in the Earth's deep mantle resulting from carbon-iron redox coupling, Nature, Vol. 472, pp. 209 – 212.

Sachan, H.K. (2001), Supra-subduction origin of the Nidar Ophiolitic sequence, Indus Suture Zone, Ladakh, India: evidence from mineral chemistry of upper mantle rocks, Ofioliti,Vol. 26, pp. 23–32.

Sachan, H. K., Mukherjee, B. K. and Bodnar, R. J. (2007), Preservation of methane generated during serpentinization of upper mantle rocks: Evidence from Fluid inclusions in the Nidar Ophiolite, Indus Suture Zone, Ladakh (India), Earth Planetary Science Letters, Vol. 257, pp. 47 – 59.

Sakai, H., Takigami, Y., Nakamuta, Y. and Nomura, H. (1999), Inverted metamorphism in the pre – Siwalik foreland basin sediments beneath the crystalline nappe, western Nepal Himalaya: Journal of Asian Earth Sciences, Vol. 17, pp. 727–739.

Schiano, P. and Clocchiatti, R. (1994),World-wide occurrence of silica-rich melts in sub-continental and sub-oceanic mantle minerals, Nature (London),Vol. 368, pp. 621–624.

Searle, M.P., Windley, B.F., Coward, M.P., Cooper, D.J.W., Rex, A.D., Rex, D., Tingdong, L.,Xuchang, X., Jan, M.Q., Thakur, V. C. and Kumar, S. (1987), The closing of Tethys and the tectonics of the Himalayas, Geological Society of America Bulletin, Vol. 98, pp. 678–701.

Searle, M.P., Simpson, R.L., Law, R.D., Parrish, R.R. and Waters, D.J. (2003), The structural geometry, metamorphic and magmatic evolution of the Everest Massif, High Himalaya of Nepal–South Tibet, Geological Society of London, Vol. 160, pp. 345–366.

Sen, K., Das, S., Mukherjee, B. K. and Sen, K. (2013), Bimodal stable isotope signatures of Zildat Ophiolitic Me´lange, Indus Suture Zone, Himalaya: implications for emplacement of an ophiolitic me´lange in a convergent setup, Intrenational Journal of Earth sciences, Geosciences of the Himalaya–Karakoram–Tibet orogen, Vol. 102, No. 7, pp. 2033 – 2042.

Sharma, K. K. (1998), Geologic and tectonic evolution of the Himalaya before and after the India-Asia collision, Proceedings of Indian Academy of Science, Vol. 107, No.4, pp. 265 – 282.

Shim, S. H. and Duffy, T. S. (2001),Raman spectroscopy of Fe_2O_3 to 62 GPa, American Mineralogist, Vol. 87, pp. 318 – 326.

Smith, D. C., Dobrzhinetskaya, L. F., Godard, G. and Green, H. (2011), Diamond Lonsdaleite - Graphite Relations Examined by Raman Mapping of Carbon Microinclusions inside Zircon at KumdyKol, Kokchetav, Kazakhstan: Evidence of the Metamictization of Diamond, Ultrahigh Pressure Metamorphism: 25 Years after Discovery of Coesite and Diamond (eds Dobrzhinetskaya, L.F., Faryad, S.W., Wallis, S. & Cuthbert, S.),Elsevier, Amsterdam, 43 – 75.

Smith, D. C. and Godard, G. (2013), A Raman spectroscopic study of diamond and disordered sp^3-carbon in the coesite-bearing Straumen Eclogite Pod, Norway, Journal of Metamorphic Geology, Vol. 31, pp. 19 – 33.

Steinman, G. (1905), Geologische Beobachtungen in den Alpen, II. Die Schardtshe Ueberfaltungstheorieund die geologische Bedeutung der Tiefseeabatze und der ophiolitschen Massengesteine, Bereichte Naturforeschenden Gesellschaft, Freiburg, Vol. 16, pp. 1–49.

Steinmann, G., (1927), Die ophiolitischen Zonen in den Mediterranean Kettengebirgen: Compte Rendu, XIVe Congres Géologique International, 1926, Madrid,Graficas Reunidas, Vol. 2, pp. 637–667.

Stephenson, B.J., Waters, D.J. & Searle, M.P. (2000), Inverted metamorphism and the Main Central Thrust: field relations and thermo barometric constraints from the Kishtwar Window, NW Indian Himalaya. Journal of Metamorphic Geology, Vol. 18, pp. 571–590.

Stern, R. J. and Bloomer, S. H. (1992), Subduction zone infancy: Examples from the Eocene Izu-Bonin-Mariana and Jurassic California arcs, GSA Bulletin, Vol. 104, pp. 1621 – 1636.

Su, W.J., Woodward, R.L., Dziewonski, A.M. (1992), Deep origin of mid-ocean-ridge seismic velocity anomalies. Nature, Vol. 360, pp. 149–152.

Thakur, V.C. and Virdi, N.S. (1979), Lithostratigraphy, structural framework, deformation and metamorphism of the south-eastern region of Ladakh. Kashmir Himalaya, India. Him. Geol., Vol. 9, pp. 11–25.

Thakur, V.C., Bhat, M.I. (1983), Interpretation of tectonic environment of Nidar Ophiolite: A geochemical approach. In: Thakur, V.C., Sharma, K.K. (Eds.), Geology of Indus Suture Zone of Ladakh. Wadia Institute of Himalayan Geology, Dehradun, pp. 21–31.

Thakur, V.C., Misra, D.K. (1984), Tectonic framework of Indus and Shyok Suture Zones in eastern Ladakh. Northwest Himalaya. Tectonophysics 101, 207–220.

Thakur, V.C. (1990), Indus Tsangpo suture zone in Ladakh – its tectonostratigraphy and tectonics, Proceed. Indian Acad. Sci. (Earth Planet. Sci.), Vol. 99, pp. 169–185.

Tribaudino, M., Mantovani, L.,Bersani, D. & Lottici, P. P.(2012), Raman spectroscopy of (Ca, Mg)$MgSi_2O_6$clinopyroxenes, American Mineralogist, Vol. 97, pp. 1339 – 1347.

Trumbull, R. B., Yang, J. S., Robinson, P. T., Di Pierro, S., Vennenmann, T. and Wiedenbeck, M. (2009),The carbon isotope composition of natural SiC (moissanite) from the Earth's mantle: new discoveries from ophiolites, Lithos, Vol. 113, pp. 612 – 620.

Ulmer, P. & Trommsdorff, V. (1995), Serpentine stability to mantle depth and subduction related magmatism, Science, Vol. 268, pp. 858 – 861.

Ulmer, P. and Stalder, R. (2001), The Mg(Fe)SiO_3 orthoenstatite - clinoenstatite transition at high pressures and temperatures determined by Raman-spectroscopy on quenched samples, American Mineralogist, Vol. 86, pp. 1267-1274.

Upadhyay, H.D. and Neale, E.R.W. (1979), On the tectonic regime of ophiolite genesis. Earth and Planetary Science Letters, Vol. 43, pp. 93 – 102.

Valdiya, K.S., 1980. Geology of the Kumaon Lesser Himalaya. The Himachal Press, Wadia Institute of Himalayan Geology, Dehra Dun.

Van Roermund, H.L.M. and Drury, M.R. (1998), Ultra-high pressure ($P > 6$ GPa) garnet peridotites in Western Norway: exhumation of mantle rocks from 185 km depth, Terra Nova, Vol. 10, pp. 295 – 301.

Vannay, J.C. and Grasemann, B. (2001), Himalayan inverted metamorphism and synconvergence extension as a consequence of a general shear extrusion, Geological Magazine, Vol. 138, pp. 253–276.

Vine, F. J. and D. H. Matthews (1963) Magnetic anomalies over ocean ridges, Nature, Vol. 199, pp. 947 – 949.

Vrijmoed, J. C. and Smith, D. C.&Van Roermund, H. L. M. (2008), Raman confirmation of microdiamond in the Svartberget Fe - Ti type garnet peridotite, Western Gneiss Region, Western Norway,Terra Nova,Vol. 20, pp. 295 – 301.

Weinberg, R.F., Dunlap, W.J. and Whitehouse, M. (2000), New field, structural, geochronological data from the Shyok, Nubra valleys, northern Ladakh, linking Kohistan to Tibet. In: Khan, M.A., Treolar, P.J., Searle, M.P., Jan, M.Q. (Eds.), Tectonics of the Nanga Parbat Syntaxis, the Western Himalaya. Geol. Soc. Spec. Pub. Geological Society of London, UK, Vol. 170, pp. 253– 276.

Whitmarsh, R.B., Manatschal, G., Minshull, T. A. (2001), Evolution of magma – poorcontinental margins from rifting to seafloor spreading, Nature, Vol. 413, pp. 150 – 154.

White, N.M., Pringle, M., Garzanti, E.,Bickle, M., Najman, Y., Chapman, H. and Friend, P., (2002), Constraints on the exhumation and erosion of the High Himalayan Slab, NW India, from foreland basin deposits, Earth and Planetary Science Letters, Vol. 195, pp. 29–44.

Wu, C., K.D. Nelson, G. Wortman, S.D. Samson, Y. Yue, J. Li, W.S.F. Kidd, and M.A. Edwards (1998),Yadong cross structure and South Tibetan Detachment in the east-central Himalaya (89-90E), Tectonics, Vol. 17, pp. 28-45.

Yamamoto, S., Komiya, T., Hirose, K. and Maruyama, S. (2009), Coesite and clinopyroxene exsolution lamellae in chromites: In-situ ultrahigh-pressure evidence from podiform chromitites in the Luobusa ophiolite, southern Tibet, Lithos, Vol. 109, No. 3-4, pp. 314 – 322.

Yang, J. et al., (2007), Diamond- and coesite-bearing chromitites from the Luobusa ophiolite, Tibet, Geology, Vol. 35, No. 10, pp. 875 – 878.

Yin, A. (2006), Cenozoic tectonic evolution of the Himalayan orogen as constrained by along-strike variation of structural geometry, exhumation history, and foreland sedimentation, Earth-Science Reviews, Vol. 76, pp. 1–131.

Zhang, L., Song, S., Liou, J, G., Ai, Y. and Li, X. (2005), Relict coesite exsolution in omphacite from western Tianshaneclogites, China, American Mineralogist,Vol. 90, pp. 181 – 186.

Zhao, W., Nelson, K. D., Project INDEPTH Team (1993), Deep seismic reflection evidence for continental under thrusting beneath southern Tibet, Nature, Vol. 366, pp. 557 – 559.

Zhao, D., Xu, Y., Wiens, D.A., Dorman, L., Hildebrand, J., Webb, S. (1997), Depth extent ofthe Lau back-arc spreading center and its relation to subduction processes. Science, Vol. 278, pp. 254–257.

APPENDIX

APPENDIX

The appendix section contains additional EMPA (APPENDIX 1) and Laser Raman spectroscopic analyses (APPENDIX 2).

APPENDIX 1

Additional Electron microprobe analyses of olivine and spinels of 1NU18 dunite, which represents the discordant dunite (correspond to table 4.1).

Elements	Olivine	Olivine	Spinel	Spinel	Spinel	Olivine	Olivine
Na_2O	0.01	0	0.02	0.02	0	0	0
MgO	51.22	50.97	13.01	12.31	12.68	51.22	51.13
Al_2O_3	0	0	17.46	14.53	16.06	0	0.01
SiO_2	41.77	41.98	0.04	0.03	0.04	41.73	41.89
P_2O_5	0	0	0	0.03	0	0	0
K_2O	0	0	0	0	0	0.01	0
CaO	0.03	0.02	0	0.01	0	0.04	0.03
TiO_2	0	0.04	0.18	0.17	0.18	0.02	0.02
MnO	0.17	0.19	0.28	0.32	0.3	0.16	0.06
FeO	6.29	6.48	15.35	15.61	15.21	6.41	6.23
Cr_2O_3	0.01	0	52.72	56.53	55.37	0.06	0
Total	99.5	99.68	99.06	99.55	99.85	99.65	99.38

Additional Electron microprobe analyses of olivine and spinels of 1NU18 dunite, which represents the discordant dunite (correspond to table 4.1).

Elements	Spinel	Spinel	Olivine	Olivine	Olivine	Olivine
Na_2O	0	0	0.01	0	0	0
MgO	11.8	11.73	50.81	51.12	50.99	51.27
Al_2O_3	13.74	12.65	0	0	0	0
SiO_2	0.05	0.03	42.11	41.93	41.76	41.9
P_2O_5	0.01	0	0.03	0.01	0	0.01
K_2O	0	0	0	0	0	0
CaO	0	0	0.06	0.06	0.04	0.07
TiO_2	0.19	0.09	0.06	0	0	0.03
MnO	0.27	0.4	0.12	0.09	0.08	0.12
FeO	16.49	16.89	6.33	6.15	6.5	6.35
Cr_2O_3	56.13	58.01	0	0	0	0
Total	98.69	99.8	99.54	99.35	99.36	99.76

Additional Electron microprobe analyses of olivine and spinels of 1NU18 dunite, which represents the discordant dunite (correspond to table 4.1).

Elements	Spinel	Spinel	Spinel	Spinel	Spinel	Spinel
Na_2O	0	0.01	0.02	0.06	0	0.04
MgO	12.28	13.61	15.41	4.76	15.53	5.32
Al_2O_3	15.03	20.84	30.6	0.23	30.46	0.29
SiO_2	0.04	0.08	0.03	3.12	0.05	3.69
P_2O_5	0	0	0	0	0	0
K_2O	0.01	0	0.01	0.02	0	0
CaO	0	0.04	0	0.17	0	0.11
TiO_2	0.08	0.08	0.03	0.58	0.1	0.44
MnO	0.27	0.25	0.32	2.33	0.18	2.03
FeO	15.13	14.62	12.15	54.84	12.63	54.29
Cr_2O_3	55.96	50.55	39.83	27.02	40.16	26.47
Total	98.81	100.07	98.4	93.13	99.12	92.68

Additional EPM analyses of olivine, orthopyroxene, clinopyroxene and spinel in a lherzolite (3) representative of the ultramafics cut by the dunite channel (correspond to table 4.5).

Elements	Opx	Opx	Opx	Opx	Olivine	Olivine	Olivine	Cpx
Na_2O	0	0	0	0	0	0.02	0.01	0.1
MgO	33.26	32.87	33.07	31.76	48.95	48.91	48.96	16.49
Al_2O_3	3.8	3.97	3.98	3.81	0	0	0	3.28
SiO_2	55.69	55.53	55.91	55.55	41.35	41.44	41.33	52.33
P_2O_5	0.03	0	0	0	0.03	0.02	0	0
K_2O	0.01	0.02	0.01	0	0	0.04	0	0
CaO	0.62	0.67	0.48	2.4	0	0.02	0.04	24.91
TiO_2	0.03	0.06	0.08	0.06	0	0.03	0	0.11
MnO	0.09	0.18	0.15	0.06	0.15	0.16	0.16	0.06
FeO	5.97	5.88	6.02	5.8	9.3	9.62	9.24	1.79
Cr_2O_3	0.91	0.75	0.8	0.63	0	0	0	0.9
Total	100.4	99.95	100.49	100.08	99.77	100.26	99.75	99.97

Additional EPM analyses of olivine, orthopyroxene, clinopyroxene and spinel in a lherzolite (3) representative of the ultramafics cut by the dunite channel (correspond to table 4.5).

Elements	Cpx	Cpx	Cpx	Olivine	Olivine	Spinel	Spinel
Na_2O	0.12	0.12	0.13	0	0	0	0.02
MgO	16.02	16.39	16.33	48.95	48.96	2.28	3.31
Al_2O_3	3.67	3.32	3.79	0.01	0	1.25	1.96
SiO_2	52.46	52.92	52.35	41.72	41.38	1.8	2.7
P_2O_5	0	0	0.03	0	0	0	0
K_2O	0	0.01	0	0	0	0	0
CaO	24.79	24.67	24.33	0.01	0.04	0.01	0
TiO_2	0.17	0.14	0.15	0.06	0.02	0.26	0.13
MnO	0.09	0.11	0.13	0.15	0.16	0.31	0.29
FeO	1.93	2.1	2.05	9.18	9.34	70.42	67
Cr_2O_3	1.01	0.93	0.79	0	0.02	17.25	17.91
Total	100.26	100.71	100.08	100.09	99.92	93.58	93.33

Additional EPM analyses of olivine, orthopyroxene and spinel in a harzburgite (1NU29) representative of the ultramafics cut by the dunite channel (correspond to table 4.6).

Elements	Opx	Opx	Opx	Olivine	Olivine	Olivine	Olivine
Na_2O	0	0.01	0	0	0	0	0
MgO	34.53	34.17	34.4	49.28	49.49	49.26	49.38
Al_2O_3	0.59	0.69	0.7	0	0	0	0
SiO_2	58.49	58.48	58.54	41.65	41.55	41.94	41.67
P_2O_5	0.02	0.01	0	0	0.04	0.01	0.01
K_2O	0.01	0	0	0.01	0	0	0
CaO	0.9	1.33	0.91	0.02	0.03	0.01	0.01
TiO_2	0	0.02	0.01	0.05	0.02	0.04	0.02
MnO	0.05	0.11	0.25	0.15	0.18	0.11	0.1
FeO	5.36	5.42	5.79	8.76	8.46	8.6	8.74
Cr_2O_3	0.3	0.39	0.36	0	0	0.08	0
Total	100.24	100.64	100.97	99.92	99.77	100.06	99.93

Additional EPM analyses of olivine, orthopyroxene and spinel in a harzburgite (1NU29) representative of the ultramafics cut by the dunite channel (correspond to table 4.6).

Elements	Spinel	Spinel	Spinel	Spinel	Spinel	Spinel	Olivine	Olivine	Opx
Na_2O	0.01	0	0.02	0	0	0.01	0	0	0
MgO	9.35	9.26	9.38	9.4	9.44	9.29	49.17	49.61	34.63
Al_2O_3	11.08	10.9	10.76	10.92	11.02	11.32	0	0	0.74
SiO_2	0.04	0.05	0.02	0.05	0.06	0.07	41.51	41.2	57.91
P_2O_5	0	0.05	0.03	0.02	0	0.05	0	0	0.03
K_2O	0	0	0.04	0	0	0	0	0	0
CaO	0	0	0.01	0.02	0.01	0.01	0.01	0.02	0.59
TiO_2	0.02	0.1	0.06	0.1	0	0.05	0.02	0	0.04
MnO	0.19	0.34	0.32	0.38	0.45	0.31	0.13	0.14	0.12
FeO	19.69	19.97	20.43	20.75	20.65	20.14	8.56	8.68	5.42
Cr_2O_3	58.36	58.09	58.74	58.19	58.14	58.15	0	0.01	0.44
Total	98.73	98.75	99.8	99.83	99.77	99.41	99.41	99.65	99.93

Additional EPM analyses of olivine, orthopyroxene and spinel in a harzburgite (1NU29) representative of the ultramafics cut by the dunite channel (correspond to table 4.6).

Elements	Opx	Opx	Opx	Olivine	Olivine	Opx	Olivine	Olivine
Na_2O	0.02	0	0	0	0	0	0	0
MgO	34.38	33.95	33.51	49.11	49.03	34.53	49.33	49.75
Al_2O_3	0.78	0.71	0.75	0	0	0.68	0.01	0
SiO_2	57.85	57.97	57.77	41.46	41.34	58.49	41.45	41.46
P_2O_5	0	0	0	0	0	0.04	0	0.01
K_2O	0	0.01	0.02	0.01	0	0	0	0.01
CaO	1.12	1.46	2.18	0.01	0	0.7	0.01	0.03
TiO_2	0.01	0.03	0.03	0	0.01	0.01	0.03	0.05
MnO	0.2	0.1	0.12	0.18	0.14	0.06	0.14	0.03
FeO	5.59	5.31	5.46	8.11	8.48	5.62	8.49	8.67
Cr_2O_3	0.42	0.44	0.35	0.03	0.02	0.36	0.01	0.02
Total	100.36	99.98	100.18	98.91	99.03	100.49	99.47	100.04

Additional Mineral chemistry data of essential minerals of 1NU27 lherzolite, which is entrapped in the discordant dunite channel (correspond to Table 4.2).

Elements	Olivine	Cpx	Cpx	Cpx	Cpx	Cpx
Na_2O	0	0.02	0.01	0.02	0.02	0
MgO	48	17.39	17.6	17.94	17.23	17.46
Al_2O_3	0.02	1.2	1	0.8	1.11	0.99
SiO_2	41.06	54.12	54.34	55.12	54.58	54.54
P_2O_5	0	0.02	0.01	0	0.05	0
K_2O	0	0.01	0	0	0	0
CaO	0.01	25.02	24.8	24.06	24.93	24.85
TiO_2	0	0.04	0.04	0	0	0.03
MnO	0.17	0.06	0.08	0.1	0.15	0.05
FeO	8.79	1.8	1.65	1.64	1.82	1.83
Cr_2O_3	0	0.71	0.68	0.5	0.74	0.5
Total	98.05	100.39	100.22	100.17	100.62	100.27

Additional Mineral chemistry data of essential minerals of 1NU27 lherzolite, which is entrapped in the discordant dunite channel (correspond to Table 4.2).

Elements	Opx	Opx	Opx	Opx	Spinel	Spinel	Spinel	Spinel
Na_2O	0	0	0	0	0	0.02	0	0
MgO	33.94	34.09	34.04	33.73	10.68	10.79	10.61	10.5
Al_2O_3	0.93	0.91	0.95	0.84	15.94	16.21	15.61	15.16
SiO_2	57.4	57.98	57.74	57.89	0.07	0.05	0.07	0.05
P_2O_5	0	0	0	0	0	0	0	0.02
K_2O	0.02	0	0	0	0	0.03	0.01	0
CaO	0.7	0.65	0.65	0.57	0.05	0.06	0.01	0.02
TiO_2	0.06	0	0	0	0.05	0.1	0.09	0.05
MnO	0.2	0.11	0.17	0.18	0.27	0.33	0.33	0.27
FeO	6.04	5.93	5.74	5.83	19.7	20.03	19.54	19.28
Cr_2O_3	0.41	0.37	0.29	0.26	51.76	50.32	52.21	53.47
Total	99.7	100.04	99.58	99.3	98.53	97.93	98.49	98.82

Additional Mineral chemistry data of essential minerals of 1NU27 lherzolite, which is entrapped in the discordant dunite channel (correspond to Table 4.2).

Elements	Spinel	Spinel	Spinel	Olivine	Olivine	Olivine	Olivine	Opx
Na_2O	0	0	0.01	0.01	0	0	0	0
MgO	10.41	10.14	10.22	48.37	48.35	48.94	48.79	32.85
Al_2O_3	14.77	14.73	14.82	0	0	0	0	1.22
SiO_2	0.02	0.06	0.06	41.14	41.16	41.04	41.18	57.3
P_2O_5	0	0	0.01	0	0	0	0.01	0
K_2O	0.01	0.01	0.02	0	0	0	0	0.01
CaO	0	0	0.01	0.03	0.02	0.01	0	1.59
TiO_2	0.09	0.03	0.11	0.05	0.01	0.02	0.05	0.05
MnO	0.37	0.25	0.32	0.16	0	0.16	0.1	0.22
FeO	19.69	19.9	19.54	8.81	8.46	8.85	8.62	5.81
Cr_2O_3	53.03	52.44	53.4	0.07	0.01	0.04	0.11	0.56
Total	98.4	97.55	98.52	98.65	98.01	99.04	98.88	99.62

Additional Mineral chemistry data of essential minerals of 1NU27 lherzolite, which is entrapped in the discordant dunite channel (correspond to Table 4.2).

Elements	Opx	Opx	Opx	Opx	Opx	Opx	Opx	Opx
Na_2O	0	0	0	0	0	0	0	0.02
MgO	33.53	28.71	32.13	33.32	33.64	33.5	33.85	32.86
Al_2O_3	1.11	0.98	1	1.05	1.02	0.98	1.04	1.03
SiO_2	57.4	56.37	57.44	57.37	57.54	57.37	57.45	57.03
P_2O_5	0	0.03	0.05	0.02	0	0.01	0	0
K_2O	0	0.01	0.01	0	0	0	0	0.02
CaO	1.01	8.42	2.84	0.69	1	0.55	0.63	1.58
TiO_2	0.02	0.08	0.02	0.06	0.05	0	0.01	0
MnO	0.14	0.11	0.09	0.16	0.16	0.15	0.18	0.17
FeO	5.84	4.48	5.54	5.93	5.75	5.96	5.91	5.84
Cr_2O_3	0.5	0.49	0.43	0.39	0.39	0.56	0.43	0.44
Total	99.54	99.69	99.54	98.99	99.56	99.09	99.5	98.99

Additional Mineral chemistry data of essential minerals of 1NU27 lherzolite, which is entrapped in the discordant dunite channel (correspond to Table 4.2).

Elements	Opx	Cpx	Cpx	Cpx	Cpx	Cpx	Cpx	Cpx
Na_2O	0.01	0.07	0.03	0.07	0.03	0.02	0.02	0.03
MgO	33.31	24.67	17.4	28.23	29.99	17.42	17.2	20.01
Al_2O_3	1.05	0.93	1.37	0.77	0.66	1.3	1.31	1.06
SiO_2	57.48	48.18	54.71	46.33	47.27	54.4	54.38	52.95
P_2O_5	0.03	0	0	0	0.01	0	0	0
K_2O	0	0.01	0.01	0.06	0.01	0	0.02	0
CaO	0.89	12.32	23.66	9.07	7.96	23.71	23.62	21.01
TiO_2	0	0.04	0.06	0.02	0.02	0	0.06	0.03
MnO	0.11	0.22	0.13	0.14	0.09	0.1	0.03	0
FeO	5.57	3.08	1.76	3.42	4.01	1.69	2.13	2.13
Cr_2O_3	0.47	0.72	0.83	0.61	0.27	0.74	0.77	0.73
Total	98.93	90.21	99.96	88.73	90.31	99.38	99.54	97.95

Additional Mineral chemistry data of essential minerals of 1NU27 lherzolite, which is entrapped in the discordant dunite channel (correspond to Table 4.2).

Elements	Cpx	Opx	Opx	Opx	Olivine	Olivine	Olivine	Olivine
Na_2O	0.01	0.02	0.03	0	0	0	0.01	0
MgO	17.48	34.19	32.85	33.61	49.25	49.27	48.79	49.11
Al_2O_3	1.27	1.16	1.15	1.09	0	0.01	0	0
SiO_2	54.28	57.66	57.56	57.63	41.63	41.05	41.73	41.48
P_2O_5	0	0.03	0	0.05	0.03	0	0.02	0.02
K_2O	0	0	0.01	0.01	0	0	0	0
CaO	23.65	0.69	2.48	1.18	0.01	0.01	0	0.02
TiO_2	0.07	0	0.05	0.01	0.02	0.03	0	0
MnO	0.04	0.09	0.15	0.17	0.19	0.17	0.05	0.1
FeO	1.81	5.5	5.05	5.59	9.05	9.04	8.76	8.91
Cr_2O_3	0.73	0.6	0.71	0.46	0.04	0	0.11	0.03
Total	99.32	99.95	100.06	99.8	100.24	99.58	99.47	99.66

Additional Mineral chemistry data of essential minerals of 1NU27 lherzolite, which is entrapped in the discordant dunite channel (correspond to Table 4.2).

Elements	Olivine	Olivine	Olivine	Opx	Opx	Opx	Opx	Opx	Opx
Na_2O	0	0	0.02	0.01	0	0	0.02	0	0.03
MgO	49.01	49.15	48.99	33.54	33.81	33.81	33.71	33.77	33.42
Al_2O_3	0	0.01	0	1.1	1.15	1.13	1.1	1.14	1.04
SiO_2	41.16	41.37	41.46	57.18	57.86	57.82	57.73	57.52	57.5
P_2O_5	0	0	0.02	0	0	0.01	0	0.05	0
K_2O	0	0	0	0	0	0	0.03	0	0.01
CaO	0.03	0.02	0.01	1.43	0.87	0.83	0.8	1.13	1.08
TiO_2	0.04	0.02	0.03	0.05	0	0	0	0.05	0.02
MnO	0.06	0	0.1	0.13	0.09	0.07	0.13	0.15	0.11
FeO	8.41	8.92	8.34	5.71	5.67	5.76	5.99	5.68	5.73
Cr_2O_3	0	0	0	0.62	0.51	0.55	0.53	0.48	0.45
Total	98.71	99.48	98.96	99.78	99.94	100	100.05	99.96	99.39

Additional Mineral chemistry data of essential minerals of 1NU27 lherzolite, which is entrapped in the discordant dunite channel (correspond to Table 4.2).

Elements	Opx	Olivine	Olivine	Cpx	Opx	Cpx	Opx
Na_2O	0	0	0	0.02	0	0.01	0.01
MgO	33.34	48.97	48.71	28.77	33.35	28.59	33.18
Al_2O_3	1.11	0	0	1.02	1.09	0.96	1.12
SiO_2	57.35	41.15	41.33	56.15	57.57	56.99	57.66
P_2O_5	0.01	0	0.04	0	0.01	0	0
K_2O	0	0	0	0	0	0	0
CaO	1.37	0.04	0.03	8.6	1.49	8.78	1.02
TiO_2	0.06	0	0	0.02	0	0.03	0
MnO	0.14	0.13	0.17	0.03	0.1	0.06	0.08
FeO	5.61	8.84	8.75	4.64	5.64	4.37	5.46
Cr_2O_3	0.51	0.04	0	0.47	0.54	0.48	0.47
Total	99.5	99.17	99.03	99.73	99.8	100.28	98.99

Additional Mineral chemistry data of essential minerals of 1NU27 lherzolite, which is entrapped in the discordant dunite channel (correspond to Table 4.2).

Elements	Cpx	Opx	Cpx	Opx	Olivine	Olivine	Olivine
Na_2O	0	0	0.01	0	0	0	0
MgO	29.21	33.39	29.5	32.49	47.07	47.21	47.34
Al_2O_3	1.07	1.1	1.12	1.11	0	0.02	0
SiO_2	56.21	57.85	56.75	56.66	40.56	40.28	40.4
P_2O_5	0.06	0.03	0.01	0.05	0.04	0	0.02
K_2O	0.01	0.01	0.01	0	0	0	0.02
CaO	7.83	1.57	7.31	1.21	0.04	0	0.05
TiO_2	0.08	0.04	0.01	0.01	0	0.04	0
MnO	0.02	0.18	0.1	0.13	0.09	0.2	0.13
FeO	4.47	5.73	4.63	5.96	9.22	9.16	8.97
Cr_2O_3	0.51	0.52	0.44	0.55	0	0	0
Total	99.48	100.42	99.9	98.18	97.03	96.91	96.92

APPENDIX 2

AP 2. Additional Raman spectra of high pressure minerals in lherzolite 1M1 (shown in chapter 4; corresponds to Fig 4.8 & 4.13) are showing all mineral phases – Coesite, *C2/c* Clinoenstatite, α – Fe_2O_3 glass, disordered α – Fe_2O_3 and disordered carbon recovered from the ultramafic part of the Nidar ophiolite.

A. 2B11 – 2B19 are additional analyses of spot 1 from the same grain as in B1 in Fig 4.8.

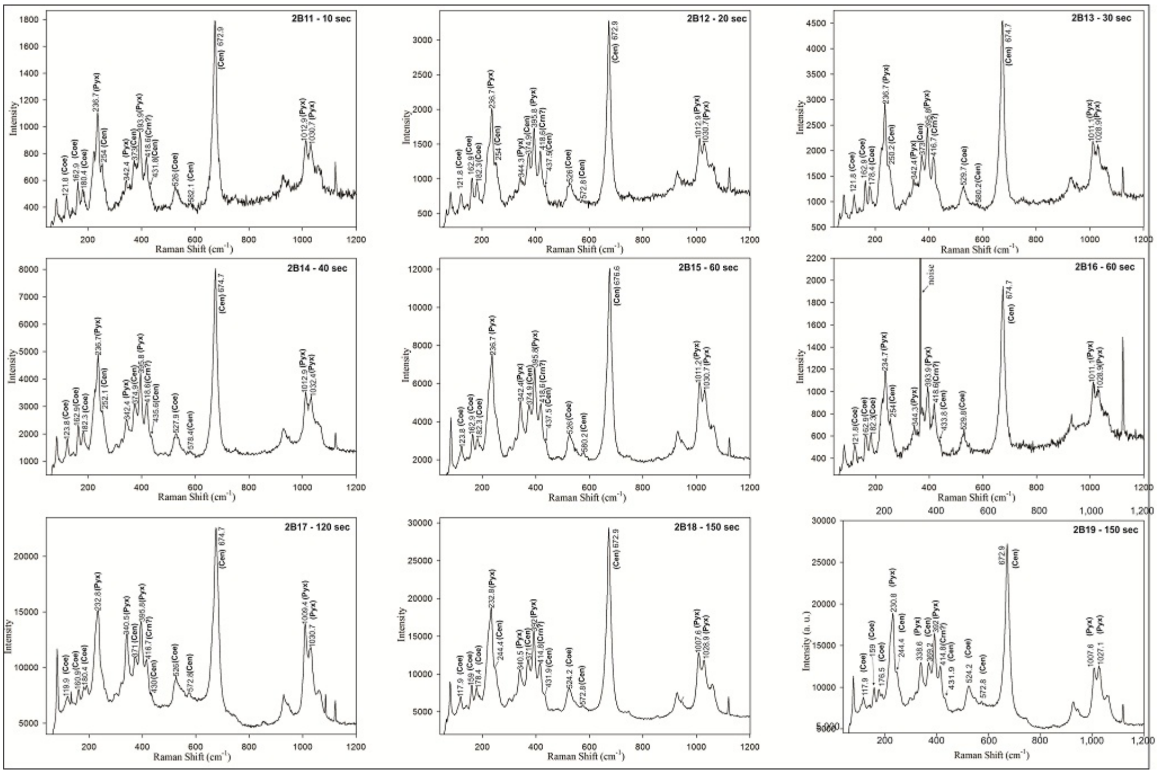

AP 2. B. 2B31 & 2B32 are additional analysis of spot 3 shown in Fig 4.8 B. Spectra 2B21 & 2B22 are corresponding to spot 2 in Fig 4.8 B. The Raman spectra of the host are showing trend of an orthoenstatite and written as “Host”. The point 5 of Fig 4.8 showing presence of disordered carbonaceous matter (Fig 2C 51 – 52).

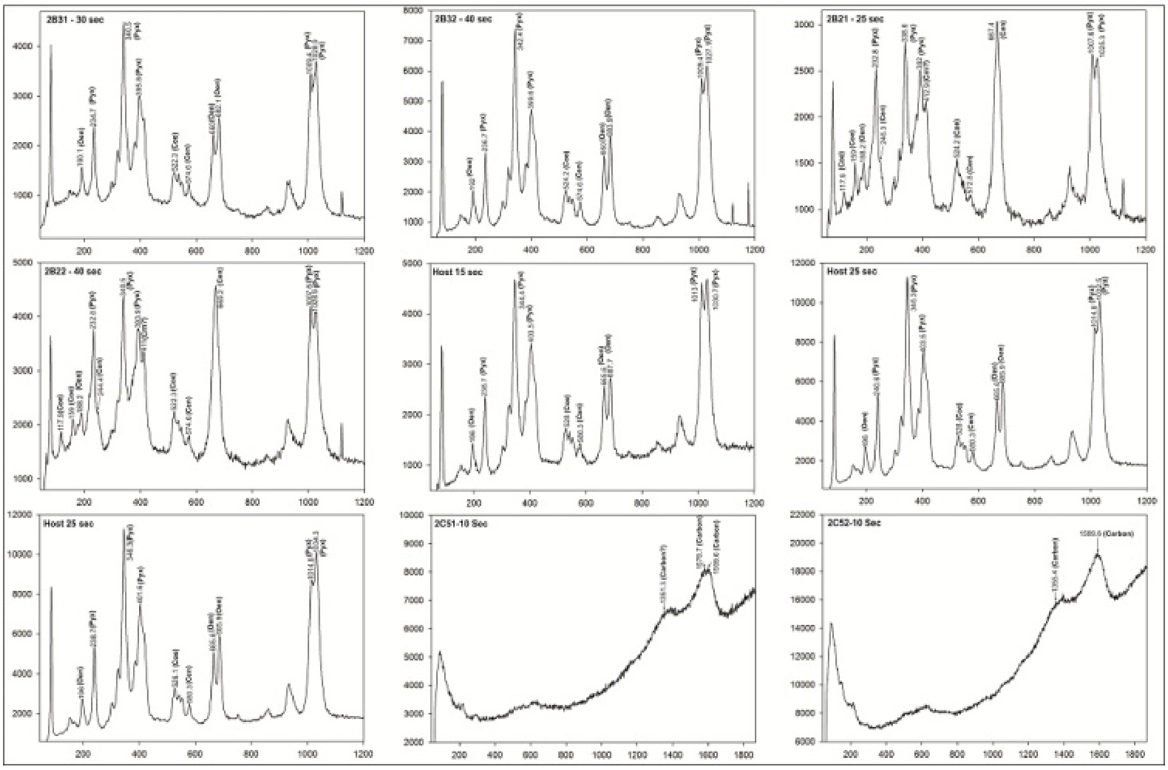

AP 2. C. 2C 53 & 2C 54 show α – Fe_2O_3 + disordered carbon which is corresponds to the spot 5 in Fig 4.8 C. The 2C61 – 2C63 spectra represent additional spectra of disordered α – Fe_2O_3 taken from different part of the same grain around point 6 in Fig 4.8. 2C41 represents point 4 shown in Fig 4.8 C.

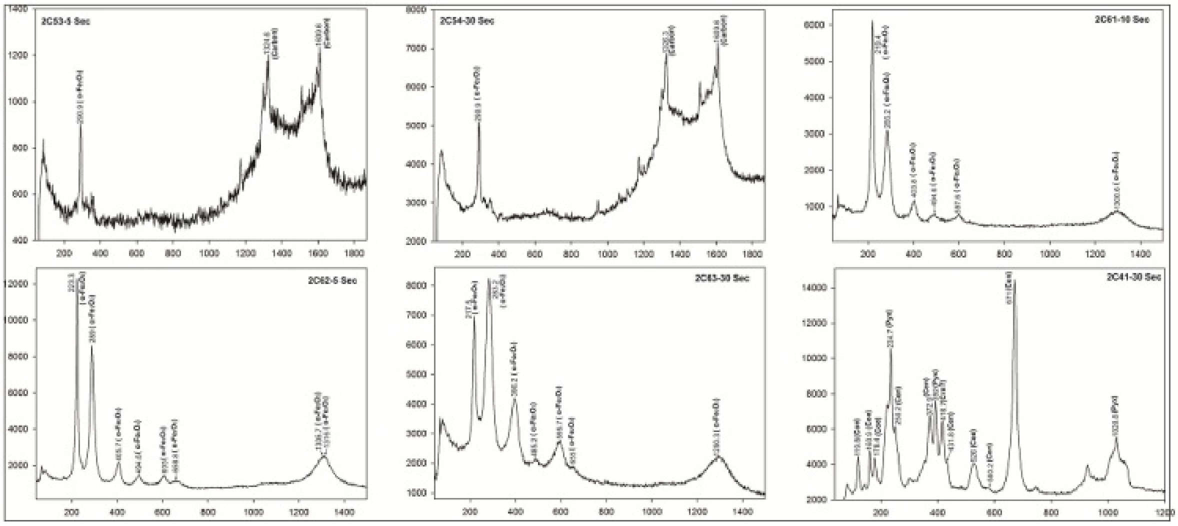

BIO - DATA

Souvik Das – Bio data

Educational history

2011	Qualified NET (National Eligibility Test).
2008	M.Sc. in Applied Geology from university of Calcutta (69.2 %).
2006	B.Sc. in Geology from University of Calcutta (82%).
2003	Higher Secondary from Sanskrit Collegiate School, Kolkata (West Bengal Council of Higher Secondary Education) and obtained 72.9%.
2001	Secondary Education from Sanskrit Collegiate School, Kolkata (West Bengal) with 82%.

M.Sc. Dissertation

It was carried out on “Development of imbricate thrust in mechanically two layer setting: an experimental investigation” under guidance of Dr. Santanu Bose (Lecturer, University of Calcutta).

PhD topic

Nature and evolution of mantle section in the Nidar Ophiolite suite, Ladakh, India under guidance of Dr. Barun K Mukherjee (Sci’ C, Wadia Institute of Himalayan Geology)

Honors and awards

WIHG Institute Senior Research fellowship on 2012

Wadia National fellowship on 2009

Berkner Travel Grant Award to attend the AGU Fall Meeting in 2011 from American Geophysical Union (AGU)

Third prize for poster presentation in International Conference on Indian Monsoon and Himalayan Geodynamics

Publications:

1. Sen Koushick, **Das Souvik**, Mukherjee Barun K, Sen Koushik., (2013), Bimodal stable isotope signatures of Zildat Ophiolitic Mélange, Indus Suture Zone, Himalaya: implications for emplacement of an ophiolitic mélange in a convergent set-up, **International Journal of Earth Sciences** Vol 102 (7) 2033-2042.
2. **Das Souvik**, Sen Koushick, Mukherjee Barun K, Mukherjee Soumyajit (2014), Natural CO_2 sequestration of altered ultramafic from the Himalayan Ophiolite, Ladakh India, **International Journal of Earth Sciences**, under review.
3. **Das Souvik**, Mukherjee Barun k, Basu Asish R (2014), Relict minerals from the mantle transition zone in the Nidar Ophiolite Complex (NOC) Ladakh Himalaya, India, **Geological Society of London**, submitted.

Conference proceedings:

International

1. Sen Koushick, **Das Souvik**, Mukherjee Barun K., 2011, “Significance ... final emplacement” In 14th Bathurst Meeting of Carbonate Sedimentologist, Bristol University, United Kingdom.
2. **Souvik Das** & Barun K Mukherjee, 2011; Supersilicic Clinopyroxene from Nidar Ophiolite Ultramafics, Ladakh Himalaya, AGU Fall Meeting, San Francisco, USA.
3. **Souvik Das** 2011; Possible path of water to the mantle through serpentine subduction: Evidence from Nidar Ophiolite, Ladakh Himalaya, Indian Monsoon and Himalayan Geodynamics, Dehradun, India.

4. **Souvik Das**, Barun K Mukherjee & Asish R Basu 2013; Mineral Relicts of the Earth's Mantle Transition Zone in Peridotites of the Nidar Ophiolite, Himalaya, India, AGU Fall Meeting, San Francisco, USA.

National

1. **Souvik Das**, Barun K Mukherjee, Koushik Sen, 2010; Serpentinization of ultramafic rocks of Nidar Ophiolite, NW Himalaya: a clue of multiphase deformation during emplacement" (RDS-I) Kolkata, India.
2. **Souvik Das** & Barun K Mukherjee, 2011; Hydration of upper mantle by serpentines: Evidence from Nidar Ophiolite, Ladakh Himalaya, Geodynamics and Metallogenesis of Indian Lithosphere, Varanasi, India.
3. **Souvik Das** 2011; Possible path of water to the mantle through serpentine subduction: Evidence from Nidar Ophiolite, Ladakh Himalaya, Indian Monsoon and Himalayan Geodynamics, Dehradun, India.
4. **Souvik Das**, Barun K Mukherjee, 2013; X discontinuity: probing through mineral phase transitions from Himalayan peridotite, page 13, Workshop on modern perspective in Himalayan Geosciences, Indian Geophysical Union, WIHG, Dehradun, India.
5. Puspendu Saha, **Souvik Das**, Santanu Bose, 2013; Analogue modeling on deformation mechanics in fold – thrust belt: implications on earthquake rupture, page 49, Workshop on modern perspective in Himalayan Geosciences, Indian Geophysical Union, WIHG, Dehradun, India.

Popular articles:

First time reporting of exsolution lamellae as an indicator of high pressure in a clinopyroxene of ultramafics of Nidar Ophiolite (photomicrograph) took place in WIHG Newsletter, 2011.

Affiliation

American Geophysical Union
Geochemical Society
Life member of Himalayan Geology
Life member of SGTSGINDIA